Depth Perception in Humans and Animals

Jared Parnell

A thesis presented for the degree of
Doctor of Philosophy

Centre for Advanced Instrumentation

Department of Physics

Durham University

England

August 2015

Abstract

This thesis has been the product of three projects which are all related to depth perception, within the core discipline of vision science. The first project was collaborative work between the University of Durham and researchers at University of California, Berkeley. These included Prof. Martin S. Banks and Bill Sprague at U.C. Berkeley, and Dr. Jürgen Schmoll and Prof. Gordon Love at the University of Durham. This project built on previous research investigating the ocular adaptations in different land-dwelling vertebrate species. We found that we could strongly predict pupil shape based on the diel activity and trophic strategies of a species, and our simulations showed that multifocal pupils may extend depth of focus. The second project was also in collaboration with U.C. Berkeley; Prof. Martin S. Banks, and Paul Johnson, which involved a study into 3D displays and different approaches to reducing the vergence-accommodation conflict. Our results showed that a focus-correct adaptive system did assist in the vergence-accommodation conflict, but monovision was less efficacious and we believe this was due to a reduction in stereoacuity. The third project considered spherical aberration as a cue to the sign of defocus. We present simulations which show that the spatial frequency content of images on either side of focus differ, and suggest that this could, in principle, drive the accommodative process.

Declaration

The work in this thesis is based on research carried out in the Centre for Advanced Instrumentation, Department of Physics and in the Department of Psychology at the University of Durham, England. No part of this thesis has been submitted elsewhere for any other degree or qualification and it is the sole work of the author unless referenced to the contrary in the text. My supervisor, Prof. Gordon Love, and I received specialist guidance on work conducted throughout this project from our collaborator, Prof. Martin S. Banks, and his students Paul Johnson and Bill Sprague, from the Vision Science Group at the University of California, Berkeley.

Publications

- Banks, M.S., Sprague, W.W., Schmoll, J., Parnell J.A.Q., & Love, G. D. (2015) Why do Animal Eyes have Pupils of Different Shapes?, *Science Advances*, 1(7)

Acknowledgements

Firstly, I would like to thank my supervisor, Prof. Gordon Love, who has imparted a great deal of knowledge and advice, throughout. I would also like to thank all of my project collaborators, including Prof. Martin Banks, Bill Sprague, Paul Johnson, and Dr. Jürgen Schmoll for all of their hard work and insight through the different aspects of each project (particularly the unrelenting determination to publish our Science Advances paper). To the other members of the Centre for Advanced Instrumentation, I extend my gratitude for their tolerance and friendship in the past 4 years. I would also like to thank all of my friends and family who have given their support, with a special thanks to Louise who had to endure my company for the final weeks before completion.

I would like to acknowledge funding from Engineering and Physical Sciences Research Council for my studentship.

Contents

List of Figures

List of Tables

Chapter 1

Introduction

Depth perception is a fundamental aspect of visual perception for the survival of many different species, including humans. Animals require vision for hunting, foraging, and the detection of predators. Depth perception is a critical aspect of visual function, which allows us to interact with our environment in a precise and efficient manner. The ability to identify the location of objects in the environment allows different species to hunt or forage for food, escape predators, use tools, and engage in social behaviours. Vision is the primary sense for most humans, although we also utilise this faculty for more than survival. We have developed many forms of visual entertainment, some of which utilise the mechanisms of depth perception to create the illusion of three dimensional (3D) images on two dimensional (2D) surfaces. This is an area which has been growing due to changes in the associated technology, although there are still challenges regarding the quality and comfort experienced by users.

We define depth as the relative distance from one object or surface to another, whereas distance is a length between two points. These two terms are related but distinct in that the former concerns relative positions while the latter is a measure of absolute positions in space. When we talk about depth perception we are referring to the identification of distances of objects in the environment relative to the observer as a consequence of sensations derived

from the visual system. This is an important distinction as two objects in the environment may be 12 centimetres apart but if they are located 1 metres from the observer then this distance will appear much greater than if these two objects are located at 5 metres.

This thesis is the culmination of three different projects, each investigating different aspects of depth perception. These projects include an investigation into vertically elongated pupils and multifocal lenses in cats; an experiment assessing the viability of monovision spectacles in reducing discomfort associated with 3D viewing; and a proposition regarding a mechanism which may allow the sign of defocus to be discerned from the power spectrum of retinal images as a consequence of spherical aberration. Although these three projects are distinct in their content, they are all related to the perception of depth.

1.1. Synopsis

This thesis presents work from the field of vision science, with a particular emphasis on depth perception. The diversity of the individual projects requires a degree of separation when presenting them as a cohesive body of work. The following is a summary of those chapters.

- Chapter 2 introduces many of the key concepts in vision science that are relevant to the successive chapters. The anatomy of the eye is explained, followed by aspects of the visual field and perception; including accommodation and its associated cues, contrast sensitivity, and visual acuity.

- Chapter 3 describes the methods used to simulate different aspects of the visual system. These simulations are used to produce some of the results given in chapters 4 and 5. The basic elements of the eye, which the simulations hope to replicate, are described. Zernike polynomials, the point spread function (PSF), and the modulation transfer function (MTF) are all defined with reference to their role in the simulations and consequent results.

- Chapter 4 describes a theory which allows the sign of defocus to be determined from

information contained in images formed by a system which exhibits spherical aberration. Defocus is used throughout this section as a reference from which we can identify the unique features of both astigmatism (a well known source of sign information) and spherical aberration. The results are based on a series of simulations which model the eye (as described in chapter 3) with different applied aberrations. Astigmatism provides sign information to the observer through the preservation of contrast in only one orientation. We propose that, when spherical aberration is present, sign information can be derived from the spatial frequency content of images on either side of focus. Our results support this hypothesis. This mechanism could, in principle, drive accommodation in the absence of other cues.

- Chapter 5 investigates the role of elongated pupils and multifocal lenses. The simulations are based on the same method used in the previous chapter, but they are adapted to model the eye of a cat. This animal has vertically elongated pupils and multifocal lenses. These results are provided in the context of a broader collaborative project which asks why animals have pupils of different shapes based on their daily activity cycles, and trophic strategies. The reasons for these evolutionary adaptations is also investigated, where various models and theories are proposed for a range of different ocular physiologies. We find that vertically elongated pupils are most common in nocturnal ambush predators, horizontal pupils in diurnal grazers (i.e. prey), and circular pupils in diurnal active predators. The theory for horizontally elongated pupils is to increase throughput and image resolution at oblique angles, and vertical pupils may increase the efficacy of stereopsis through the fusion of vertical contours. Multifocal lenses may increase depth of focus, but our results suggest that the vertically elongated pupil does not necessarily allow usage of the multifocal lens in bright conditions as suggested by Malmström and Kröger (2006).

- Chapter 6 details the results of two psychophysical experiments which assess the potential benefits of monovision as a means to improving simulated three dimensional

viewing. It is proposed that this benefit may lie in the reduction of the vergence-accommodation conflict, and while this effect might hold, we found that participants did not perform was well when wearing the monovision lenses as compared with traditional polarising glasses, and participants stated a preference for the traditional method. The decline in performance may be associated with reduced stereoacuity, although this may not account for the subjective preference for the traditional method.

- Chapter 7 summarises the results and conclusions from each chapter.

Chapter 2

The visual system

This chapter includes theory related to several of the following results chapters. We discuss the anatomy of the eye, with an emphasis on human vision, as this is fundamental to each chapter and the basis of depth perception. The visual field, including visual/stereo acuity and contrast sensitivity, are then discussed. These elements are critical in the fidelity of ocular imaging and metrics regarding visual performance. We then discuss accommodation (the ability to focus on objects at different distances), and different cues which give rise to this response, including vergence which is related to stereoacuity and the means through which we produce the illusion of depth in chapter 6. We discuss accommodation and its associated cues as these are also fundamental to depth perception; where monochromatic aberrations are particularly relevant to the results in chapter 4, where we discuss spherical aberration as a potential cue to the sign of defocus. The section on chromatic aberration is relevant to chapter 4 because this is considered to be one of the most prevalent cues to accommodation in humans, but it is also highly relevant to section 5.1.7 where we investigate multifocal lenses as a means of reducing chromatic aberration in animals with different shaped pupils.

2.1. Anatomy of the eye

The eye is a sensory organ which provides humans with an ability to perceive their environment by way of the light entering the eye, activating photoreceptors in the retina which send electrical signals through the optic nerve to the brain, of which approximately 27% is associated with visual function, which appears large when compared with areas such as auditory processing which is associated with 8% of the cortex (Chalupa & Werner, 2004). This process is very complex and there are many stages which alters the role light has in forming our perception of the world, from the moment it is refracted through the structures of the eye (Artal & Tabernero, 2010), to the extraction of shapes and features in the retina and neural structures of the eye (Fairhall *et al.*, 2006), as well as a great deal of complex processing which occurs in different areas of the brain (Milner & Goodale, 1995; Thorpe *et al.*, 1996).

Light, often reflected from objects within the environment, first passes through the cornea, the aqueous humour, and then through the iris to the crystalline lens, which utilises the contraction and relaxation of the ciliary muscles to change the shape of the lens, allowing the light from a given object to be focused on the retina after travelling through the vitreous humour (figure 2.1).

The structure and shape of the eye is maintained by a fairly rigid structure called the sclera, this is the white part of the eye which is externally visible. The cornea is a transparent area on the anterior surface of the eye. The sclera and cornea are composed of similar material (both connective tissue) but the difference in opacity is associated with the structure of collagen fibres, where the organisation is irregular in the sclera and more consistent in the cornea. The cornea does not receive any blood flow (presumably as this would interfere with transparency) but receives nutrients from the tear film on the outer surface of the cornea and the aqueous humour in the interior surface. The cornea is responsible for about 80% of the eyes focusing power, with the remaining 20% from the crystalline lens. As such, medical conditions such as keratoconus can cause thinning of the cornea, resulting in severe visual distortions (Hess & Carney, 1979). The iris acts as an aperture, stopping light after it has

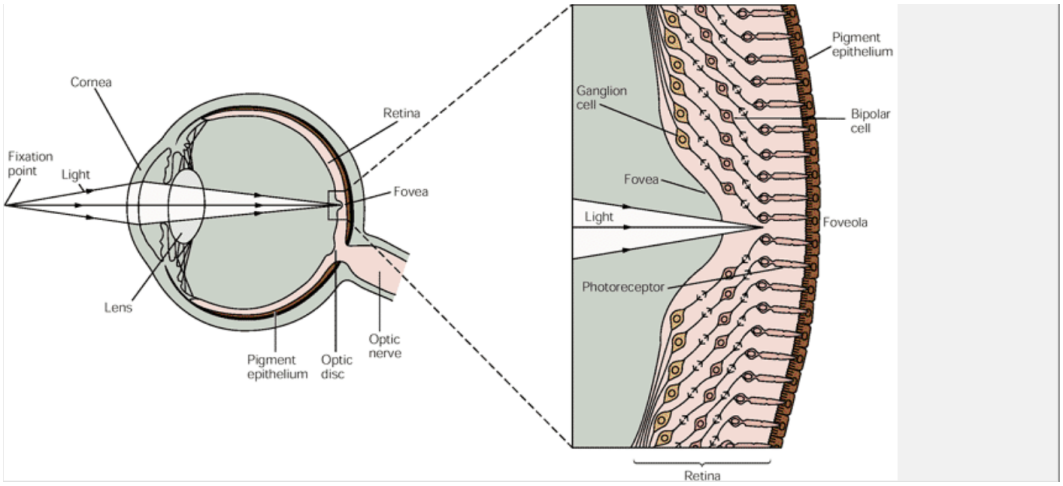

Figure. 2.1: the passage of light through the structures of the eye, until focused on the retina (Tessier-Lavigne, 2000).

passed through the cornea. This structure is responsible for controlling the amount of light entering the eye. The iris consists of a structure called the stroma, which is a fibrous tissue that contracts and dilates with integral pupillary muscles. This part of the eye is heavily pigmented, and gives the eye its colour (Forrester *et al.*, 2015).

2.1.1. Crystalline lens

The crystalline lens is located near the front of the eye, just behind the iris (pupil), and is around 10mm in diameter with a 4mm axial depth. This lens is responsible for the accommodation response (ability to focus) in humans, whereby the ciliary muscle which surrounds the lens contracts and relaxes to change its shape. This alters the refractive power of the lens allowing light from different distances to become focused on the retina. The lens itself is primarily composed of three structures; the lens capsule, which is a membrane which surrounds the lens; the lens epithelium, which is responsible for regulating the flow of nutrients in and out of the lens as well as developing new lens fibres during growth; with most of the remaining lens consisting of lens fibres which are structured and transparent to increase refraction. The lens itself does not receive any nourishment from blood, but

absorbs nutrients and ions from the aqueous and vitreous humours on either side (Forrester *et al.*, 2015).

The lens tends to stiffen with age, and consequently the extent to which it can alter its shape decreases. This results in a reduction in the range of accommodation of adults from around the age of 40-50 years. Presbyopia, and cataracts, are conditions which are often responsible for ophthalmic corrections such as intraocular lenses, and laser eye surgery. These often involve the application of monovision, where the one eye is permanently focused at distance, and the other for near vision; or multifocal lenses, where each eye receives a number of different focal points (Nijkamp *et al.*, 2004; Richdale, 2006; Fernandes, 2013).

2.1.2. Retina

The retina is composed of several layers, and each of these layers is composed of different types of cells. When the light reaches the retina it passes through these different cellular structures before activating the photoreceptors (figure 2.1). The light that they receive is then converted into electrical signals (in the form of graded potentials, which feed through to the ganglion layer which are responsible for transmitting impulses to the optic nerve) which are passed from the photoreceptors to the next layer; consisting of bipolar, amacrine, and horizontal cells. These cells pass information to the retinal ganglion cells, which direct the impulses to the optic nerve. There is also an additional layer behind the photoreceptors called the retinal pigment epithelium (RPE). This layer is responsible for absorbing scattered light (or reflecting it in some animals with a section of the RPE called the tapetum lucidum), and is responsible for a number of different functions including the transport of ions and nutrients to the photoreceptors which do not have any direct blood supply from the choroid (the vascular system that lies between the retina and the sclera). There are blood vessels on the inner most surface of the retina and these extend from a single artery, that passes through the back of the eye, close to the optic nerve. These vessels supply blood to the inner layers of the retina, while the choroid supplies the outer layers (Kiel, 2010; Forrester *et al.*, 2015). Although it is interesting to note that many species of bird have a structure called

the pecten, this is a vascular structure which does not radiate vessels across the retina but still supplies the inner layers with blood. This is associated with an increase in the efficacy and acuity of the avian eye (Mann, 1924; Crozier & Wolf, 1944; Brach, 1977).

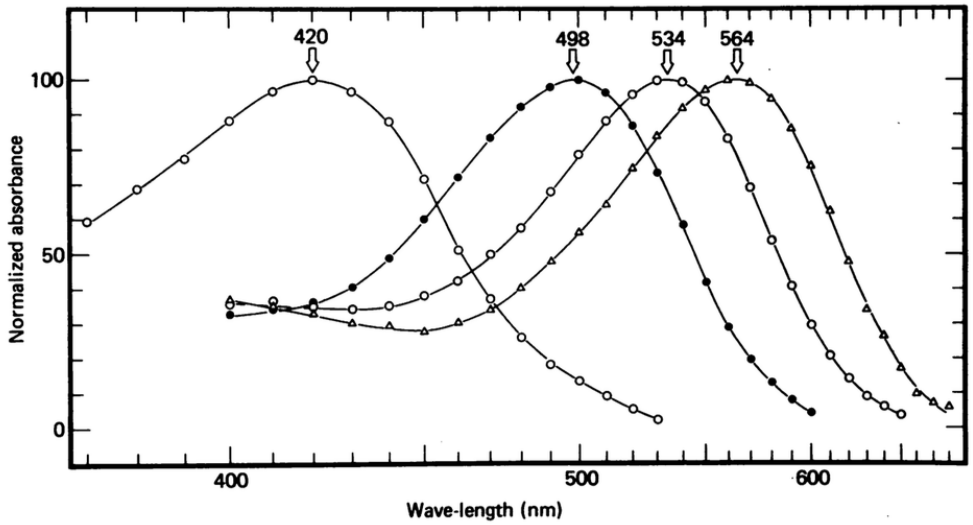

Figure. 2.2: This figure taken from Bowmaker and Dartnall (1980) shows the mean absorbance spectra of the four types of photoreceptor in the human eye. The curve labelled 498 is the mean of the absorbance of 11 rods (scotopic vision), and the three cones types (responsible for high acuity colour vision) are; curve 420 is the mean of three blue-sensitive cones; 534 is the mean of eleven green-sensitive cones; and 564 is the mean of nineteen red-sensitive cones.

The photoreceptors are the layer of cells primarily responsible for the collection of light, and the conversion of light into graded potentials. Light is collected by other cells, such as retinal ganglion cells, but their function is less well understood; theories include the regulation of the circadian clock and pupillary reflex (Berson *et al.*, 2002; Markwell *et al.*, 2010). Photoreceptor cells absorb photons, and this produces graded potentials (a disruption to the cells biochemical equilibrium) which travel from these photoreceptor cells at the posterior of the retina through each layer until it innervates the ganglion cells (Rodieck, 1998, Ch. 3) and these cells produce action potentials that travel through the optic nerve to the brain. There are two types of photoreceptors in the eye, these are called cones and

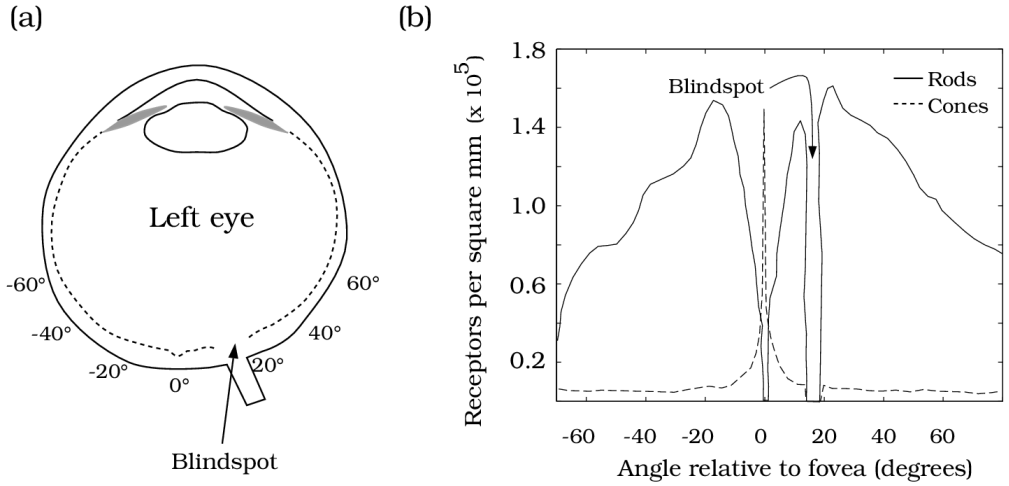

Figure. 2.3: the fovea had the highest density of cone photoreceptors and is the area responsible for the highest area of visula acuity. Panel (a) shows the position of the retina and blind spot with an angular scale indicated around the posterior surface of the eye. Panel (b) shows the density of rods and cones around the fovea, and the location of the blind spot (Wandell, 1995)

rods. The first is responsible for high acuity vision, and the perception of colour. There are (typically) 3 types, each sensitive to different wavelengths of light, roughly equating to red, green, and blue colours. The spectral sensitivity of all four different photoreceptor types (rods/red, green, and blue cones) can be seen in figure 2.2. Cone photoreceptors are also directionally sensitive. Light entering the eye at the periphery falls at an increased angle of incidence on the retina and, due to the directional sensitivity of cone photoreceptors, the neural response of the cell is reduced. This phenomenon is called the Stiles-Crawford effect (Stiles, 1937; Westheimer, 2008).

The retina has a central visual point called the fovea, which is located within an area called the macula. The fovea, extending out into the macula, has the highest count of cone photoreceptors. This axis which aligns with the fovea is called the visual axis and this is separated by approximately 6° from the optical axis of the eye (Pettigrew & Sanderson, 1986). The density of cone receptors, and its morphology, result in the highest levels of visual acuity as compared with any other position on the retina. It is called the foveal pit as it is a

slight depression in the surface of the retina, and there is no vascular structures which means that this area of the retina is entirely dependent on oxygen supplied by the choroid (Riva & Cranstoun, 1994; Pinz *et al.*, 1998). The shape, position, and photoreceptor density around the fovea can be seen in figure 2.3. The retina can be imaged using an opthalmoscope as shown in figure 2.4 with several key areas highlighted (Stanford University School of Medicine Website, 2015).

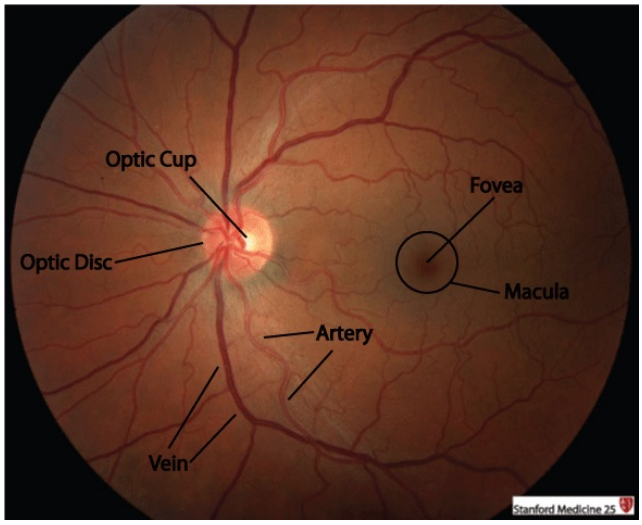

Figure. 2.4: this image of the fundus (posterior surface) of the eye was taken with an ophthalmoscope and labels have been added to highlight the position of the optic cup, optic disk, examples of veins and arteries, the macula and within it the fovea. From Stanford University School of Medicine Website (2015).

2.2. The visual field

The normal monocular visual field of typical adult extends, approximately, 100° laterally, 60° medially, 60° upwards, and 75° downwards. There is a central area of higher sensitivity called 'central vision' which is the inner 30° of the the full visual field. There is also a 'blind spot' which occurs where the optic nerve exits, and the ophthalmic artery enters. This spot is located 12-17° temporally, and 1.5° inferiorly from fixation (Spector, 1990). In this area, called the optic disc (highlighted in figure 2.4), there are no photoreceptors,

and as a consequence there is no information collected over an area with a 7.5° diameter (Armaly, 1969). Although there is no perceptual information available from this part of the retina, we are not consciously aware of the blind spot under normal conditions, but certain tasks and tests can be performed which will allow subjective identification of its size and location (Ramachandran, 1992).

2.2.1. Acuity

Visual acuity is often the most common test of an individuals visual function, and it is often measured through the use of a Snellen Chart (Snellen, 1863), although an alternative test has been developed, called the logMAR (Logarithm of the Minimum Angle of Resolution) chart, which is considered to be more accurate due its design (Bailey & Lovie, 1976). The latter test is considered better due to the use of logarithmic spacing and sizing between each letter. These two charts can be seen in figure 2.5.

Stereoacuity is the ability to which people can extract information which is dependent on binocular vision. This may include the perception of the depth of objects, or tasks related to occlusion. There are a number of tests which measure stereoacuity, these include random-dot stereograms, and contour-based stereotests, such as the Titmus fly test (Millodot, 2004). Stereoacuity is typically high at a young age and studies have found that may decline in old age, but not necessarily in conjunction with standard visual acuity and the reasons for this decline are unclear (Greene & Madden, 1987; Brown *et al.*, 1993; Garnham & Sloper, 2006).

2.2.2. Contrast sensitivity

Contrast sensitivity is a measure of how accurately an observer can differentiate areas of varying luminance. It is similar to visual acuity, in that it measures the visual performance of an individual, but it also takes into account the contrast of the stimulus. The visual acuity tests (such as Snellen and logMAR) always present letters in high contrast, i.e. black letters on a bright white background. In some medical conditions, such as glaucoma; ocular hypertension; Parkinson's disease; and diabetes, we find that visual acuity is still fairly

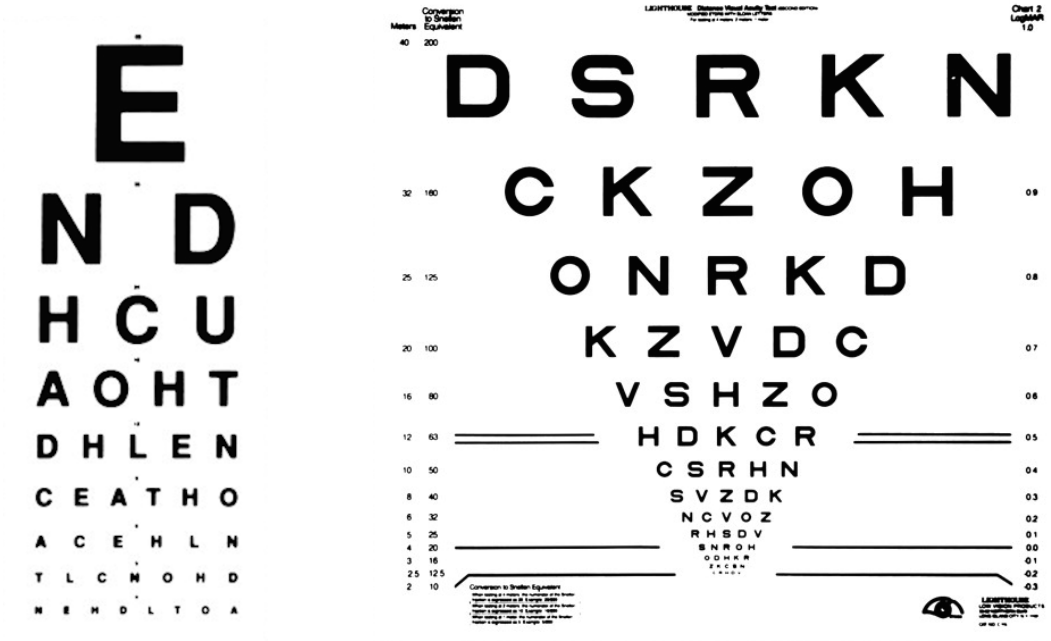

(a) Snellen (b) logMAR

Figure. 2.5: two visual acuity charts. The first is an early design which is based on the visual acuity score where 20/20 is considered optimal vision. The second is the logMAR chart which features letters that decrease in size and spacing logarithmically. This provides greater clinical accuracy (Bailey & Lovie, 1976).

high but contrast sensitivity is degraded such that they may perform well in a visual acuity task, but would have difficulty performing the same task when the pedestal intensity is closer to stimulus intensity (Regan & Neima, 1984; Stamper, 1984). In figure 2.6, we see a visualisation of the contrast sensitivity function as described by Campbell and Robson (1968) in panel 2.6a, and we see an adapted visual acuity chart, by D. G. Pelli (1988), which accounts for contrast sensitivity loss in figure 2.6b.

Sensitivity to spatial frequencies reaches a maximum at around 45 cycles/degree (cpd), and peaks at around 3-5 cpd. In comparison, the sensitivity of a cat is believed to peak at around 0.3 cpd (Stamper, 1984). The fovea is the area of the retina which is responsible for the highest levels of contrast sensitivity, and this reduces at increasing eccentricities (Thibos *et al.*, 1996).

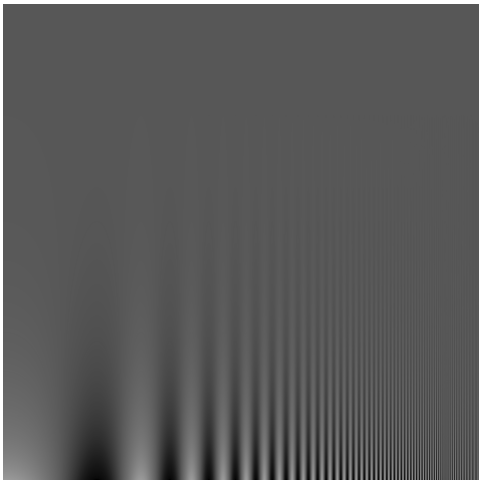

(a) Campbell-Robson Contrast Sensitivity Chart

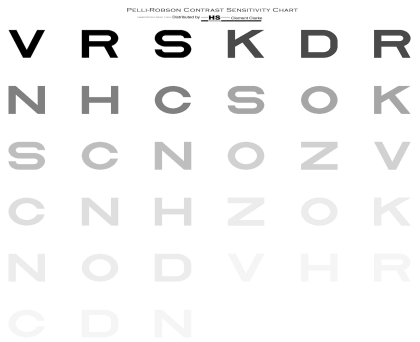

(b) Pelli-Robson Contrast Sensitivity Chart

Figure. 2.6: two charts that highlight the effect of contrast as well as acuity.

2.3. Accommodation

The eye has evolved mechanisms which allow dynamic control of its refractive power to resolve images on the retina. In humans, this occurs primarily through changes in the shape of the crystalline lens. The ciliary muscle which surrounds the lens can contract and relax which alters the curvature of the lens. This causes the refractive power to increase and decrease so that images at different distances can be brought into focus.

Monocular accommodation occurs in response to a number of cues such as scale, motion parallax, and object recognition, but subjects often accommodate in the correct direction when these are removed as viable cues (Chen *et al.*, 2006). This ability has been attributed to the aberrations of the eye (Kruger & Pola, 1986; Flitcroft, 1990; Wilson *et al.*, 2002; Chin *et al.*, 2009), i.e longitudinal chromatic aberration (LCA) and monochromatic aberrations (MCA). It is also possible that directional cues are derived from other phenomena such as microfluctuations (Gray *et al.*, 1993), or the Stiles-Crawford effect (Fincham, 1951). This study aims to identify which monochromatic aberrations could provide a directional accommodation cue when other aberrations have been removed. Kruger *et al.* (1995) found that

accommodation was significantly affected by the removal or reversal of chromatic aberration but in one subject accommodation was unaffected by either condition (removal or reversal). The accommodative ability in this individual was attributed to sign information derived from monochromatic aberrations, such as spherical aberration.

The lens tends to harden with age, and this correlates with the onset of presbyopia and the decline the accommodative range (Pau & Kranz, 1991). The power of the lens is typically considered to be around 15 dioptres in younger adults, but this drops to 8 dioptres at age 40, and 1-2 dioptres by age 60 (Forrester *et al.*, 2015).

2.3.1. Vergence

The accommodative response (the ability to focus on objects) is intrinsically linked to the vergence response (the rotation of the eyes to mutually align the visual axis with objects in the environment). In a natural situation an observer will view objects within the environment and as these objects get closer to the observer the eyes must rotate to maintain fixation but because the distance also decreases so must the eyes refocus to reduce the blur error. As the eyes rotate to align with a new, or approaching, object the focal power of the crystalline lens also changes to bring that object into focus. As these actions occur in a complimentary and parallel fashion in everyday viewing they have become functionally linked, i.e. focal distance and vergence distance are the same in normal viewing, consequently changes in vergence evoke a change in focal power and vice versa. In the case of 3D displays, the illusion of depth (i.e. the appearance that an object is closer or farther from the depth at which it exists) is created by changing the disparity of images, but there is no associated shift in focal distance. It is suggested that this conflict can result in headaches and discomfort in a number of observers, particularly when the magnitude of disparity exceeds certain thresholds. The extent to which the illusion of depth can be created is also limited by these thresholds due to increased blur error and vergence comfort (Shibata *et al.*, 2011).

The extent to which a typical individual can retain a clear 3D image from binocular

stimuli has been well documented as part of ophthalmic investigations for vision correction. The ability to alter their accommodation and vergence responses, and still retain a well-focused single image is limited, and defined by Fry (1939) as the *zone of clear single binocular vision* (ZCSBV), at the greatest extent of which the individual may well still experience discomfort. The area in which the vergence-accommodation conflict is minimised to a tolerable level is called *Percival's Zone of Comfort* (Percival, 1892). Percival (1892) defined this zone as the central third of the ZCSBV. Sheard (1934) also defined a 'zone of comfort' but either author based their estimates on slightly different criteria, namely the extent of this zone relative to the position of 'phoria lines'. Phoria lines, drawn through dioptric space, indicate the the angle at which an eye (monocular) will rest when comfortably accommodated to a given stimulus. This eye rotation occurs due to the complimentary nature of vergence and accommodation. In the typical observer this line falls close to the natural viewing line along which the vergence distance and focal distance are the same. It doesn't follow this trend exactly because people tend to be slightly *exophoric* when the focal distance is close, and *esophoric* when the vergence distance is further. Exophoria is characterised by an under-rotation of the eyes relative to focal distance, while esophoria is the over-rotation of the eyes relative to focal distance. Percival's zone of comfort assumes that the most comfortable zone is within the middle 1/3 area of the ZCSBV, while Sheard assumes that the area of discomfort extends from the lines of phoria towards the central line by 1/3. The area within the shaded zones in figure 2.7b are considered the maximum extent for comfortable binocular vision in an average population. Figure 2.7a shows the maximum and minimum extent to which a typical individual can converge and diverge the eyes to maintain clear binocular vision (i.e. before images misalign in either eye and become double vision).

Although there are a number of cues that can be attributed to binocular vision, such as vergence (and occlusion etc), it also appears that subjects can accommodate in the correct direction in the absence of these cues (Campbell *et al.*, 1958). This is attributed to a range of properties that exist during monocular vision including monochromatic and

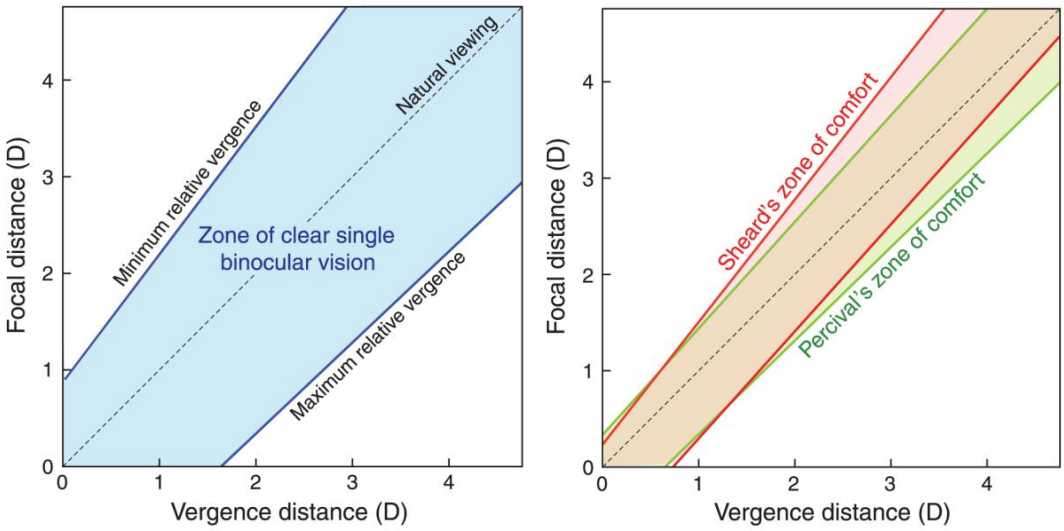

(a) The maximum and minimum vergence distance for binocular fusion.

(b) The zones of comfort when viewing fused-stereo images.

Figure. 2.7: The left hand figure (a) shows the difference between focal distance and vergence distance within which an individual can maintain a single fused image from stereo stimuli. The right hand figure (b) shows the difference between focal distance and vergence difference within which an individual will experience comfortable stereo-fused images (Shibata *et al.*, 2011).

chromatic aberrations, microfluctuations, and potentially the Stiles-Crawford effect (which is not extensively discussed within the scope of this thesis).

2.3.2. Monochromatic aberrations

The human eye is a complex organ with a number of structures which are optically imperfect. The surfaces of these structures, which the light passes through, can introduce aberrations to the wavefront entering the eye, although it is possible that these aberrations actually assist in the accommodation process (Gambra *et al.*, 2010; Yi *et al.*, 2011). It is primarily the aberrations of the crystalline lens that may provide cues to the direction, and possibly the magnitude, of required accommodation changes, although aberrations that are introduced due to other structures in the eye might also contribute to this process (Hofer *et al.*, 2001; Wilson *et al.*, 2002; Gambra *et al.*, 2010). The correction of these errors in the optometric

domain primarily concern defocus and astigmatism but it is known that the structures of the eye produce wavefront error of greater complexity than these low-order aberrations alone. The more complex aberrations are known as high-order aberrations due to the manner in which they are characterised through Zernike polynomials. Defocus alone produces a blur, which is identical in character at either side of focus, but it is known that certain aberrations produce a different blur error for a given magnitude, and its inverse, at either side of defocus.

It is also important to note, however, that studies have shown a decrease in certain aberrations when they are measured across the entire structure of the eye, as when compared with the lens or cornea independently. This suggests that the crystalline lens is, to some degree, compensating for the aberrations of the cornea (Artal & Guirao, 1998). Porter *et al.* (2001) found that aberrations of the crystalline lens were symmetrical in both the left and right eyes, suggesting that the development was genetically determined, but this is in contrast to Marcos and Burns (2000) who did not find a significant level of symmetry. This, however, could be due to differences in sample sizes (Porter: n=109; Marcos: n=2).

In a study by Phillips and Stark (1977), it was proposed that blur alone, was ''the sufficient neurological stimulus to accommodation". In this study, subjects were placed in front of a projector, of which the focusing motor was controlled in closed loop in line with a slit-lamp optometer, or alternatively in open-loop with a oscilloscope. This enabled the researchers to specify a point of focus and control the defocus of the projected image in response to the refractive state of the subjects eye. It was found that defocus alone drove the accommodation response but at the instance the image changed defocus, a 'hunting' response was detected. This is characterised as a forward and backwards shift in refractive state while the subject attempted to determine the sign of defocus (Phillips & Stark, 1977).

The effect of isolated monochromatic aberrations was studied by Wilson *et al.* (2002). Initially they measured the participants natural aberrations, and took these measurements into account when using computer code to produce point spread functions (PSF - defined in section 3.0.6) that did or did not contain defocus sign information (as shown in Figure 2.8). They then presented subjects with this point source through an aperture conjugate with

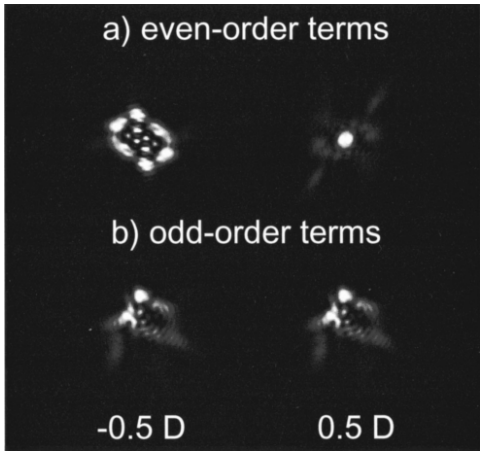

Figure. 2.8: PSFs from Wilson *et al.* (2002) showing the difference in the PSF at -0.5D and 0.5D for a subject (SN) when the experimenter applied even-order aberration terms (shown in a) or odd-order aberration terms (shown in b). The cue is derived from differences in the PSF as shown in a), while aberration terms which do not convey sign information are shown in b). The magnitude of these differences also changes as a function of pupil size, as the pupil size decreases so does the RMS of aberration values (i.e. diffraction becomes the dominate effect).

their pupil while the subjects ability to accommodate was reduced through the application of cyclopentolate hydrochloride. The participants were given approximately two minutes of training to teach them the difference between different PSFs at magnitudes on either side of focus. A point source was the presented with a positive or negative defocus and the subject was required to identify the sign of the defocus component (i.e. whether the change in blur was characteristic of a positive or negative magnitude of defocus). It was found that this ability increased as a function of pupil size, where smaller pupils reduced the ability to identify the direction of defocus, while larger pupils increased the rate at which observers specified the correct direction. This effect was associated with an increase in the RMS (root mean square) of the wavefront error associated with each pupil size, particularly when this error was associated with even-order terms, i.e. those for which the PSF is different either side of focus (Wilson *et al.*, 2002).

Chen *et al.* (2006), conducted a study which assessed the ability of 6 subjects to accommodate stimuli in different conditions; where high-order aberrations were removed with an

adaptive optics system, and where high-order aberrations were unaltered, with the exception of the those detected in the beamsplitter and other optical elements. Any potential cue from chromatic aberration was removed by lighting the target with monochromatic light (550nm), while microfluctuations were unaltered and unrecorded. It was found that four of the 6 subjects could accommodate, with only slight variations in accuracy, to the defocus error, while one subject could not accommodate at all to the condition in which high-order aberrations were removed. Finally, subject AP could not accommodate in either direction, with or without the presence of high-order aberrations. It was later found that this subject was able to correctly accommodate to varying defocus values when the target was illuminated with polychromatic light. The conclusions of this study indicate that there is significant inter-individual variability in responses to changes in accommodative cues. In addition to these results, the effect of high-order aberrations on depth of focus was also estimated from the recorded aberrations of 13 subjects, and, despite high-order aberrations increasing depth of field, there was no measured effect on accommodative response gain or latency. This also suggests that the removal of high-order aberrations does not improve accommodative response in any measurable way (Chen *et al.*, 2006).

These studies suggest that the accommodative function of the human visual system may, in some instances, utilise high-order aberrations to determine the sign of defocus for a given stimulus but their significance is variable between individuals.

2.3.3. Chromatic aberration

Chromatic aberration, or dispersion, occurs because of the variances in refraction of different wavelengths of light through the structures of the eye. Longitudinal chromatic aberration causes the image on the retina to form such that the spread, or defocus, varies for each wavelength of light. An example is shown in figure 2.9 This causes a change in intensity of the light activating different photoreceptors in the retina, which could provide the observer with a cue to the sign of defocus (Campbell & Westheimer, 1959; Kröger *et al.*, 1997).

In a study by Chin *et al.* (2009), the role of monochromatic aberrations were investigated

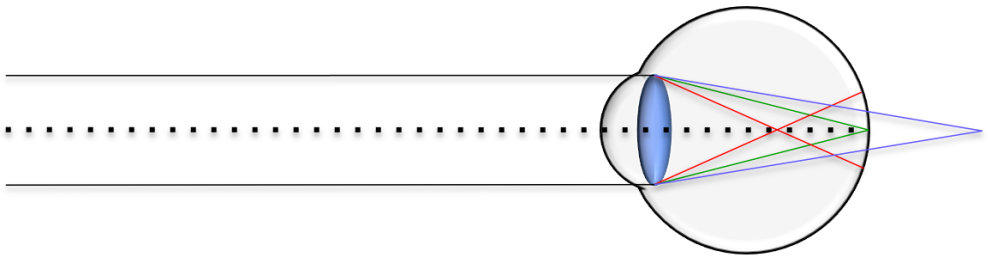

Figure. 2.9: The effect of longitudinal chromatic aberration on white light as it passes through the eye. White light enters the eye from left to right in the diagram. Each wavelength is refractive to different degrees, which results in a different focal point for each. Three wavelengths, equivalent to red, green, and blue, have been highlighted in the diagram.

through experimentation with an adaptive optics system. This allowed the removal or reversal of the monochromatic aberrations of the subjects eye. The subject viewed a maltese cross illuminated with monochromatic light (550 nm), the position of which was varied with a Badal optometer to ensure that the luminance and scale of the target remained constant. This removed visual information which may have provided the subject with a means of determining the sign of defocus, with the intention of isolating monochromatic aberrations as the only available cue. Responses during the study were incorrect with greater frequency when the target was moved in an outward step and when aberrations were inverted. The results of this study suggest that monochromatic aberrations can, for some observers, play an important role in the accommodative process. The variability in observers may occur as an effect of the specific aberrations present in their eye, which were not recorded during this study (Chin *et al.*, 2009).

In a similar study conducted by Aggarwala *et al.* (1995), subjects were required to view a Maltese cross as it was moved sinusoidally at 0.2 Hz, across an amplitude of 1 Diopter. Their accommodative response was recorded as the stimulus was illuminated in 12 different lighting conditions; including 10 monochromatic wavelengths, a white light illumination and an achromatised white light (for which longitudinal chromatic aberration is minimised). It was found that the accommodative gain and phase lag was least when the target was

illuminated with non-achromatised white light. It was also found that these metrics were smaller for central wavelengths of light when compared with those at the extremes of the visible spectrum. The differences between the monochromatic and achromatic conditions were minimal (statistically similar) but the difference between these 11 conditions and the white light condition was significant ($p < 0.01$). These results suggest that longitudinal chromatic aberration plays a significant role in the determination of the sign of defocus in human accommodation (Aggarwala *et al.*, 1995). Also, despite there being no control for high-order aberrations or microfluctuations, the significance of the difference between conditions where longitudinal chromatic aberration were present, and those where it was not, are sufficient to support the chromatic aberration theory of accommodation control. The results of Aggarwala *et al.* (1995), are consistent with previous results such as those of (Kruger & Pola, 1986).

2.3.4. Microfluctuations

Microfluctuations (MFs) are an aspect of the ocular system that could give rise to a directional cue. This phenomenon is defined as an oscillating change in the focal power of the crystalline lens, which often occurs with both a high frequency component (HFC) and a low frequency component (LFC). The HFC occurs at a frequency of 1 Hz or greater, while the LFC is considered to be less than 1 Hz, with the magnitude of these fluctuations tended to occur at a power less than 1 Dioptre (Monticone & Menozzi, 2011), although this measure varies throughout the literature, such as Charman and Heron (1988) where the LFC is defined as < 0.5 Hz, and the HFC > 0.5 Hz. The magnitude of these microfluctuations also varies throughout the literature, but one significant study assessed the perceptual detectability of microfluctuations. Winn *et al.* (1989) found that the magnitude of microfluctuations more than spanned the depth of focus and so assumed that this was sufficient without the need for a sub-threshold blur mechanism. The eyes studied in this report were under cycloplegia, and as such, the pupil would have been very dilated, reducing the depth-of-field and increasing the potential effect of accommodative microfluctuations.

Studies have shown that the LFC component is more pronounced when the subject has smaller pupils, while the HFC is more pronounced when the pupil is large. This is assumed to be a consequence of the change in depth-of-field. When there is a limited depth of field, the magnitude of the oscillations do not need to be large to maintain optimum focus, while at a larger depth-of-field the oscillations are larger but less frequent (Campbell & Westheimer, 1959, 1960). Although a later study found that the LFC changed as a function of pupil diameters less than 2 mm, there was little change above this size. There was also no change in the HFC as a function of pupil size (Gray *et al.*, 1993).

There have also been a number of other variables that appear to influence the magnitude and frequency of microfluctuations. One of the most significant of these correlations was between MFs and cardiopulmonary signals. There was early evidence to suggest that the HFC was only an artefact of the periphery of the crystalline lens, a consequence of localised resonance due to tension, and so did not influence accommodative state (Charman & Heron, 1988). Winn *et al.* (1990b) contested this position; they found that the HFC was consistent across the entire lens and not limited to the periphery, consistent with the mathematical model proposed by Koretz *et al.* (1984). They also conclude, however, that the sign of accommodative change is unlikely to be inferred by MFs, as previous studies have suggested that this is not possible in monocular viewing conditions where cues such as stimulus size are removed (Stark & Takahashi, 1965) and that a more likely function of MFs is the maintenance of the steady-state response. However, Kotulak and Schor (1986) claim that accommodation can be stimulated by blur stimulus that is below the human perceptual threshold. Stark and Takahashi (1965) also stated that further investigation was required to determine the source of the components of MFs (Winn *et al.*, 1990b).

Winn *et al.* (1990a) also attempted to discern the origin of microfluctuations. They found that there was a significant correlation between arterial pulse rate and the HFC (defined between 1 Hz and 2.3 Hz). There have been several studies that have confirmed this correlation (Eadie, 1995; Wirm & Gilmartin, 2007). Collins *et al.* (1995) also supported this finding, but also discovered an association between LFC and the respiratory cycle. In

a study by Hampson *et al.* (2005), the hypothesis that there is a link between the HFC and arterial pulse rate was considered tenuous. Monticone and Menozzi (2011) state that this hypothesis is controversial.

There is also evidence that individuals with astigmatism might make cyclic changes in accommodative state, between the two focal points incurred by an astigmatic aberration (Stark *et al.*, 2003). This would suggest that the subject is utilising an oscillation of the crystalline lens to attain the optimum focus of the presented stimulus. The literature presents a compelling case for the position that microfluctuations are regulated by cardiopulmonary and respiratory systems, and their function is primarily in the maintenance of steady-state accommodation.

The role of microfluctuations is not studied in the scope of this thesis, but it is relevant within the scope of accommodative cues. The way in which the visual system interpretes and combines different cues is unknown, and this may play a role in accommodation control. High level cues (those that exist from cognitive sources, such as parallax, shadowing/tone, occlusion, and size/shape) are often present along side lower level cues such as those discussed (monochromatic aberrations, chromatic aberrations, and microfluctuations). It is unknown how the brain interprets these cues in parallel or which cues would take precedence in the presence of conflicts.

Chapter 3

Modelling the eye

Light that enters the eye is focused on to the retina, but this process is imperfect. Aberrations are introduced to the wavefront as it passes through the cornea and lens. If the eye was to fixate on a point of light in the distance, then in an ideal optical system this point would be focused on the retina as a single point. In an aberration-free system, this would still not occur due to diffraction, which is a spread of light on the retina due to the interaction of light with the aperture, or pupil. When this occurs in an optical system the spread of light is characterised by concentric rings around the central point. This spread of light is called the Airy disk.

The human eye is considered to be close to diffraction-limited at pupils sizes of around 2 mm and below. This means that image quality primarily becomes a determinant of the diffraction effects of the pupil. Above this 2 mm threshold, image quality becomes increasingly determined by aberrations, an inherent aspect of the structures of the eye, which increase exponentially with pupil size. There are also effects from chromatic aberration, which occurs due to changes in the refractive index of the structures of the eye as a function of the wavelength of the light entering it (as described previously).

The image of a monochromatic point source formed on the retina can be approximated as the modulus squared of the Fourier transform of the complex wavefront at the pupil

of the eye. We can also approximate the polychromatic point source as a summation of monochromatic PSFs at different wavelengths. In order to accurately characterise the aberrated wavefront we use Zernike polynomials.

3.0.5. Complex pupil function

The aberrated wavefront is measured as deviation from a planar wave, which would be represented computationally by an array of zeros. Zernike polynomials provide a mathematical approach to describing this deviation. They are named, most commonly, by a two number system, Z_n^m, where n is the radial frequency and m is the angular frequency with n $\geq$ m. The Zernike modes ($Z_n^m(\tau,\theta)$) are used to describe a wavefront as,

$$Z_n^m(\tau,\theta) = N_n^{|m|} R_n^m(\tau) cos(m\theta), \tag{3.1}$$

for the even functions, and,

$$Z_n^{-m}(\tau,\theta) = N_n^{|m|} R_n^m(\tau) sin(m\theta), \tag{3.2}$$

for the odd functions, where τ and θ are polar coordinates giving the radial coordinate (0-1) and the angular coordinate (0-2π), respectively. The radial component ($R_n^m(\tau)$) is the given by the polynomial,

$$R_n^m(\tau) = \sum_{s=0}^{\frac{n-m}{2}} \frac{(-1)^s (n-s)!}{s!(\frac{n+m}{2}-s)!(\frac{n-m}{2}-s)!} \tau^n - 2s, \tag{3.3}$$

and the normalisation constant, N_n^m, is given by,

$$N_n^m = \sqrt{\frac{2(n+1)}{1+\delta_{m0}}}, \tag{3.4}$$

where $\delta_{m0} = 1$ for $m = 0$, and $\delta_{m0} = 0$ for $m \neq 0$ (Kronecker delta function). The normalisation function ensures that the polynomial has the correct root means square (RMS)

error. This means that for any polar coordinate on the Zernike circle, the product of the normalisation factor and the Zernike expansion coefficient will give its deviation from the zero mean for that coordinate.

The different Zernike modes, in increasing order, are shown in a typical Zernike pyramid in figure 3.1. Each of these Zernike circles can be combined, using the equations above, to produce increasingly complex wavefronts.

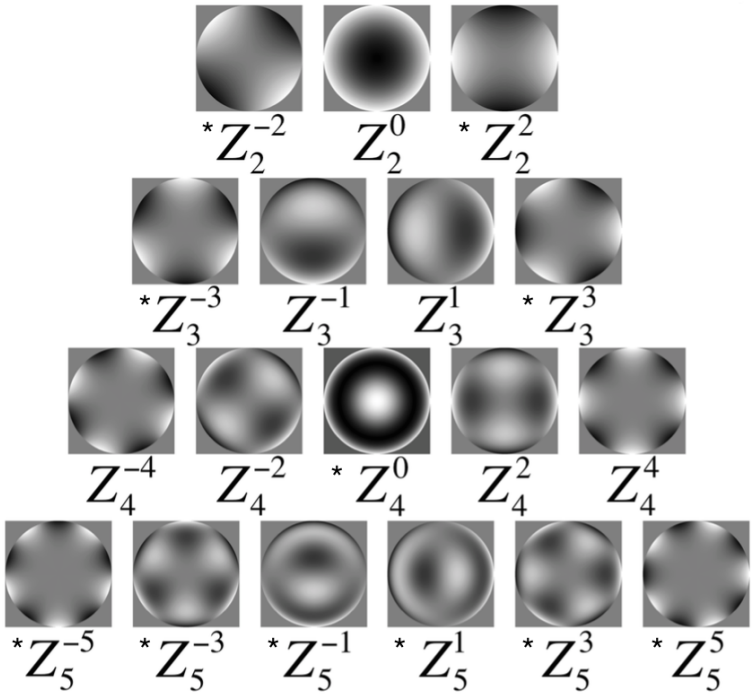

Figure. 3.1: this pyramid shows each Zernike polynomial, each described by two numbers, Z_n^m, where n is the radial component and m is the angular component. The vertical position species the radial value, and the horizontal position specifies the azimuthal angle, where the number of polynomials on each row is n+1 (Young, 2011). The terms marked with an asterisk indicate the even-order terms, where -2,2 and 2,2 are astigmatism, and 0,4 is spherical aberration.

Once we have modelled the wavefront deviations through the use of Zernike polynomials, we multiply the complex function with the pupil function to replicate produce the complex pupil function. We then take the Fourier transform of this function to produce the PSF,

which is a better metric for describing visual performance than the Zernike term on its own. Complex or large wavefront errors do not necessarily translate to poor optical quality due to consequent spread of light (i.e. some aberrations might negate the effects of others despite increasing the RMS error of the wavefront), but the PSF and MTF will give a greater indication of image quality (Applegate *et al.*, 2002).

3.0.6. PSF

The PSF is the image of a point source formed by an optical system. An ideal optical system would image a single point source as a single point in its image, but due to the effects of diffraction and aberrations, this is not the case. The consequent spread of light is called the point spread function, and this can degrade images as each point in an image will affect surrounding points which increases blur and reduces image contrast. The PSF ($I(\tau, \theta)$) is the intensity of the Fourier transform of the complex pupil function ($p(\tau, \theta)e^{-i\frac{2\pi}{\lambda}W(\tau,\theta)}$), given by,

$$I(\tau, \theta) = \left|\mathfrak{F}(p(\tau, \theta)e^{-i\frac{2\pi}{\lambda}W(\tau,\theta)})\right|^2, \tag{3.5}$$

where λ is the wavelength of the simulated light entering through the pupil, the pupil function is $p(\tau, \theta)$, and the wavefront is $W(\tau, \theta)$. We calculate the intensity by taking the modulus squared of this Fourier transform ($\mathfrak{F}$). The PSF is then normalised such that its sum equals 1, equivalent to the power input from the point source. The image formed by the optical system is the convolution of a perfect image of an object with the PSF. As such, it can used in estimates relating to image quality because degradation in image quality can be attributed by the spread of light from each point in the scene. Examples of the PSFs are shown in 2.8, which highlights their (a)symmetry around 0 dioptres of defocus depending on the order of the relevant Zernike terms. In this thesis we use the PSF as measure of imaging performance of an eye with certain pupil shapes, and aberration characteristics. We can also use the PSF to calculate the MTF of the optical system.

3.0.7. MTF

The optical transfer function (OTF) is the complex function of which the MTF is the real part, and the phase transfer function (PTF) is the imaginary part, as,

$$OTF(\nu) = MTF(\nu)e^{iPTF(\nu)} \tag{3.6}$$

where ν is the vector describing the spatial frequencies and their directions. The MTF contains information regarding the intensity at which spatial frequencies are transmitted from object to image through the optical system, and the PTF describes the phase shifts of those spatial frequencies (i.e. high contrast might be present in spatial frequencies where the phase has been inverted). The spatial frequency cut-off (C), below which spatial frequencies will have 0 contrast, is given by the equation,

$$C = \frac{D}{\lambda} \tag{3.7}$$

where D is the diameter of the pupil, and λ is the wavelength of the simulated light. As is clear from this equation, increasing the size of the aperture (or pupil in our simulations) will increase the spatial frequency range in the (retinal) image. Although this effect will only hold when the optical system is aberration-free, as the magnitude of aberrations will increase with pupil size.

In this thesis we calculate the MTF as the squared modulus if the OTF. The modulation transfer function of the eye describes the change in contrast of different spatial frequencies when imaged through an optical system. If we take the squared modulus of the Fourier transform of the PSF we acquire information about the transfer of contrast at different spatial frequencies between the object and the image as a product of the optical systems. The fidelity of contrast in the image is degraded due to optical effects such as aberrations or, in an aberration-free system, diffraction. In a perfect optical system all spatial frequencies would be reproduced perfectly in the image, in this case the MTF will have a value of 1 (perfect contrast), but this cannot occur in any system where a pupil is present (due to

diffraction).

The MTF defines the contrast fidelity of an imaging system, and as a consequence is related to the CSF of the optical system. The CSF (described in 2.2.2) provides a model of the minimum difference in contrast that can be perceived by an individual. This is dependant on the MTF as this will describe the maximum contrast information available to the observer. The CSF takes into account additional effects such as photoreceptor density, spectral sensitivity, and other cognitive effects.

3.0.8. Summary

In this thesis we model the eye with computational Fourier optics. The PSF formed on the retina is the Fourier transform of the complex pupil function. This is a sufficient model for describing the characteristics of different aberrations and pupil functions relevant to our analyses. This model also permits the modelling of chromatic aberration by the summation of individual polychromatic PSFs. We used Eq. 5.3 to estimate the magnitude of chromatic aberration in dioptres. Although this approach is qualified by its level of accuracy, it provides a sufficient and computationally efficient means of modelling all elements considered in our hypotheses.

Chapter 4

Spherical aberration as a cue to the sign of defocus

The accommodation process occurs in response to objects at different distances to bring an image into sharp focus on the retina of the eye. This is achieved through a contraction and relaxation of the ciliary muscle around the crystalline lens in the eye. The eye will become focused at a point, depending on the curvature of this lens, and when an object is presented at a distance which is closer or further from this point the eye will adjust the focal position. This change in focus can be positive or negative, towards or away from the observer (and point of best focus), and the eye will often move in the correct direction which suggests that information is available from the senses which allow the direction of change in focus to be known before the muscle contracts or relaxes. In a natural situation, the participant may have cues such as size and scale from their knowledge of their environment (Campbell *et al.*, 1958), and vergence and parallax, which is the position of objects relative to the visual axis of either eye (Takeda *et al.*, 1999; Stark *et al.*, 2002; Hoffman *et al.*, 2008). When all of these cues are removed by using a constant object adjusted so that it retains a constant size and the observer has one eye covered so that they only have monocular cues, it appears

that they can still perform this task with a high degree of accuracy (Campbell *et al.*, 1958).

The three leading theories regarding a salient cue to the sign of defocus (i.e whether a stimulus is closer or further from the observer's focus) under monocular conditions include chromatic aberrations, monochromatic aberrations, and microfluctations. There has also been reference to another cue based on the Stiles-Crawford effect. Chromatic aberration is one of the strongest theories based on previous studies, but there are a limited number of cases where occasional participants can still accommodate in the absence of chromatic aberration. The cause of this is unknown. Microfluctuations pose a potential cue, and have not been extensively studied. These are continuous oscillations of the lens with respect to its refractive power. The frequency component with greatest gain, and lowest frequency, appears to be correlated with the respiratory system which suggests a relationship between the autonomic nervous system and the ciliary muscle (Collins *et al.*, 1995). This would need to be studied independently but given its presence in all participants it seems unlikely to be the mechanism responsible in the limited number who accommodated without chromatic aberration. The mechanism which involves the Stiles-Crawford effect, proposed by Fincham (1951), provides the observer with a cue to the direction of accommodation through the differing stimulation of photoreceptors depending on whether the light on the retina is converging or diverging (i.e. hyperopic or myopic). This has been studied to a limited extent (primarily by Kruger *et al.*), and in each instance the results of such studies have proved inconclusive (Kröger *et al.*, 1997, 2001; Kruger *et al.*, 2004). It is also assumed that this mechanism may be present in each participant. Although the specific parameters and individual sensitivity to different accommodation cues is unknown.

In this study we present an alternative mechanism which suggests that high order aberrations can provide a cue to the sign of defocus. Monochromatic aberrations have been studied as a cue to accommodation response. Studies have found an effect of other even-order aberrations (Kruger & Pola, 1986; Flitcroft, 1990; Wilson *et al.*, 2002; Chin *et al.*, 2009) but the mechanisms and perceptual artefacts that enable this cue have not been discussed. Stark *et al.* (2003) investigated astigmatism combined with microfluctuations to find

whether participants exhibited greater cyclic changes in accommodation in the presence of astigmatism. They found that these changes increased in variability in three of their seven participants. In parallel with one of their previous studies (Strang, 2000), they believe that this benefits visual acuity.

We propose a mechanism through which an individual can determine the sign of defocus using information present in the aberration characteristics of both astigmatism and spherical aberrations. Previous studies have suggested that these even-order aberrations play a role in the directional control of the accommodation response. It is suggested that the sign information is contained in the differing shape of the PSF on either side of focus (Wilson *et al.*, 2002). This effect does not occur in odd-order aberrations, as such they will not be discussed within the scope of this chapter beyond the inclusion of defocus as a example of typical results for odd-order aberrations.

In the case of astigmatism, we propose that sign information is contained in the relative contrast of vertical and horizontal contours. In the case of spherical aberration we describe a difference in the power spectrum of retinal images on either side of focus. It is these characteristics in retinal images from either side of focus that we believe may, in principle, drive the accommodation response in the correct direction in the absence of other cues. It is also important to note that we have assumed a constant spherical or astigmatic aberration term which may not hold in natural accommodation. These aberrations may increase or decrease with changes in the curvature of the lens, and size of the pupil, as a consequence of accommodation changes. We do not have a model for this change, and this analysis assumes a fixed magnitude to determine what information, if any, is present and may be used by an observer.

4.1. Aberration Characteristics

The images formed by systems with varying aberrations have differing characteristics. The blur error associated with coma is different to that of astigmatism at equal magnitudes of defocus. This blur error does not differ either side of focus (i.e. for equal positive and

negative magnitudes of defocus) when we apply coma, but other aberrations do differ either side of focus. These include astigmatism and spherical aberration, both of which have been noted in previous literature as possible cues to the sign of defocus, i.e. the blur characteristics produced by the aberration might provide the observer with a cue to the sign of defocus. In the case of defocus, the PSF and the associated retinal image is identical either side of focus as seen in figures 4.1a and 4.1b.

(a) -0.5D of defocus (b) 0.5D of defocus

Figure. 4.1: The USAF-1951 test pattern aberrated with 0.5 dioptres of defocus. These are equal magnitudes of defocus with a negative (a) or positive (b) sign, but as the PSF for defocus is identical either side of best focus so is the retinal image.

This means that defocus does not contain information in its aberration characteristics that will provide an observer with a cue to the sign of defocus. There is no additional information other than blur to inform the process of refocussing the eye in either direction. The change in focus would consequently need to be 'hunting' in either direction to determine which increased contrast in the image. This is an effect that can be seen in a study by Campbell *et al.* (1958) where chromatic aberration was removed as a cue as well as spherical aberration and it was found that participants adjusted their focal power in an incorrect direction before the correct direction was determined. The changes in accommodation when the subject has all natural cues available can be seen in figure 4.2a, and the effect when cues

from chromatic aberration and spherical aberration are removed can be seen in figure 4.2b.

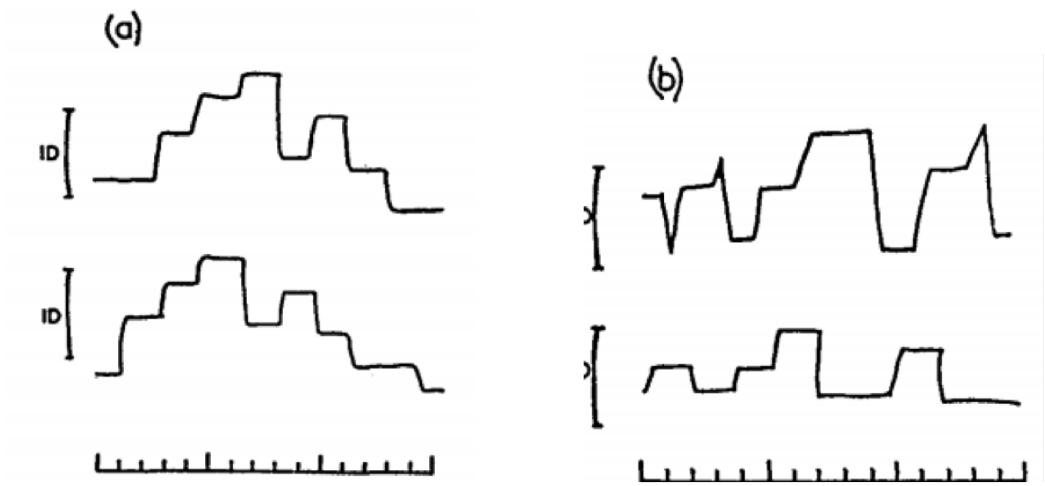

(a) Observer response when all of their natural accommodation cues are present

(b) Observer response when chromatic aberration and spherical aberration were not present

Figure. 4.2: This figure, taken from Campbell *et al.* (1958), shows a participants subjective response estimating the position of a moving stimulus. The lower trace in a and b shows the position of the stimulus, the upper trace shows the participants estimation of the change in distance. The left plot shows the results of allowing the participant to retain accommodation cues, while the right plot shows the effect of removing chromatic and spherical aberration.

This is not true for astigmatism which contains an asymmetric axis whereby positive defocus values are orthogonal or negative defocus values. This is referred to as the axis of astigmatism. As a consequence of this effect, astigmatism produces very different aberration effect in the PSF on either side of focus. When we look at complex images convolved with this PSF (i.e. the simulated retinal image) we see that vertical contours retain high contrast on one side of best focus while horizontal contours do so on the other side of focus. This can be seen in figures 4.3a and 4.3b.

This is also true for spherical aberration which also produces two different point spread functions at equal magnitudes either side of focus, but these PSFs do not differ with the same distinct orientation changes as seen in the case of astigmatism. When we apply spherical aberration to the optical system, in combination with a signed defocus term, we get a PSF

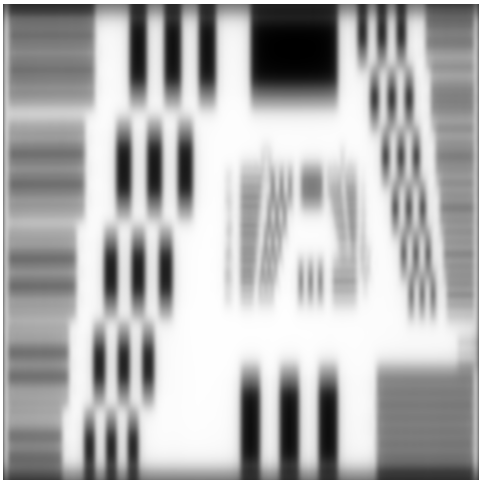

(a) -0.4D of defocus and 0.4D of astigmatism

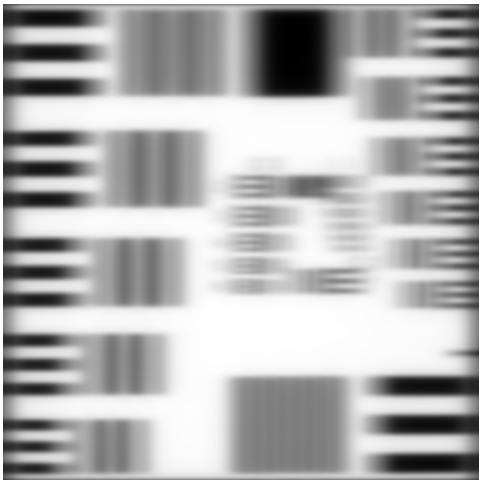

(b) 0.4D of defocus and 0.4D of astigmatism

Figure. 4.3: This is the same test pattern aberrated with 0.4D of spherical aberration. The negative defocus term (4.3a) combined with astigmatism produces sharper vertical contours, while in the positive defocus term (4.3a) produces sharper horizontal contours. It is possible that an observer could use this information to determine the sign of defocus.

which is circular and rotationally symmetric but at equal positive/negative magnitudes we see that the Airy pattern differs in size and power throughout each of the concentric rings. When we convolve this with an image to estimate the retinal image, we see that there is a change in the power spectrum of the associated images. On one side of focus the image retains higher contrast content at the low spatial frequencies while the image for the opposing sign retains contrast at the lower spatial frequencies, as seen in Figures 4.4a and 4.4b. It is this difference in the power spectrum in the images produced with spherical aberration that we wish to quantify and propose as a potential cue to the sign of defocus.

In order to assess the information which may be perceptually available to an observer we conducted a series of simulations which decompose the frequency components transferred to the retina through the optics of the eye. This is taking into account diffraction, monochromatic aberrations, and the contrast sensitivity of the eye. Our initial investigation measured the sum of the absolute difference of images in a sequence of aberrated images, but this method did not easily lend itself to imposing perceptual thresholds. As an alter-

(a) -0.5D of defocus and 0.4D of spherical aberration

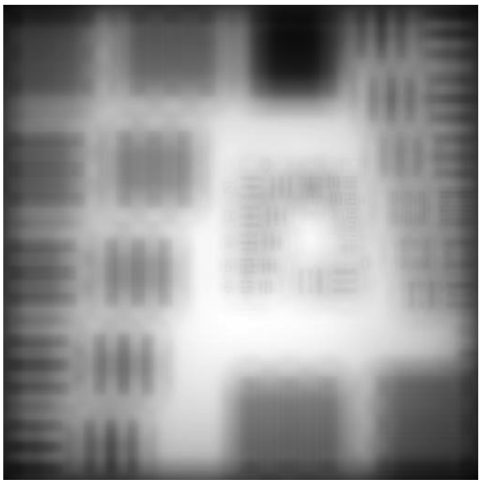

(b) 0.5D of defocus and 0.4D of spherical aberration

Figure. 4.4: These images show the effect of spherical aberration on the USAF-1951 test pattern. The left hand plot shows this stimulus image aberrated with 0.4D of spherical aberration and -0.5D of defocus. The right hand plot has the same spherical term (0.4D) but with 0.5D of defocus. These images are not identical, the difference in their power spectrum differs either side of focus. This is shown in the differences between the low spatial frequency bars located at the outer edge of the stimulus and the higher spatial frequencies closer to the centre.

native we opted to use contrast measures, and the MTF of our model to better describe the relationships between images on either side of focus. We hope that this will show that monochromatic aberrations can, in principle, be used to drive the direction of the accommodation response. This includes a novel proposition regarding the role of spherical aberration as a cue to the sign of defocus (the difference in the power spectrum of retinal images formed either side of focus).

4.2. Methods

The simulations conducted aim to show the difference in contrast between images formed at different points in dioptric space. This is to give an indication of whether such differences could provide a cue to the sign of defocus, enabling accommodative responses in the correct direction. It is unknown whether this response is ballistic (i.e. the magnitude of change in

focus is known before the movement is initiated, or whether the correct position is estimated from information during the accommodative process).

4.2.1. Methods - Contrast in sinusoidal gratings

Figure 4.5 shows each of the stimuli which were used throughout the experiment. A sinusoidal grating was generated at 5 cycles/degree. This was then used as the primary stimulus in the experiment, although other stimuli were used for illustrating the effect of aberrations on different aspects of a complex image, these included rotating the primary stimulus by 90°, and doubling the spatial frequency. We used spatial frequencies of 5 and 10 cycles per degree as they have a fairly large degree of separation but also fall on either side of, yet close to, the peak (8cpd) of the analytical contrast sensitivity function described by Mannos and Sakrison (1974) which is defined in 4.3.

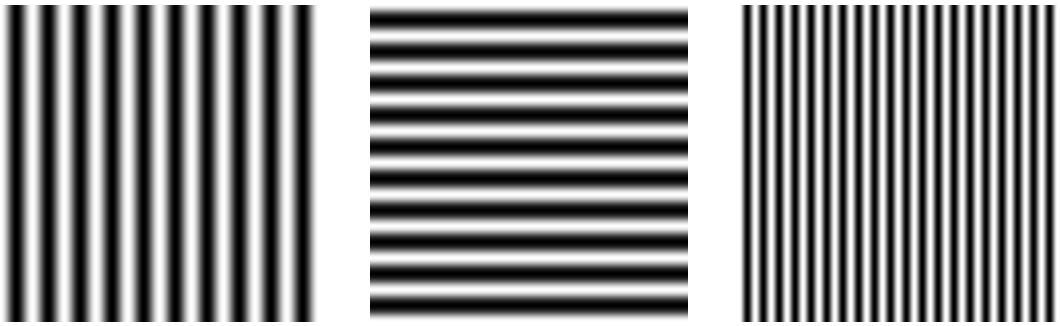

(a) Vertical sinusoidal grating at 5 cycles/degree.

(b) Horizontal sinusoidal grating at 5 cycles/degree

(c) Vertical sinusoidal grating at 10 cycles/degree

Figure. 4.5: These three images show the stimulus that was used throughout the simulations in which contrast was the relevant metric. These were used as Michelson contrast can be easily calculated, and the spatial frequency content is consistent. These images are 2° by 2°, and 1° section was cropped from the centre following convolution with the PSF. The baseline stimulus was a sinusoidal grating with a spatial frequency of 5cpd (a), and we rotated this stimulus 90° (b) for the astigmatism analysis. We used a grating at 10cpd (c) for the spherical aberration analysis.

Zernike polynomials were used to characterise the wavefront error for different monochromatic aberrations. Each mode was studied individually focusing on even-order terms (e.g. astigmatism and spherical) which were known to produce odd-error cues (i.e. a change in

characteristics of the blur pattern/point spread function depending on the sign of defocus). A series of point spread functions (PSFs) were generated by taking the Fourier transform of the wavefront combined with the pupil function. In this simulation, the pupil was fixed at 3mm, and 0.4D of a defined even-order aberration was applied to the wavefront, in addition to a magnitude of defocus. The simulated light illuminating the stimulus was fixed at 550nm. The PSF was then convolved with the stimulus image to simulate the formation of the image on the retina. Initially the aberrated image was calculated at 2°, and then a section was cut from the centre of the image. This removed any convolution artefacts around the edge of the image, which arose due to an applied border prior to convolution.

The sinusoidal grating will also only contain contours of a defined orientation; in the case of these simulations, vertical or horizontal. This distinction is not a necessary consideration with aberrations which are orthogonal such as defocus and spherical aberration, but the effect of orientation when applying aberrations such as astigmatism is distinct. We used gratings of either orientation when measuring the effect of astigmatism, but only a vertical sinusoidal grating when measuring the effects of spherical aberration.

In order to correctly identify the contrast in the aberrated sinusoidal gratings we used Michelson contrast (Michelson, 1927), defined as,

$$C = \frac{I_{max} - I_{min}}{I_{max} + I_{min}} \tag{4.1}$$

where C is the contrast of the image, I_{max} is the maximum intensity in the image, and I_{min} is the minimum intensity in the image. This metric is limited in the requirement that the image contain light and dark areas of similar area, such as those found in a sinusoidal grating. This requirement led to the specification of a sinusoidal grating as the stimulus image and enabled the correct identification of contrast when analysing images formed on the retina. It is also known, however, that sinusoidal gratings can limit the effect and characteristics of aberrations; at certain magnitudes the grating will change phase rather than contrast, an effect that must be taken into account when analysing the results.

We then aberrated the image with a range of defocus values, -1D to +1D in 201 steps, while applying a magnitude of either spherical aberration or astigmatism. We also analysed defocus in isolation to highlight the effect of an aberration which does not convey sign information (this could have included coma for example). The contrast for each image was then calculated using Equation 4.1. The difference in contrast between every image in the range of 201 defocus points was then calculated to create an array of contrast differences values of shape 201x201. Difference was calculated by,

$$D = \left| R_c^1 - R_c^2 \right| \tag{4.2}$$

where D is the difference in contrast between the two images, R_c^1 is the contrast of the first simulated retinal image, and R_c^2 is the contrast of the second simulated retinal image.

This method was intended to provide insight into the positions within the series which might produce a perceptually distinct blur error. Each of these values (the difference in contrast between two images) was then plotted to produce a heat map of values where a diagonal represented null values, where each image was compared against itself. This figure would indicate positions within the dioptric range where the difference in contrast was so low that it could be considered perceptually indistinct to an observer.

4.2.2. Methods - MTF Analysis

Following our analysis of contrast in images which contained specific spatial frequencies, we broadened the analysis to assess the affect over a range of spatial frequencies. We achieved this by comparing the MTF of the optical system at different points in dioptric space as a function of spatial frequency. Initially we compared each positive value in our dioptric range (-2D to 2D in 201 steps) to a negative value of equal magnitude (i.e. -2D vs 2D, -0.5D vs 0.5D). In this manner we can identify each position in the array where the MTF is very similar and this should provide insight into the differences in contrast at different focal positions over a range of spatial frequencies. We limited the range of spatial frequencies

from 0cpd to 60cpd as the estimate of the upper limit of the resolution of the human visual system is approximately 50cpd (Russ, 2006).

We then wanted to identify any positions within the range which might provide the observer with an incorrect depth cue (IDC) confounding the identification of the correct depth (i.e. where the difference in contrast is low due to aberration effects, but at a position which does not equal that of the stimulus). Our previous comparison of the MTF at equal magnitudes would identify if the transfer of contrast to the retina was the same at relative positive and negative positions but it might be the case that -0.5D is not the same as 0.5D, but instead is similar to the MTF at -1.1D. This is the case when we look at horizontal slices through the MTF in a system with astigmatism (figure 4.10c).

In order to further understand the image perceived by an observer we also need to take into account other aspects of the visual system. The eye is particularly sensitive to specific spatial frequencies as demonstrated by the contrast sensitivity function as described in previous literature (Campbell & Robson, 1968; Mannos & Sakrison, 1974).

4.2.3. Methods - MTF and CSF

We then wanted to know more about how an observer would perceive a scene based on the spatial frequency information that was available. In order to achieve this we need to know how the optics of the eye affected contrast in the retinal image, as well as the sensitivity of the eye to the spatial frequencies that were available at the retina. We used the Fourier based model of the eye, described previously, to derive the MTF of the visual system. We then multiply this by the contrast sensitivity function of the retina (known as the neural contrast sensitivity function). Mannos and Sakrison (1974) defined an analytical model for the contrast sensitivity function (CSF) as,

$$CSF(f) = 2.6[0.0192 + 0.114f]exp[-(0.114f)^{1.1}] \tag{4.3}$$

where f is the spatial frequency in cycles per degree. This model was based on observations by participants who made subjective assessments of images which contained different spatial frequency information. The authors used a fixed luminance which produced a pupil size of approximately 3mm. This pupil size is close to diffraction limited so Young *et al.* (2013) divided the CSF described in 4.3 by the MTF of a diffraction limited system with a 3mm pupil. We have followed the same method to estimate the neural contrast sensitivity function (NCSF). Once the NCSF has been calculated we can multiply it by the MTF for our simulated aberrated system to produce an estimated CSF for an eye with spherical aberration. This 'aberrated CSF' has been referred to as the clinical contrast sensitivity function (Dai, 2008), as it indicates how an observer would subjectively describe a scene taking all aspects of their visual function into account.

4.3. Results

This section details the results from three simulations. The first assesses the difference in contrast of defocused images with different aberrations, the second compares the differences in the MTF for our simulated visual system, and the third combines the modulation transfer function and contrast sensitivity function to estimate the perceptual availability of information as a consequence of these aspects of the visual system.

4.3.1. Contrast Data

In the first instance we analysed defocus as a standalone aberration term. As described in section 4.2, we simulated a visual system with applied aberrations, we then measured the contrast of the retinal image. This was conducted for a series of values in dioptric space, and compared each retinal image to every other in that dioptric range. The result of this analysis is shown in Figure 4.6.

The figures in this section show the difference in contrast between retinal images at different distances. The ordinate and the abscissa show the values in the dioptric range. The intersecting value, shown by a colour value in the heatmap, indicates the absolute

difference in contrast between these two retinal images. The diagonal from the lower left to the upper right represents all values compared with themselves (i.e. -0.75D vs. -0.75D)

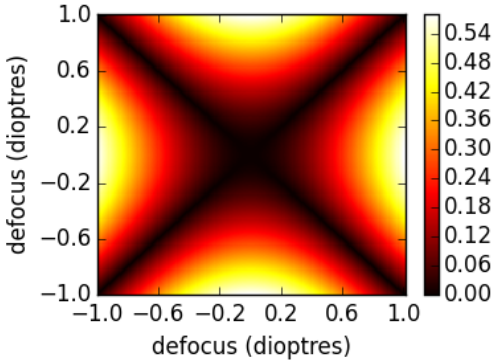

Figure. 4.6: The diagonal from the lower right to the upper left indicates that this aberration is symmetric in contrast either side of focus (i.e. -0.75D is identical to 0.75D). This is the expected result when looking at defocus.

The ordinate and the abscissa show the dioptric values between -1D and 1D. The intersecting coordinate in the figure shows the difference in contrast between the two relevant values. The black diagonal extending from the lower left to the upper right represents values of zero, where the same image is being compared against itself. There is also a black diagonal from the upper left to the lower right. This shows that there is also no difference between values of equal magnitude regardless of the sign of the dioptric value (i.e. -1D is the same in contrast as 1D, and -0.75D is the same as 0.75D). This indicates that defocus is a symmetric term which cannot be used to determine the sign of defocus as no information exists to differentiate the positive from the negative values. The same trend would also exist if we were to alter the spatial frequency of the stimulus image.

If we perform the same analysis and include an astigmatism term of 0.5D, we find that the cross shape that was evident in the case of spherical is now shifted off centre as seen in Figure 4.7a. At this point it is prudent to note that we are using a vertically oriented sinusoidal grating, and that astigmatism exhibits a change in the orientation of the elongation in the PSF on either side of focus. The PSF, for example, may be extended in the vertical

axis through the positive values and horizontally in the negative values. This change from a vertical to horizontal elongation in the PSF results in a retention of contrast in either vertical or horizontal contours within the retinal image.

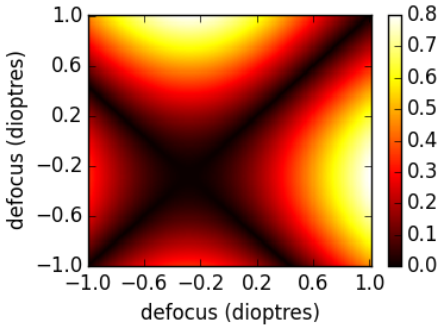

(a) Vertical sinusoidal grating

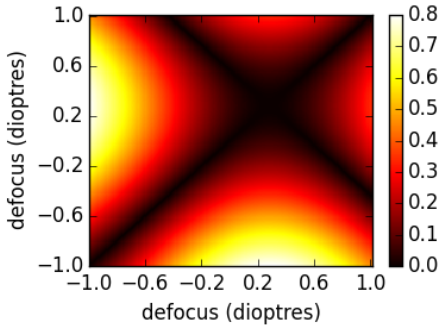

(b) Horizontal sinusoidal grating

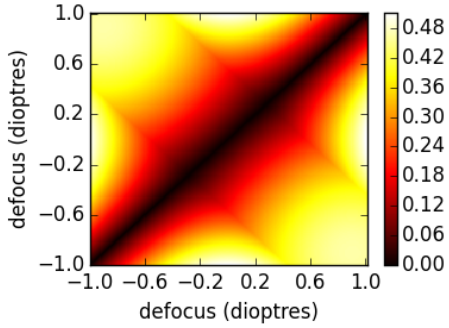

(c) The mean values between a and b

Figure. 4.7: These figures show the difference in contrast between a series of retinal images when the stimulus contains vertical contours or horizontal contours. It is this difference in the contrast of either vertical or horizontal components which may play a role in the determination of sign information. (c) shows the mean values between (a) and (b).

If we then repeat this analysis with a sinusoidal grating which is horizontal (i.e. perpendicular to the previous stimulus), we find that the cross is now offset in the other direction as seen in Figure 4.7b. In order to assess the total effect of an image which contained vertical and horizontal components, we took the mean of the two plots to determine any positions within the dioptric range where the difference in contrast would be sufficiently low to be perceptually indistinguishable. Figure 4.7c suggests that such a position does not exist.

It is the effect of astigmatism on the contrast of perpendicular contours either side of best focus which may provide an observer with a cue to the direction of accommodation. This effect on perpendicular contours does not occur in the case of spherical aberration. The PSF from an optical system with spherical aberration is rotationally symmetric. This means that the effect of convolving the PSF with the stimulus image will be the safe regardless of the orientation of the sinusoidal grating (only results using a vertical sinusoidal grating are included). Figure 4.8a shows the effect of spherical aberration on the plot above. This plot would appear identical when we rotate the sinusoidal grating, this means that no sign information is available from the orientation of contours in the image, unlike the example of astigmatism shown in figures 4.7a and 4.7b.

As the PSF of spherical aberration is rotationally symmetric, we cannot change the orientation of contours to provide a necessary change in the differences in contrast. Although, as shown in figure 4.4, the spatial frequency content of images either side of focus may differ. If we then perform this analysis on a sinusoidal grating which has a spatial frequency of 8cpd (from 4cpd), then we see that the lowest region of difference is offset relative to the previous figure. This is shown in Figure 4.8b. This suggests that there may be differences in the spatial frequency content of images either side of focus.

When we combine these two figures, as described in the astigmatism example, we see in figure 4.8c that there are no additional positions in dioptric space where contrast is as low as the positions on the diagonal from lower left to upper right (this diagonal represents the images which are compared with themselves). These examples have included only two spatial frequencies but to see what the effect is over a larger range of values we can look at the MTF of our simulated ocular system. The analysis of the full MTF will provide insight into the perceptual availability of sign information in the retinal image when spherical aberration is present.

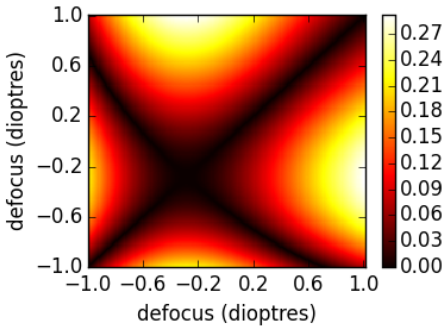

(a) Stimulus containing 4cpd

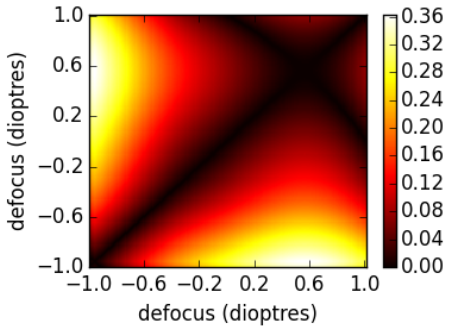

(b) Stimulus containing 8cpd

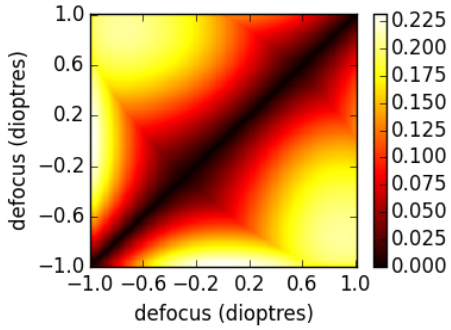

(c) The mean values between a and b

Figure. 4.8: These figures show the difference in contrast between a series of retinal images when the stimulus is either a sinusoidal grating of 4cpd, or 8cpd. Spherical aberration appears to produce a different response on either side of focus as a function of the spatial frequency content of the stimulus. When we take the mean of these two figures (a and b), we see that there are no positions within this range which have a particularly low difference in contrast.

4.3.2. MTF Data

In this analysis we compared the absolute difference between the MTFs for optical models containing different defocus values. We generated the MTF of the visual system for a series of defocus values with spherical aberration applied. The first analysis in this series compared each MTF in the negative range with each MTF of equal magnitude from the positive range of defocus values such that -0.5D would be compared against 0.5D, and -0.25D would be compared against 0.25D. If we perform this analysis for aberrations which are odd-order,

such as defocus and coma, we find that all values in the figure are zero (i.e. all of the positive and negative values are identical suggesting that sign information does not exist) as illustrated in figure 4.9a.

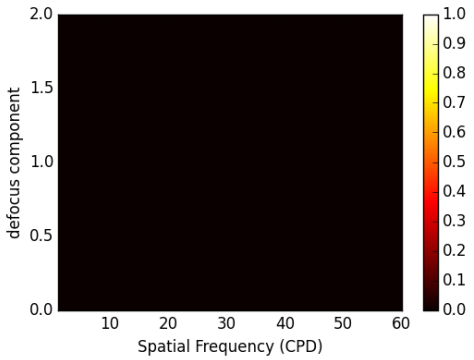

(a) Defocus

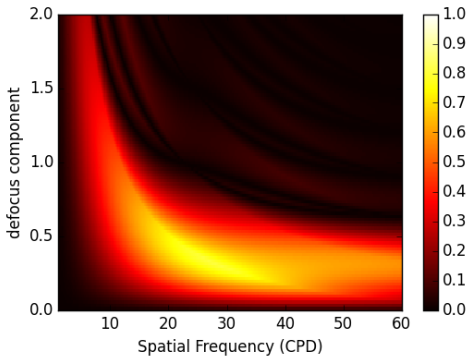

(b) Astigmatism

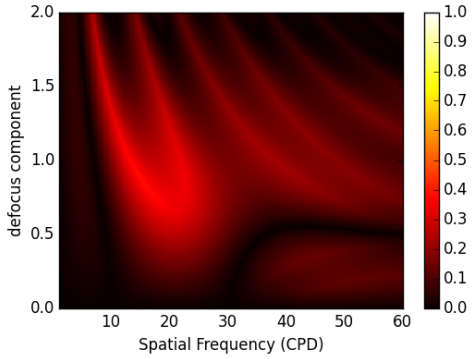

(c) Spherical

Figure. 4.9: The figures show the difference in the MTF at equal magnitudes either side of focus. The ordinate indicates the magnitude of defocus that is being compared. The abscissa shows the spatial frequency of the MTF. The height of the heatmap indicates the difference in the MTF (where 1 is 100% different, and 0 is identical). (a) shows the results of this analysis when only defocus is present in the optical model. We see that the figure is uniformly identical suggesting there there is no difference between positive and negative defocus values at equal magnitude. (b) shows the results when we apply 0.4D of astigmatism. This shows that for defocus values between 0.2D and 0.6D there is a high degree of difference between the MTFs. This trend persists at higher defocus values but only for lower spatial frequencies due to the low pass nature of the optical system. (c) shows the results for a model with 0.4D of spherical aberration. There is a smaller difference between the MTFs but it persists across a broader range of spatial frequencies and defocus values.

Although if we perform this analysis on even-order aberration terms, such as astigmatism or spherical aberration, we can identify positions in the range of defocus values where there is little difference in the transfer of contrast through the optical system. Figure 4.9b shows the difference in the MTF at equal magnitudes either side of focus. The ordinate shows the magnitude of the positive and negative values being compared. The abscissa shows spatial frequency and the heatmap indicates the absolute difference in the MTFs either side of focus. We can see that for each value that is compared either side of focus, the magnitude of difference is fairly high. This suggests that, for horizontal contours, the differences in contrast in the retinal image either side of focus are considerable. We need to repeat this analysis for vertical contours to ensure that no sign information exists in this component. If we now perform the same analysis with spherical aberration as the fixed Zernike term we see that there are a range of spatial frequencies which retain comparable contrast throughout a range of defocus values. This is shown by the dark column in 4.9c that extends through the whole dioptric range at about 14-15cpd. The difference in all other spatial frequencies should convey sufficient information to act as a potential cue to the sign of defocus. The magnitude of difference is not massive but may be sufficient to present a perceptual difference in the contrast of different spatial frequencies in the retinal image. The perception of contrast is also subject to Weber's Law, whereby the perception of change in a stimulus decreases as the magnitude of stimulus increases. In this case, the observer would be more aware of changes in contrast when the global contrast of either image is low. This means that the black areas on the heatmap may not provide a clear indication of perceptual availability, and further work on this figure may include values which are the ratio of global contrast. The perceptual availability of these cues is further discussed in section 4.3.3.

The following analysis is designed to show locations within the dioptric range which would yield an incorrect depth cue. This may include defocus positions that are not of equal magnitude but due to the aberration characteristics exhibit similarities in image formation. This analysis requires a point to be selected as a reference, we have used 0.25D. We generate the MTF for this ocular model, including 0.4D of an even-order term, and 0.25D of defocus.

This is then compared against the MTF for all other positions in the dioptric range. Figure 4.10a shows the effect of this analysis when we only apply defocus.

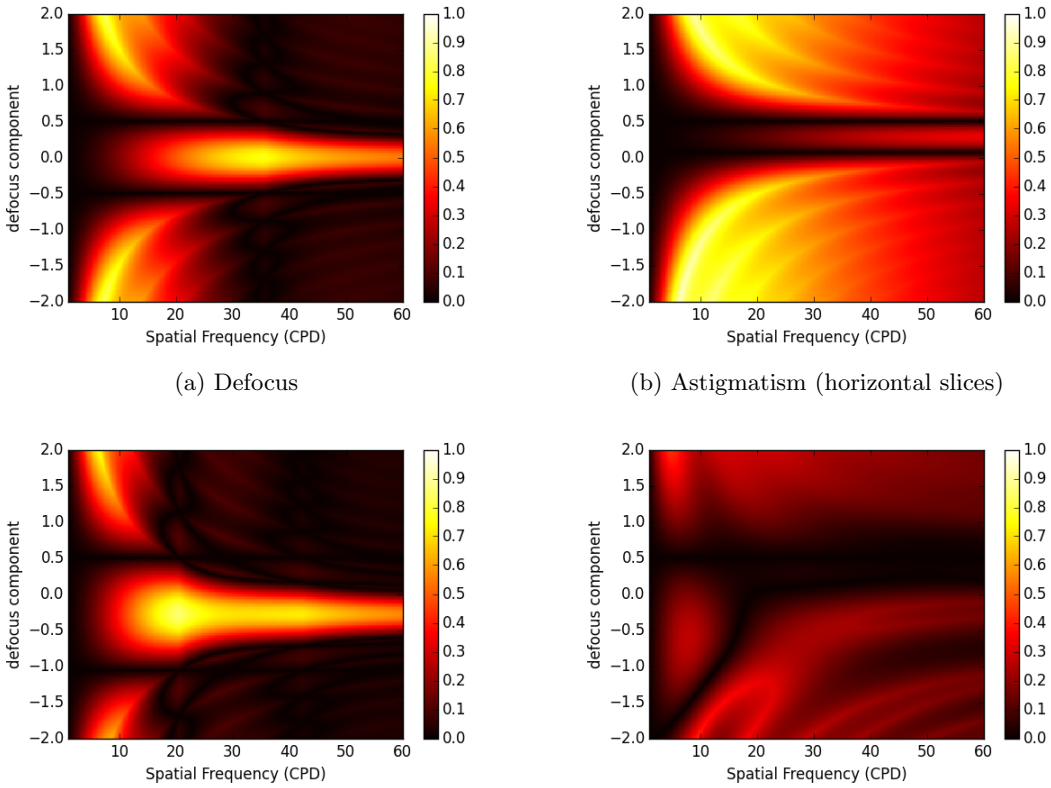

(a) Defocus

(b) Astigmatism (horizontal slices)

(c) Astigmatism (vertical slices)

(d) Spherical

Figure. 4.10: These figures show the differences between a reference MTF (0.5D defocus) and all other MTFs in the range selected (-2D to 2D defocus). (a) shows the effect when we compare the reference MTF to all other MTFs when defocus is the only aberration in the system. We see that our reference point is identical to itself and the MTF at -0.5D. In (b) we have applied 0.4D of astigmatism and taken slices horizontally through the MTF. We see that 0.5D is identical to itself and a position at 0.1D. In (c) we take vertical slices through our astigmatic MTF and we find that there is another position at -1.1D which is identical to our reference MTF. (c) gives the results when we apply 0.4D of spherical aberration. We see that there are no identical positions throughout the range of all sptail frequencies, although some spatial frequencies are similar through a range of defocus values.

The dark slice at 0.5D represents the series of values compared against themselves (as our reference point is 0.5D), but we also see that there is another dark slice at -0.5D. This occurs because there is no difference in the MTF at 0.5D and -0.5D. The presence of such

a feature suggests that defocus is not a valid cue to the sign of defocus as the visual system may identify 0.5D or -0.5D as the same point and as such could not correctly identify the direction of accommodation based on this information.

These results show that, in the case of astigmatism and spherical, contrast is transferred through the optical system in such a way that differences are retained either side of focus which may provide a cue to the sign of defocus. In order to further understand what an observer might experience, and if these cues are perceptually available, we can consider the contrast sensitivity function of the eye. This function describes the degree to which a human, at a neural level, is sensitive to different levels of contrast in a retinal image.

4.3.3. MTF and CSF Data

In order to assess what effect these changes have to the observer, and if the changes in spatial frequency content are sufficiently large to be considered a perceptually available cue to the sign of defocus, we combined the MTF of the simulated visual system with the typical contrast sensitivity function of the eye. This produces an estimate of the 'clinical contrast sensitivity function', which is the contrast sensitivity function of a subject tested subjectively under clinical conditions. Our estimate of this function, for an ocular system with 0.4D of spherical aberration is shown in Figure 4.11 (this plot was reproduced following personal communication; Love, 2015).

Figure 4.11 shows spatial frequency (CPD) on the abscissa, and contrast sensitivity on the ordinate. We have plotted 21 curves; 10 curves from -0.5D to -0.05D, 0D, and then 10 curves from 0.05D to 0.5D. The blues curves represent all of the negative values (the first blue curve to intersect the x-axis represents -0.5D), the green curve (obscured by others) represents 0D, and the red curves represent all of the positive values (where the first curve to intersect the x-axis represents 0.5D). We have also plotted the diffraction limited contrast sensitivity function as a black curve, all of the other curves also have an added 0.4D of spherical aberration.

This effect can be compared with aberrations terms which are not different either side

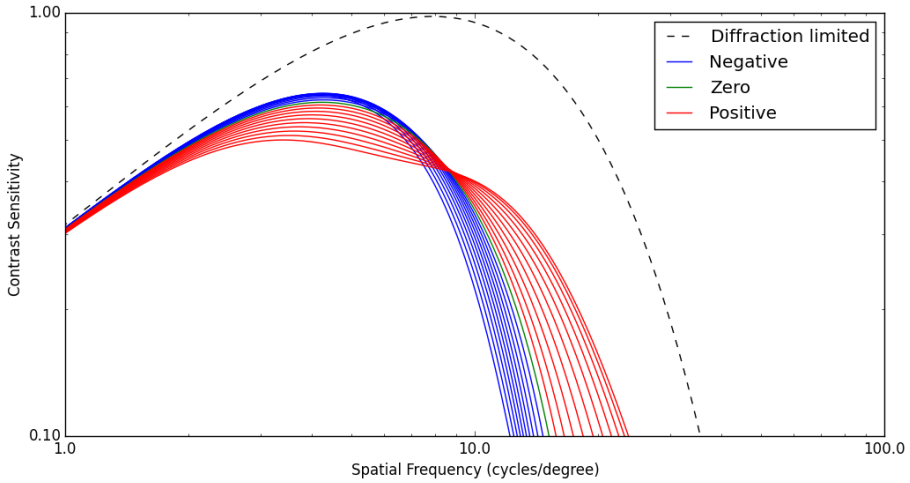

Figure. 4.11: This figure shows the effect of spherical aberration on the clinical CSF. The abscissa shows spatial frequency, and the ordinate shows contrast sensitivity. The black dotted curve represents the analytical contrast sensitivity function as defined in eq. 4.3 (Mannos & Sakrison, 1974). We apply 0.4D of spherical aberration to the simulated wavefront, and then add a defocus term in a series of steps from -0.5D to 0.5D. We calculated the MTF for each of these defocus positions, and multiply it by the CSF to find the clinical CSF at each position. The series of blue curves represents the clinical CSF at all of the negative values in the series, the green curve at best focus (with 0.4D of spherical aberration), and the red curves represent the positive values. The relative position of the red and blue curves at high and low spatial frequencies is the artefact of interest.

of focus. Figure 4.12 illustrates this point by showing a series of curves plotted with the same method as described in 4.11 but the only aberration term in this simulated wavefront is defocus.

In this figure each of the curves for the positive and negative values at either side of focus are overlapping as they are identical. This would suggest that there are no differences in the perception of images on either side of focus based on the MTF and CSF in our simplified model of a typical visual system.

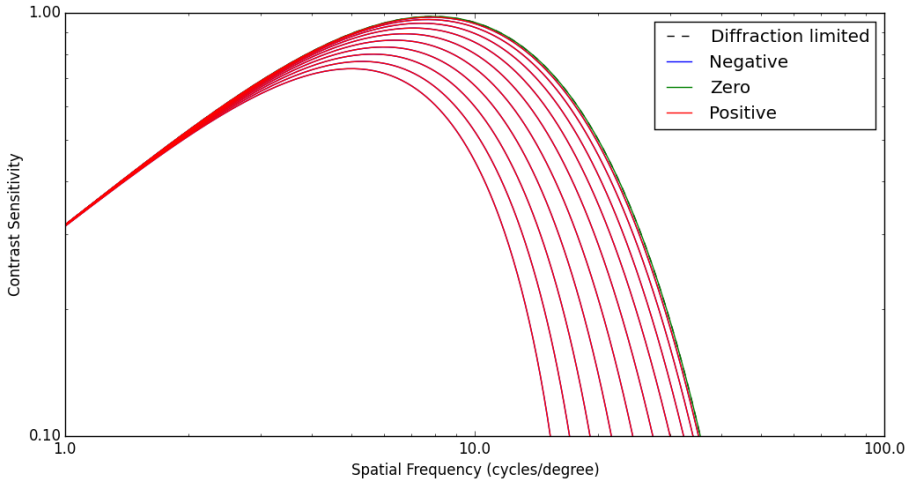

Figure. 4.12: This figure illustrates the effect of plotting the same data as above but when we have only applied defocus to the wavefront (i.e. no aberrations are present). This curve would be of similar appearance for all even-order functions, those that do not convey sign information. The critical point here is that the blue and red curves overlap, there is no difference in the perceived contrast on either side of focus.

4.4. Discussion

The results show that individual even-order Zernike aberrations can produce differences in contrast in images formed either side of focus which may be of sufficient magnitude to provide a potential cue to the sign of defocus. We have shown, through a series of different approaches, that the information available in images either side of focus differs depending on the presence of different monochromatic aberrations.

4.4.1. Discussion - Defocus

In section 4.3.1, we showed that there is no difference in images which are formed at either side of focus at equal magnitudes. Figure 4.6 shows that the Michelson contrast is identical for images formed at positions of equal magnitude either side of focus. This suggests that you could not differentiate sinusoidal gratings at 5cpd at equal magnitudes either side of focus. We extend this investigation to include other spatial frequencies in 4.3.2 where we

measure the MTF for our optical model. Initially we compare positions at equal magnitudes on either side of focus and this confirms that there are no positions where the MTF is noticeably different. We then take a single reference point (0.5D defocus), and compare this to all other points in the sequence. We find that 0.5D is identical to -0.5D which suggests that the oberver would not be able to differentiate these points, but we also find that when we extend too far the differences become negligible, this is likely to be due to the degree of contrast loss in the retinal image. In our final assessment of defocus (section 4.3.3) we combine the MTF with the CSF and find that all positive and negative positions overlap and as such, the observer of our model would not be able to distinguish positive from negative defocus. These results are expected, and provide a basis from which we can identify effects in the even-order aberrations discussed next.

4.4.2. Discussion - Astigmatism

The difference either side of focus is apparent in the instance of astigmatism where vertical and horizontal contours exhibit reduced contrast depending on the sign of the defocus term. In theory this will allow an observer to identify the position of an object relative to optimal focus depending on the axis of sharp contrast in the retinal image relative to the sign of defocus and the axis of astigmatism specific to the observer. In figure 4.7 we see that there is a difference in the contrast of images when multiple contour orientations are considered. Figure 4.7a shows that there is an IDC in the range, slightly offset with respect to the defocus case (4.6). If we assess the affect when the stimulus image contains horizontal contours (figure 4.7b), we find that the range of IDC values are offset in the other direction. When we take the mean of these two plots we find that there are no images within the range which have a similar contrast when we consider 5cpd and 10cpd in isolation.

The MTF of our optical model was then assessed to take account of the full spatial frequency range. We found that there were large differences in the MTF at low defocus values and at low spatial frequencies (over a larger range of defocus values) as shown in figure 4.9b. When we searched for IDC within the dioptric range, using 0.5D as our reference

point (while astigmatism remained fixed at 0.4D), we found that 0.1D was similar when we looked at horizontal slices through the MTF and another at -1.1D but when taking vertical slices through the MTF. As these IDC would be accounted for in the image through the presence of vertical or horizontal contours, the visual system should be able to differentiate (assuming that the stimulus contains sufficient orthogonal content).

We did not perform the final analysis which combined the MTF with the CSF, as our primary concern relates to the significance of spherical aberration as a cue to the sign of defocus, and the effect of astigmatism is well documented and highlighted through the previous analyses.

4.4.3. Discussion - Spherical Aberration

The potential cue to the sign of defocus is less clear in the case of spherical aberration. A change in vertical and horizontal contours does not occur because this aberration term is rotationally symmetric. The effect on the horizontal axis will be the same as that of the vertical axis. Although this effect on perpendicular contours does not occur, the PSF is still different on either side of focus. The data shown in 4.11 suggests that another mechanism may be perceptually available, sign information may be available through differences in the power spectrum in the retinal image at different points on either side of focus. This effect is not available in other aberrations terms such as those which are odd-order terms, or astigmatism which does contain sign information through a different mechanism (the effect on contrast of orthogonal contours).

Figure 4.8 shows our analysis of contrast using different sinusoidal gratings as our stimulus when spherical aberration is applied. We see in plot 4.8a and plot 4.8b that we need to change the spatial frequency content of the stimulus, rather than the angle of the contours as demonstrated in the astigmatism case (figure 4.7), to produce a change comparable to that seen in the astigmatism case. This suggests that there is information present in images either side of focus, but where this mechanism was dependant on the orientation of contours in the stimulus image, we now find that it is the spatial frequency content which

is the relevant source of information for determining the sign of defocus. This is extended to a greater range of spatial frequencies in figure 4.9 and figure 4.10. In plot 4.9c we see that there is a persistent difference in the MTF at equal magnitudes on either wide of focus (with the exception of certain ranges of spatial frequencies at specific defocus values). This suggests that information may be contained within the retinal image which an individual may be able to detect. Plot 4.10d attempted to identify any positions which may create an IDC (i.e. a position where the observer could not differentiate information). Using 0.5D as our reference point and scanning through the dioptric range we find that there are no points which are equivalent, with the exception of a range of values that are similar extending from 0.5D through to -2D with decreasing spatial frequency.

In order to further understand the information available to an observer we combined the MTF with the CSF to produce figure 4.11. Here we see the negative dioptric range (-0.5D to -0.05D) plotted in blue, 0D plotted in green, and the positive values (0.05D to 0.5D) plotted in red. The curves do not overlap as seen in the defocus example (figure 4.12). The negative values have increased sensitivity at low spatial frequencies and this attenuates as spatial frequency increases. The observer is less sensitive to positive values at low spatial frequencies but remains higher at greater spatial frequencies. This suggests that the information available to an observer may be contained in the power spectrum of retinal images, and differences in these images (such as those shown in figure 4.4) may provide a cue to the sign of defocus. This would require further psychophysical investigation.

4.5. Conclusions

The simulations conducted in this experiment suggest that individual monochromatic aberrations maybe provide information in the formation of retinal images either side of focus to allow an observer to discriminate between the images formed, and subsequently determine the sign of defocus. This cue may not exist in all members of a population as the magnitude and shape of aberrations will be unique to each individual. These results give an indication that, in principle, high-order aberrations defined by specific even-order Zernike terms could

a sufficient signal to assist in a correct accommodative response. These analyses may assist in explaining the instances in which observers could still focus in the correct direction when other cues such as chromatic aberration were removed such as in the study by Chen *et al.* (2006), or instances where these aberrations affected the direction or magnitude of accommodation changes such as in the study by Chin *et al.* (2009). We have proposed a novel mechanism which, in principle, allows an observer to identify the sign of defocus from images either side of focus when spherical aberration is present. This is a mechanism which has not been previously investigated to the authors knowledge. It is unclear what content may be required in a stimulus for an observer to use the aberration characteristics as a cue to positive or negative changes in focal position. The spatial frequency content of natural images tends to vary, as well as the contrast of contours due to other effects such as structure, shape, occlusion, shadowing, foreshortening, etc. It is currently unknown if spherical aberration does indeed play a role in the disambiguation of sign information, and if it is a necessary mechanism given the possible presence of chromatic aberration or astigmatism.

Chapter 5

An investigation into elongated pupils and multifocal lenses

The preceding chapters are related to depth perception in humans. This chapter will consider the effects of different ocular physiologies throughout different species. In particular, the optical benefits of vertically, or horizontally, elongated pupils and multifocal lenses. The first section of this chapter covers the area of the project that was completed collaboratively with colleagues at U.C. Berkeley, as well as Durham University. The latter part details the results of simulations of vertically elongated pupils and multifocal lenses.

The physiology of the eye varies considerably between different species. The eye can be positioned at different locations on the head, they may be of different colours or shapes, the light collecting properties and neural processing can also differ. This project was primarily concerned with the shape of the pupils in land-dwelling vertebrates. We propose optical benefits and the selective pressures which might have led to their evolution. The pupil may be circular, vertically elongated, horizontally elongated or a range of other shapes (e.g. pinhole, keyhole and W-shaped). The primary hypothesis for elongated pupils has been to increase the control of retinal illumination. Hammond and Mouat (1985) show that feline

species can change the area of their pupil, and subsequent throughput, by 135-fold as seen in Fig. 5.1. Roth and Kelber (2004) showed that this figure was 300-fold in the eyes of Gecko species. In comparison the control of pupillary area in humans is 15-fold (De Groot & Gebhard, 1952). These figures suggest that a elongated pupil gives significantly greater control of retinal illumination, which maybe prove beneficial to species who may encounter extreme variations in ambient light; "a moonlit night can be 100 million times darker than a day with bright sunshine" - Kelber and Roth (2006).

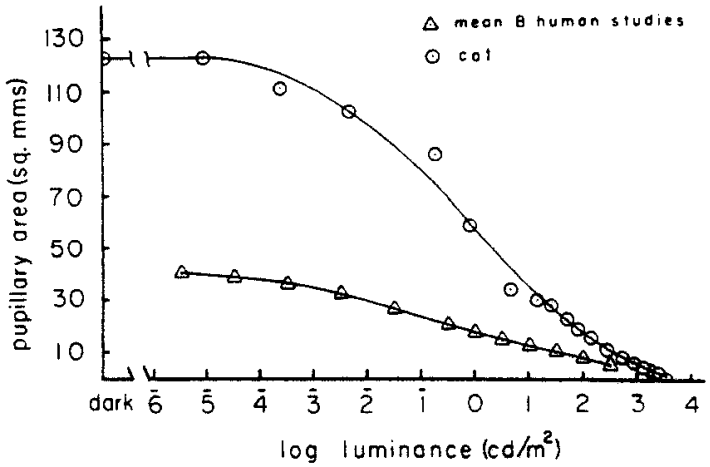

Figure. 5.1: Feline and human pupil area changes with luminance - Wilcox and Barlow (1975)

Previous studies suggest that there tends to be a propensity towards vertically elongated pupils in small predatory animals that have forward facing eyes (Malmström & Kröger, 2006). Animals which exhibit strong orbit convergence often have a larger binocular overlap, this can benefit depth perception for hunting prey. In primates this advantage is described by the visual predation hypothesis, and arboreal locomotion (Cartmill, 2002). Changizi and Shimojo (2008) contest this, arguing that while many predatory animals have forward facing eyes, there are many herbivorous or omnivorous species that have forward facing eyes. They state that the distinction between these two evolutionary traits is the environment

and mass of the body, rather than the diet, of the species concerned. They state that a primary advantage of binocular vision is the ability to see through cluttered environments such as forests while lateral eyes are often found in species whose primary domain are open spaces. The analysis found that convergence increases in predatory animals as a function of body mass, but also in non-predatory animals as a function of body mass and environment. (Changizi & Shimojo, 2008).

The eyes might be positioned on the head such that the optical axes of the eye are parallel (forward-facing), or they may be highly lateral, in some instances this angle of laterality is so great that the animals might have binocular field in both the forward and backwards directions (Johnson, 1901). In a later paper by Heesy (2005), orbit divergence was measured and used for the laterality data in our study. Orbit convergence was defined as the degree to which the optical cavities in the skulls of different animals diverge from its central axis (approximately the spinal column). Heesy (2004) states that frontal-eyed and lateral-eyed descriptions can not be derived from measurements of orbit convergence as some species have lateral orbits but forward facing eyes. This can be attributed to the position of the eyes in the orbit, the position of the post-orbital bar, or the vertical rotation of the orbit in the skull. The number of species for which these confounds present a problem is minimal and so this study assumed that orbit convergence was a sufficient approximation for forward- and lateral-eyed descriptions.

The daily activity of different species might also vary. There are species specifically adapted for activity during the day, others at night, some at dawn and dusk, while some exhibit sporadic activity throughout a 24 hour period. In some instances the behaviour of an animal might vary depending on the conditions of its environment (Sperry *et al.*, 2010), or environmental pressures, which are often anthropogenic (Prange *et al.*, 2004).

The work conducted for this project was distributed between Durham University and University of California, Berkeley. The entirety of the project is summarised in section 5.1 where each task is described and contributors detailed. The feline eye model was developed as part of this project then further extended for inclusion in this thesis. This work is detailed

in Section 5.1.7.

5.1. Collaborative Work

The eyes of different species in different environments exhibit different characteristics. We focused on land-dwelling vertebrates and attempted to characterise taxonomical information for each species (n = 224), we then extrapolate relationships which might predict pupil shape (Bill Sprague, Jared Parnell). We also looked at the functional advantages of vertically elongated pupils and horizontally elongated pupils as they may perform against circular pupils in a range of tests, including ray tracing models (Jürgen Schmoll, Durham University; Martin S. Banks & Bill Sprague, U.C. Berkeley - see section 5.1.5), and real-imaging with a modified camera (Gordon Love & Colin Dunlop, Durham University - see section 5.1.4). We also investigated the relationship between height and defocus as a predictor of pupil orientation (Bill Sprague & Martin S. Banks, U.C. Berkeley - see section 5.1.2), as well as the presence and extent of cyclovergence in lateral eyed species with horizontal pupils (Gordon Love & Jared Parnell, Durham University; Martin S. Banks, U.C. Berkeley; Jenny Read, Newcastle University - see section 5.1.6).

The different aspects of the project suggest that pupil shape can be predicted, with a high degree of certainty, from factors such as trophic strategy (foraging mode) and diel activity (primary period of activity in a daily cycle). This relationship between ecological niche and pupil shape suggests there must be a functional role in the evolution of different pupil shapes. As such, we propose a range of theories that may support the role of a given pupil shape for a specific species. These include factors such as shoulder height; predator detection; stereopsis; and, potentially, the f-ratio and consequent depth of focus of an animals eye (the list of all species included in the study is available in the appendix).

5.1.1. Taxonomy and Statistical Analysis

The statistical analysis was primarily conducted by Bill Sprague, and Prof. Martin S. Banks at U.C. Berkeley. Data collection was conducted by Bill Sprague, and Jared Parnell. The

hypothesis was that pupil shape could be predicted from information relating to the trophic strategy and daily activity cycles of a given species. The pupils shapes we designated as independent for this study were vertically elongated, horizontally elongated, vertical sub-circular and circular (the few horizontal sub-circular species we encountered were characterised as circular). Each of these pupil shapes are shown in Figure. 5.2.

(a) Vertical (b) Sub-circular (c) Circular (d) Horizontal

Figure. 5.2: Different pupil types (specific to our analyses). (a) vertically elongated pupil of a cats eye; (b) sub-circular pupil of a Eurasian lynx; (c) circular pupil of a human eye; (d) horizontally elongated pupil of a cows eye (Suren Manvelyan, 2014)

The predictors we used were diel activity and trophic strategy. Diel activity is the time of day in which the species was most active, which included nocturnal (primarily active at night), diurnal (primarily active during the day), and polyphasic (active at different times throughout the day, this included cathemeral and crepuscular). The second factor, trophic strategy, includes: active; where species pursue prey over a distance, ambush; where the species pounces on its prey after lying in wait or stalking over smaller distances, prey; where the species is passive, this is a broad characterisation which includes animals which graze or engage in herbivorous foraging.

The number of species in each category is listed in table 5.1. This table shows, for our analysis, the independent variables as rows (trophic strategy and daily activity), with the dependant variable comprising the columns (pupil shape: vertical, horizontal, circular, and sub-circular).

The values in table 5.1 were subjected to statistical analysis to assess their relationships. Initially relative risk (RR) was defined as a measure of the likelihood of different pupils shapes relative to a reference condition, in this instance horizontal pupils (Eq. 5.1). We

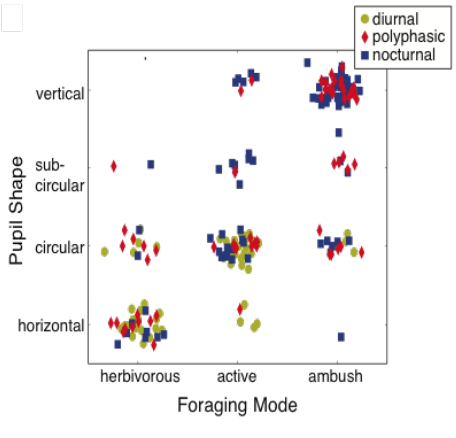

Pupil shape	Relative-risk ratio	Confidence interval	P
Circular			
activity	1.18	(0.61, 2.17)	0.602
foraging	17.65	(6.71, 46.38)	< 0.00001
Sub-circular			
activity	4.28	(1.68, 10.90)	0.002
foraging	31.06	(9.01, 107.12)	< 0.00001
Vertical slit			
activity	6.21	(2.40, 16.05)	< 0.00001
foraging	393.47	(96.93, 1597.19)	< 0.00001

Figure. 5.3: The left hand plot shows the division of each species by pupil shape and foraging mode, while the markers indicate diel activity type. The right hand table shows the statistical analysis on this dataset, where a relative-risk ratio greater than 1 indicates a likelihood that changes in the taxonomical category will predict the specified pupil over a horizontally elongated pupil. The significance values (P) represent the results of multinomial logistic regression between each taxonomical category and the pupil shape indicated compared with horizontal pupils.

selected this pupil shape as the weighting of the data points in figure 5.3 show the greatest difference between horizontal and vertical when moving from diurnal to nocturnal, and herbivorous prey to ambush predator. We defined relative risk as,

$$RR(PupilShape, a_i, f_j) = \frac{p(PupilShape|a_i, f_j)}{p(HorizPupil|a_i, f_j)} \tag{5.1}$$

where a_i is the i-th diel activity (1 = diurnal, 2 = polyphasic, 3 = nocturnal) and f_j is the j-th trophic strategy (1 = prey, 2 = active, 3 = ambush).

We then assessed the probability of predicting the pupil shape using multinomial logistic regression (analysis by Bill Sprague). This provided relative risk ratios which indicate the probability that that pupil type would change from horizontal pupil to the specified pupil type as each taxonomical category was incremented (Fig. 5.3). The overall effect of foraging mode and diel activity in predicting pupil shape was highly significant: $\chi^2 = 219.9$; $p < 1^{-15}$.

In some instances the specific taxonomy of a species was difficult to define due either

	Pupil Shape	*horizontal*	*circular*	*sub-circular*	*vertical*	*all*
Activity	**Foraging Mode**					
diurnal	*herbivorous*	18	5	0	0	23
	active	4	27	0	0	31
	ambush	0	4	0	0	4
polyphasic	*herbivorous*	10	6	1	0	17
	active	1	9	2	2	14
	ambush	0	6	5	22	33
nocturnal	*herbivorous*	8	2	1	0	11
	active	0	13	7	5	25
	ambush	1	6	3	46	56
all		42	78	19	75	214

Table 5.1: The number of species in each category

		Pupil Shape	*circular*	*sub-circular*	*vertical*
Constant	**Subset**	**Comparison**			
Activity	*diurnal*	*herbivorous to active*	24.3	4.50	4.50
		active to ambush	5926	40001	40001
	polyphasic	*herbivorous to active*	15	20	2.00E+05
		active to ambush	6667	25002	1.10E+05
	nocturnal	*herbivorous to active*	5.20E+05	5.60E+05	4.00E+09
		active to ambush	0	0	0
Foraging Mode	*herbivorous*	*diurnal to polyphasic*	2.16	18002	1.80
		polyphasic to nocturnal	0.417	1.25	1.25
	active	*diurnal to polyphasic*	1.33	79998	79998
		polyphasic to nocturnal	14446	35002	25002
	ambush	*diurnal to polyphasic*	1.50	50001	2.20E+05
		polyphasic to nocturnal	0	0	0

Table 5.2: The results of the risk ratio calculations with horizontal pupils as the reference condition. The cells coloured red indicate that the calculation was affected by the division of 0 (10^{-4}).

to limited data, or ambiguity in the activity as some animals exhibited combinations of behaviour or atypical behaviour in certain conditions. An example is the differences in diel

activity in a single species of snake living at different latitudes. This may be attributed to their cold-blooded nature and the relative temperatures in different geographical localities, these changes can also occur seasonally (Sperry *et al.*, 2010). In light of these facts, it is also worth noting that approximately 50% of the species included in this study were snakes, sourced primarily from Brischoux *et al.* (2010). We subsequently conducted the statistical tests on both the full data set, and a subset which excluded all snakes. This was to ensure that the initial relationships held when the selection bias was not weighted towards snake species. In this condition it was found that the overall effect was still highly significant: $\chi^2 = 102.5$; $p < 1^{-15}$.

5.1.2. Height vs. Defocus

We also looked at other factors such as the height and fixation distance as a means of predicting pupil shape, extending the theory proposed by Malmström and Kröger (2006) which suggests that vertically elongated pupils are found in species with small body mass while this propensity declines as body mass increases. The collaborators at U.C. Berkeley; Martin Banks and Bill Sprague, developed a series of figures which highlight the effects of height and relative fixation distances on defocus (Fig. 5.4).

These figures highlight the limited depth of focus for shorter animals. We propose that vertically elongated pupils occur with greater frequency in smaller animals as a means of retaining contrast in vertical contours for the purpose of improving stereopsis through disparity. While defocus error is still retained for horizontal contours such that depth information is retained. This effect may be further enhanced due to the effect of foreshortening on objects in the visual field. It should be noted that some species exhibit vertically elongated pupils but are lateral-eyed, such as some reptilia (crocodile, alligator, gecko etc). This may provide them with the ability to estimate depth from the blur gradient associated with horizontal contours while the increased DOF associated with vertical contours may assist with object recognition. Although this argument would also apply to horizontal pupils in the perpendicular orientation.

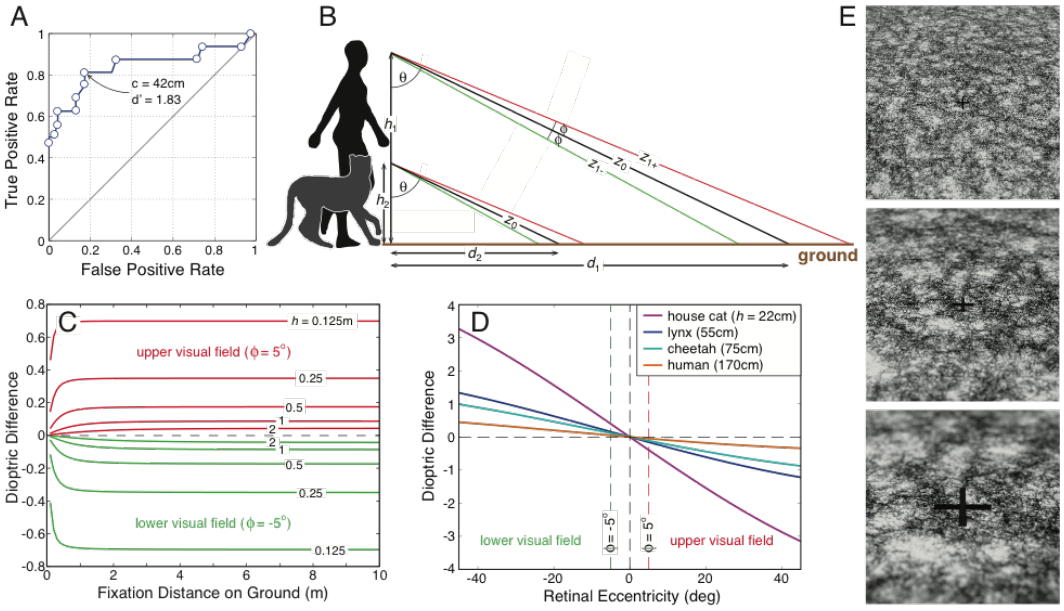

Figure. 5.4: A) gives the ROC curve when height is used to predict vertical pupil shape against other shapes from shoulder height. B) shows the relative distance along the ground (d_1, d_2) at which a Human (h_1) and a Cheetah (h_2) might attend assuming the same viewing angle (θ). Z_{1+} and Z_{1-} represent angles $\pm 5°$. This arrangement is assumed for curves shown in C) & D). C) shows the dioptric difference for a range of different heights where the green curves represent Z_{1-} and the red curves represent Z_{1+}. D) shows this discrepancy extended beyond the limits of $Z_{1\pm}$, as the viewing angle increases away from the point of focus, the distance of the retina extends away from the visual axis and the magnitude of defocus decreases as a function of height. E) shows three images generated with a virtual camera (4.5mm aperture, 30° FOV) at a fixation angle (θ) of 56° but different distances to target (top to bottom; $Z_0 = 0.6$, 0.2 and 0.1 metres).

5.1.3. Eye Laterality

Pupil shape also appears to have a correlation with eye laterality. It appears that animals with forward-facing eyes often have vertically elongated or round pupils, while lateral-eyed animals often have more horizontally elongated pupils. In our dataset we found that of the 42 herbivorous prey animals, 36 have horizontal pupils. Laterality data was only known for 27 of these species but we found that 26 of these 27 terrestrial animals categorised as prey have laterality angles greater than 87° (Banks *et al*, 2014).

It must be noted that with each of these trends, there are exceptions, and cases which

could be considered ambiguous due to the specific characterisation of the given animal. An exception might include crocodiles, which have lateral-eyes and vertically elongated pupils, or the Mongoose which has forward-facing eyes and horizontally elongated pupils. The position of the eyes on the head also occurs as a spectrum of values across many species, and so the division of lateral-eyed and frontal-eyed descriptions can tend towards ambiguous.

5.1.4. Optical Effects of Elongated Pupils

We also assessed the visual effects of elongated pupils of different orientations. Gordon Love (Durham University) took a series of images with a digital camera modified (by Colin Dunlop, Durham University) to position a rotatable slit (12mm x 1mm) in the pupil plane of the camera. This set-up enabled visualisation of the optical effects of an elongated pupil in different orientations. It was found, as confirmed through previous simulations, that vertical contours remained in sharp focus through a greater depth of field when the slit pupil was oriented vertically while horizontal contours had a shallower depth of focus and so appeared blurred closer to the focal plane. When the pupil was oriented horizontally, horizontal contours remained sharp through a greater depth of field, while vertical contours became blurred away from the focal plane (Fig. 5.5). It is hypothesised that the presence of sharper vertical contours in the visual field may assist in the vergence process, which could increase the speed or accuracy of stereopsis.

5.1.5. Sheep's Eye Model

The benefits of the horizontally elongated pupil were also analysed through model of the sheep's eye. The model was developed in Zemax® by Jürgen Schmoll at Durham University. The hypothesis was that the horizontally elongated pupil may allow a greater lateral field of view. It was found that the horizontally elongated pupil enabled more light to hit the retina from greater field angles as compared with the circular pupil.

The results shown in 5.6, suggest that the horizontally elongated pupil might confer the advantage of retaining a high throughput for large field angles at which image quality is higher as compared with the circular pupil model. This may facilitate vision at a sufficiently

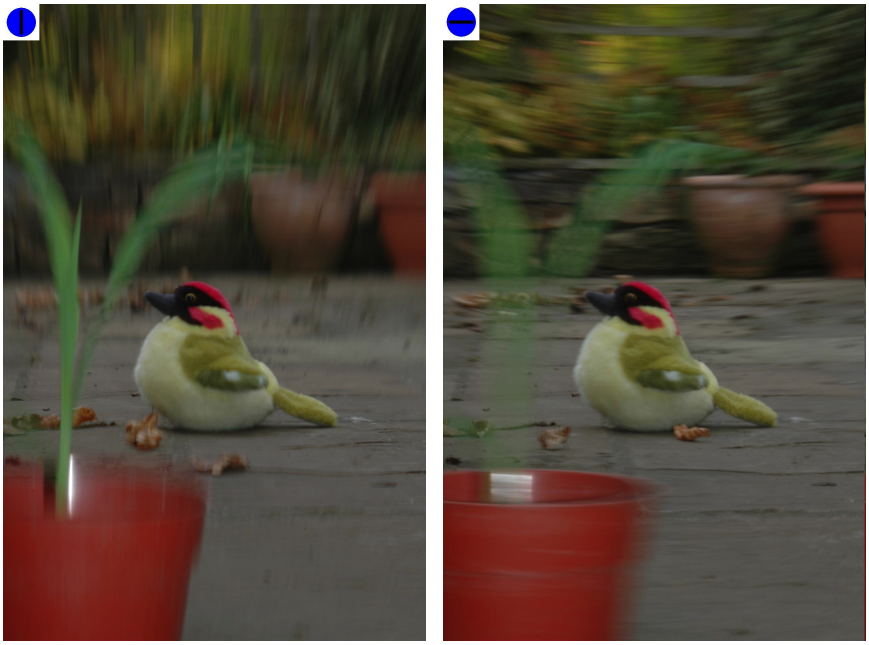

(a) Vertically elongated (b) horizontally elongated

Figure. 5.5: Images taken with a camera modified with a rotatable slit aperture. When the pupil is orientated such that the longest axis is vertical, the vertical contours in the image are sharper over a greater DoF. The opposite is true when the pupil is horizontal, i.e. horizontal contours are sharper over a larger DoF (Gordon Love & Colin Dunlop, CfAI, Durham)

high resolution to detect predators in a wide field of view, potentially in front of, and behind the animal in question. This eye shape retains depth of focus for horizontal contours, which may also aid locomotion over variable terrain should the need to flee a detected predator arise.

5.1.6. Rotational Optokinesis

Heath, Northcutt, and Barber (1969) described the phenomenon of rotational optokinesis in Reptiles, whereby an animal can rotate the optic bulb in the head to retain a constant alignment of the pupil relative to the ground plane. In species where the eyes are positioned laterally on the head it is necessary to rotate each eye in opposing directions to maintain correct alignment. The rotation of the optic bulb in opposite direction is called cyclover-

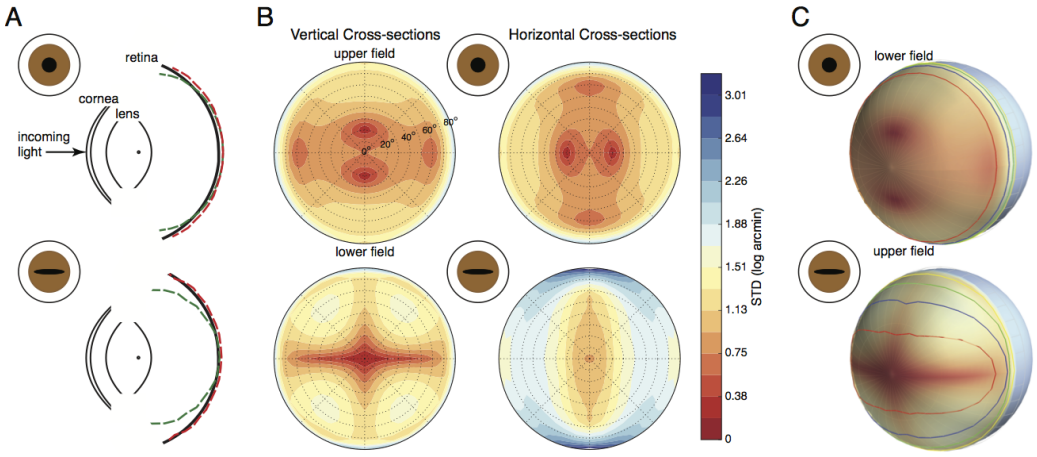

Figure. 5.6: Throughput and image quality based on a model sheep's eye A) The model of the sheep's eye designed in Zemax®. The black curves represent different surfaces in the eye. These surfaces include, from left to right, the anterior and posterior surfaces of the cornea (radii 11.66 and 13mm; thickness 0.8mm, refractive index 1.382), the anterior and posterior surfaces of the lens (radii 9.17 and -8.12mm, thickness 9mm, refractive index 1.516), and the retina (radius 12mm). The red curve is the focal plane for vertical line objects, and the green curve is the focal plane for horizontal line objects. B) Cross-sections of the PSF for each pupil shape. The upper plot shows the PSF for a circular pupil (2.8 x 2.8mm) and the lower plot for the horizontally elongated pupil (8 x 1mm). The centre of each plot represents the optic axis. The dashed circles represent different eccentricities. The heat-map corresponds to the standard deviation of the PSF where red represents the smallest deviation (i.e. the smallest point spread). The left hand figures are vertical cross-sections of the PSF while the right hand figure shows horizontal cross-sections. C) These figures show the vertical cross-sections of the PSF (lefthand side of panel B), with a measure of throughput overlaid as coloured lines (red, blue, green, and yellow for 80%, 60%, 40%, and 20%, respectively.).

gence. Heath *et al.* (1969) found that some species exhibited this behaviour while others did not. In one experiment, a Caiman Sclerops was placed in a darkened box which was then either rotated to invoke gravitational changes, or an artificial horizon was manipulated. The magnitude of this response is illustrated in Fig. 5.7. The response only occurred when the stimulus change was gravitational. This effect still occurred when the spinal column was severed behind the skull, but stopped when the fluid of the inner ear was drained. However rotational optokinesis did not occur in the species Coleonyx veriegatus (Gecko) and to a significantly lesser degree (rotations of $0°$ to $-30°$) in Dryophis nasutus (Green Vine Snake).

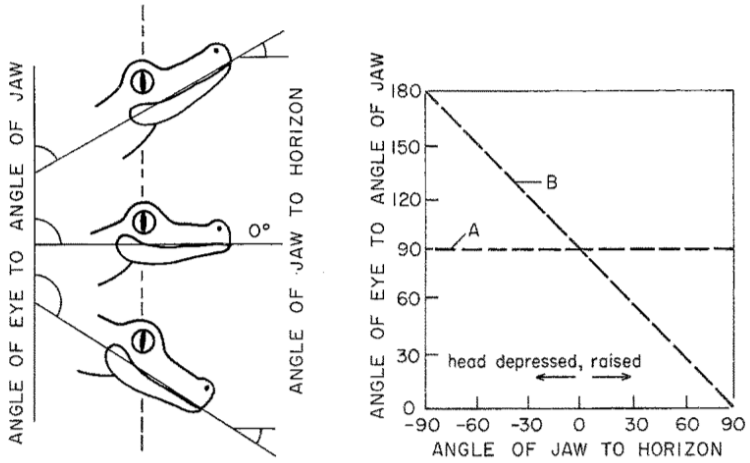

Figure. 5.7: Rotational Optokinesis as defined by Heath *et al.* (1969), the left hand image shows eye rotation relative to the angle of the head. The right hand plot shows the magnitude of change in eye rotation relative to the head and horizon.

This phenomenon was investigated by taking pictures of different animals with their heads in difference positions relative to the ground plane. These primarily included domesticated species such as sheep, horses and deer. It was found that many of these lateral-eyed species with horizontal pupils exhibited cyclovergence up to $\sim 70°$, maintaining pupil orientation with the ground plane, as their heads rotated to feed. We have found that effect present in a number of grazing species with horizontally elongated pupils, including sheep, deer, and goats. We believe this is to maintain the orientation of the pupil with that of the horizon, such that the optical properties of the horizontal pupil persist at different head angles.

5.1.7. Conclusions

This section has covered the work which was conducted by different members of the collaborative team for the animal eyes project. We have shown a statistical trend which can predict pupil shape with a high degree of probability, and extended the research on different facets of the ocular properties of different eye physiologies. The next section covers the work on feline pupils, vertical slit pupils and multifocal lenses, which was conducted by the author,

for inclusion in the animal eye project as well as this thesis.

5.2. Vertically elongated pupils and multifocal lenses

The previous section (Section 5.1) discussed the collaborative work on the prevalence of different shaped pupils as a variable of diel activity and trophic strategy, and some of the effects and functions of these shapes. This section details the authors contribution to that body of work with an investigation into vertically elongated pupils, the optical effects of multifocal lenses, and the combination of these ocular attributes.

Elongated pupils occur in animals in both vertical and horizontal orientations, in animals with both lateral and forward-facing eyes. It appears that horizontal pupils are common in species which are prey, while vertically elongated pupils are an adaptation found primarily in ambush predators (Section 5.1.1). Multifocal lenses are another evolutionary adaptation which, existing literature suggests, are used to reduce chromatic aberration caused by the incorrect imaging of different wavelengths as a function of their refractive index in the tissues of the eye (Kröger *et al.*, 1999; Land, 2006; Malmström & Kröger, 2006). Kröger *et al.* (1999) suggest that elongated pupils provide the ability to utilise all zones of the multifocal lens when the pupil is in different constrictive states.

> "In eyes with mobile irises, multifocal lenses are correlated with pupil shapes that allow all zones of the lens, with different refractive powers, to participate in the imaging process, irrespective of the state of pupil constriction." - Kröger *et al.* (1999)

There are also several land-dwelling species, such as house mice, which exhibit circular pupils and multifocal lenses. It appears that a primary distinction between species with each eye type is their period of activity during the day; many animals with elongated pupils and multifocal lenses appear to be crepuscular while the house mouse is primarily nocturnal (Land, 2006). There also appears to be a difference between genera within the felidae family; Malmström and Kröger (2006) found that those with smaller eyes tended to have elongated

pupils with multifocal lenses while larger eyed felidae had round pupils and monofocal lenses. They stated that this relationship was also found in other families such as Canidae.

Multifocal lenses occur in different species, including species within the same family. Kröger *et al.* (1999) suggests that this adaptation has occurred to reduce chromatic aberration as broadband light passes through the structures of the eye. This functionality is also cited by Malmström and Kröger (2006) as an explanation of the correlation between elongated pupils and multifocal lenses. Malmström and Kröger (2006) suggests that the elongated pupil allows the animal to utilise all of the refractive zones of a multifocal lens when the pupil is constricted in bright light conditions as shown in Fig. 5.8.

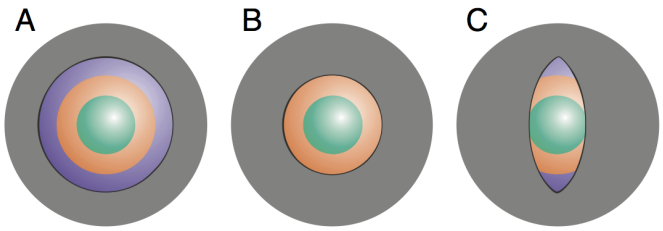

Figure. 5.8: Functional advantage of the vertically elongated pupil from Malmström and Kröger (2006); A) shows the fully dilated pupil with all zones exposed, B) the effect of a circular pupil i.e. the outer zone is occluded, C) the vertically elongated pupil exposes all areas of the multifocal lens while reducing pupil area

The simulation was developed with the intention of comparing elongated pupils and round pupils, of similar pupillary area so to identify the optical benefits relevant to the studied animal, in this instance the domestic cat. This was later extended in consideration of the theory that the elongated pupil enabled some animals to utilise a multifocal lens in varying light conditions, such as during mesopic lighting; as many felines are crepuscular (Kröger *et al.*, 1999). This also provided the opportunity to assess the benefit of multifocal lenses by comparing consistent pupil shapes with varying lens architectures. This project utilised a simulation model that was initially developed for modelling the optical qualities of the human eye, and then modified for assessing the effect of varying eye physiologies, in particular, the potential benefits of elongated pupils and multifocal lenses.

5.2.1. Methods

The simulation model developed to study the optical quality of the feline visual system is based on the same model and properties of used in the study of the human visual system (see introduction on monochromatic aberrations for details). The model was adapted according to estimated parameters specific to the feline eye. Initial tests were conducted using figures from (Hammond & Mouat, 1985) but these were later adapted to emphasise the effect of the elongated pupil. The pupil function was changed in shape such that a vertical height and horizontal width could be specified and an ellipse would be generated based on these values. This approximation of the shape of the feline elongated pupil, i.e. elliptical rather than 'marquise', was considered sufficiently representative for investigations into its optical effects.

The model simulated monochromatic light close to the centre of the visible spectrum (∼580nm), this allowed the efficacy of the model to be tested against the diffraction limit for that given wavelength. Once the reliability of the model was confirmed, additional wavelengths were simulated (201 values ranging from 450 nm to 650 nm). The PSF for each wavelength was generated then each summed to produce a PSF for broadband light. The retina has varying spectral sensitivity and so each wavelength was appropriately weighted with the coefficient W (Eq. 5.2) as,

$$W = -((3.0 * 10^8)/\lambda - 5.4 * 10^5)^2/(5.0 * 10^4)^2 \tag{5.2}$$

where, W is the weight and λ is the wavelength of the light in nanometers (Love - PC, 2013). Equation 5.2 roughly equates to the CIE luminosity function which describes spectral sensitivity in humans, and we used this as an approximation to the feline visual system as we were not aware of an equivalent model for this species. The associated curve can be seen in Fig. 5.10 (left).

As well as a variance in spectral sensitivity of photosensitive cells in the retina, each wavelength also has a different refractive index through the structures of the eye, which

results in chromatic aberration. The magnitude of chromatic aberration was calculated in Dioptres (D), as,

$$D = 1.7312 - (0.63346/((\lambda * 10^6) - 0.21410)) \tag{5.3}$$

where D is the defocus value in diopters and λ is the wavelength of light in metres (Banks - PC, 2013). The associated curve can be seen in Fig. 5.10 (right). The modelling of the multifocal lens was achieved by creating three individual pupil functions, rather than modelling independent lenses. The amplitude spread function for each of these pupil areas was then summed and squared to produce a complete point-spread function. The total power of this point-spread function was compared with the total for the pupil area to ensure consistent power transfer from the wavefront entering the pupil to the image plane. Figure 5.9a shows the total pupil area. Figure 5.9b shows the outer zone; Figure 5.9c the middle zone; and Figure 5.9d the inner zone.

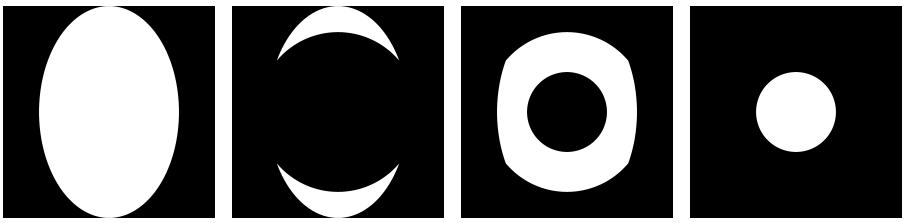

(a) Full Pupil (b) Outer Zone (c) Middle Zone (d) Central Zone

Figure. 5.9: Pupil functions simulating a multifocal lens

The refractive index of each zone was set by applying a magnitude of defocus to the wavefront for its PSF calculation. The outer zone was set to -0.4 D, the middle zone was set to +4 D, and the central zone was set to 0 D. The refractive offset (i.e the refractive index of the lens) was then applied to the magnitude of chromatic aberration for each wavelength according to Eq. 5.3 (see 5.10.

It was decided that the appropriate metric to compare image quality in different eye physiologies was the Strehl ratio. The Strehl ratio in this context was defined as the peak of the PSF of the chromatically aberrated model, against the peak of the PSF in a diffraction

limited model with no chromatic aberration. This metric was used to compare two different pupil sizes (12x12 mm and 12x1.5 mm) for four different optical conditions as follows, circular monofocal, vertically elongated monofocal, circular multifocal, and vertically elongated multifocal.

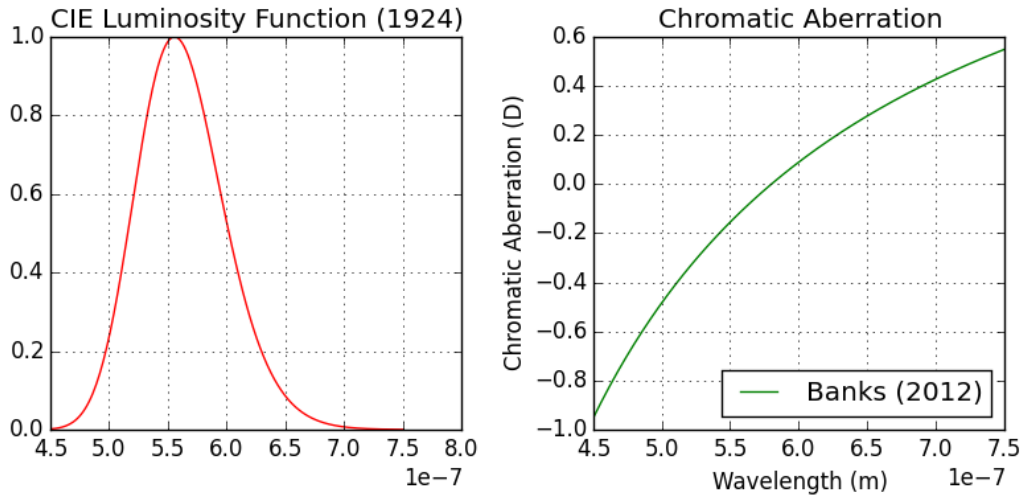

Figure. 5.10: The left hand figure shows the curve associated with spectral sensitivity of the human retina (Love, 2012); while the right hand figure shows the magnitude of chromatic aberration as a function of wavelength (Banks, 2012)

The analysis was then adapted to include pupil sizes based on measurements from real cats. The selected sizes were 12x12mm; associated with scotopic conditions, 10.6x7mm; associated with mesopic ambient light, and 6x1.5mm; associated with photopic conditions (Hammond & Mouat, 1985). This is intended to give an indication of the potential image quality and consequent effects of either a multifocal or monofocal lens through a range of different dilation states.

5.2.2. Results

The results of the four different artificial pupil simulation conditions (circular monofocal, vertically elongated monofocal, circular multifocal, and vertically elongated multifocal) show that the multifocal lens extends depth of field when the pupil is circular but this benefit

is lost when the pupil constricts to a vertically elongated pupil due to occlusion of the peripheral zones of the lens. This increased depth of field also reduces image quality at optimal focus (0D), when compared with the monofocal lens model.

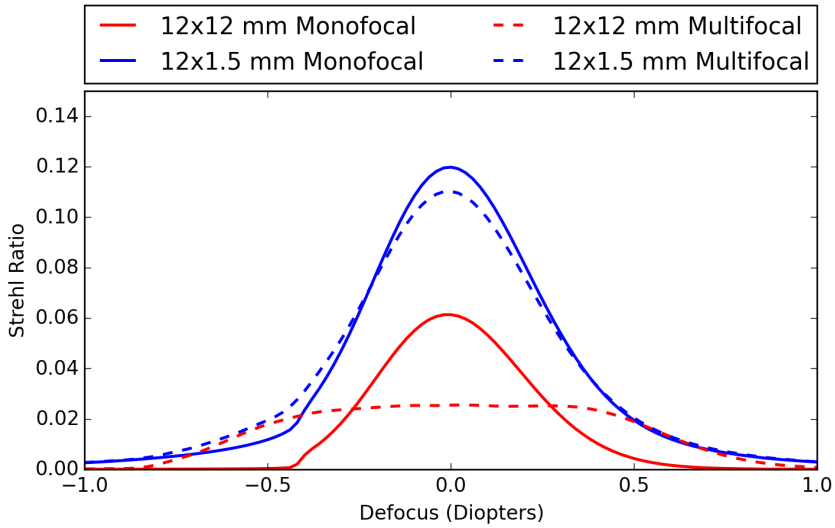

Figure. 5.11: Strehl Ratio for different pupil conditions (Circular pupil = 12mm x12mm; vertically elongated pupil = 12mm x 1.5mm). In this instance, Strehl was defined as the peak of the PSF of the model with chromatic aberration over the peak of the model which was diffraction limited eye.

Fig 5.11 shows the consequent Strehl ratio for different pupil and lens configurations, as described above. In the case of the circular pupil, it can clearly be seen that the multifocal lens increases image quality at greater defocus values, but the quality at 0D (best focus) is significantly degraded. In the elongated pupil condition, the multifocal lens only gives marginally increased depth of field, and the change at 0D is also reduced.

The pupil values selected for Figure 5.11 were artificial and intended only to show the extreme effects of the elongated pupil against a circular pupil. In order to assess the effect of pupil shape on image quality in real cats eyes, average pupil sizes were selected from Hammond and Mouat (1985) for different ambient light conditions.

The results shown in Fig. 5.12 indicate that when the pupil is constricted, the outer zones of the multifocal lens are occluded and the benefits associated with such a lens architecture

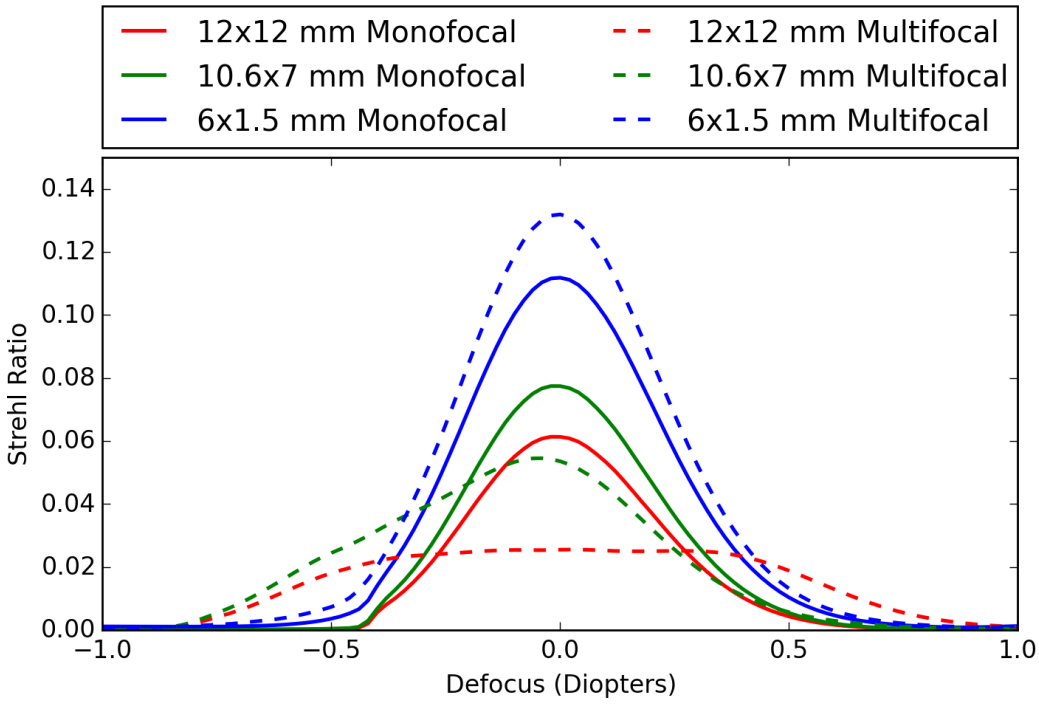

Figure. 5.12: Strehl Ratio (as previously defined) for different pupil sizes which match those of a cat, as measured by Hammond and Mouat (1985).

are lost. This can be seen as a close fit of the curves for the monofocal and multifocal lenses in the 6x1.5mm condition, suggesting that neither lens provides a particular advantage over the other. In the 12x12 mm condition, the peak of the curve is lower and broader in the multifocal condition suggesting a greater depth of focus, while in the monofocal condition the curve is narrower, suggesting a lesser DOF, but the image quality at best focus is greater than the multifocal condition. The mesopic state (10.6mm x 7mm) produces similar curves for the multi and monofocal conditions but the multifocal condition shows an increased DOF for negative defocus values. This is attributed to an increased area in the zone which has a negative refractive power, while the zone which produces a positive focal point is extensively occluded. It should be noted that this effect arises due to the arbitrary shape and power of the multifocal zones. Physiological data regarding the shape and power of the multifocal lens is unknown, and as such we assigned arbitrary parameters to this aspect of the model.

The model could be improved following biological measurement of these properties.

The effect of the defocus shift on the PSF in different conditions was also studied. This showed that, in line with the Strehl ratio results, the PSF spot size increased in the monofocal condition but this benefit declined when the pupil constricted to an elongated aperture. Malmström and Kröger (2006) suggested that the purpose of the multifocal lens was to correct chromatic aberration (CA). In order to assess the effect of the multifocal lens for correcting CA, we produced colour PSF images which estimate the spot size for different wavelengths at different defocus values.

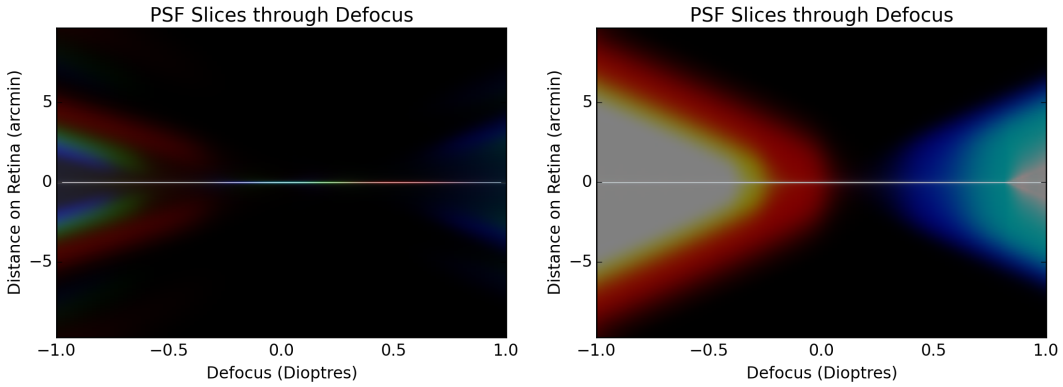

(a) Slices (12x12mm) from multifocal lens (b) Slices (12x12mm) from monofocal lens

Figure. 5.13: Plots generated by taking slices through the PSF, for a circular 12x12mm pupil, at different dioptric steps (abscissa), giving the horizontal extent on the retina (ordinate). Figure a shows slices through the PSF for a multifocal lens. Figure b shows slices through the PSF in the monofocal model. The colour indicates magnitude as real RGB values representing defocus across the spectrum due to chromatic aberration

It can be seen in Fig. 5.13 that the effect of the multifocal lens considerably decreases PSF spot size across a range of defocus values, equivalent to increasing depth of focus as discussed in reference to Fig. 5.11 and Fig. 5.12. This suggests that the lenses do improve chromatic aberration by decreasing spot size but whether this is secondary to the increase in depth of focus is unclear.

The effect of the multifocal lens in the artificially elongated pupil condition (12x1.5mm) is less clear, there is a noticeable decrease in spot size for vertically aligned contours (vertical

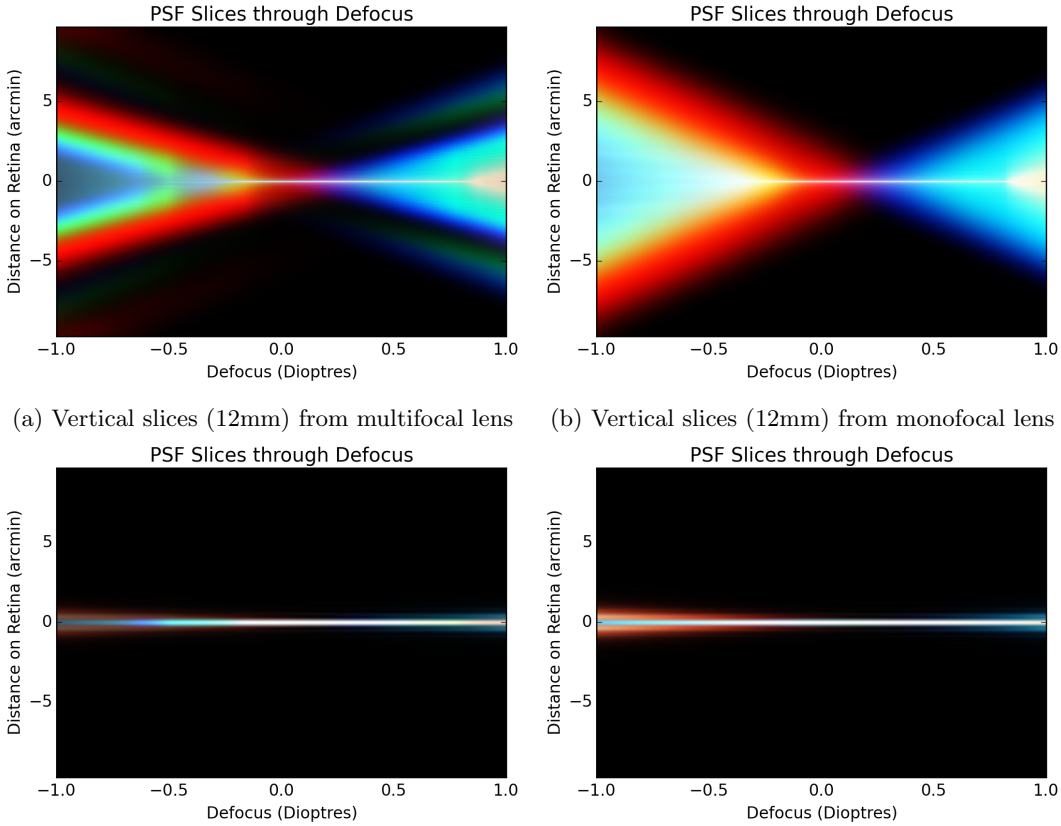

(a) Vertical slices (12mm) from multifocal lens

(b) Vertical slices (12mm) from monofocal lens

(c) Horizontal slices (12mm) from multifocal lens

(d) Vertical slices (12mm) from monofocal lens

Figure. 5.14: Plots generated by taking vertical or horizontal slices through PSF's generated for a number of different defocus values. The top row are vertical slices and the lower row are horizontal slices. The left column is the multifocal lens, and the right column is the single zone (monofocal) lens.

slices), but the effect is considerably less distinct when compared with the circular pupil condition.

5.2.3. Conclusions

The results of this simulation suggest that the functional benefits of the elongated pupil with regards to the multifocal lens, i.e. that the elongated pupil allows the transmission of light through all refractive zones of the multifocal lens as described by Malmström and Kröger (2006), is not supported. It seems plausible that the multifocal lens allows increased depth

of field when the pupil is fully dilated. This is further supported by Kelber and Roth (2006), who noted that many nocturnal animals will only have colour vision during day (photopic, i.e. the use of cones) or dusk (mesopic, i.e. low cone use, poor colour vision) conditions, and will be colour-blind in night conditions when many species use only rod photoreceptors (scotopic vision, i.e. rods only, no colour vision). The only species for which colour vision at night has been confirmed is nocturnal species of Hawkmoth and Gecko (Kelber & Roth, 2006). Although at present, there is a little conclusive behavioural evidence of colour vision in cats independent of lighting conditions. Kelber, Vorobyev, and Osorio (2003) states that it is not known if cats have two or three cones types (di- or trichromatic colour vision) at the retinal level. The effects of chromatic aberration will degrade visual quality when the light is composed of more than one wavelength. It may have other implications for accommodation where the chromatic spread is necessary to determine monocular depth cues, but visual quality may be a greater priority in animals with small f-numbers.

It should be noted that, in this simulation, the area of each of the three multifocal zones were the same as each other. This may not be representative of the physiology of the cats eyes but we do not have physical measurements of either the area or refractive index of different zones to refine the simulation. However, given that the maximum vertical extent of the pupil is halved in the fully constricted state, it seems plausible that the outer zones would be occluded, suggesting that the multifocal lens serves as an adaptation for scotopic, or possibly mesopic, vision, and that the elongated pupil does not serve to enable the functionality of the lens in different dilation states. It is tentatively proposed that the multifocal lens serves as a means of increasing the depth of focus in species where it is limited by the f-ratio of their visual system. While the elongated pupil may provide greater control of pupillary area as well as other advantages for binocularity and depth perception as discussed in section 5.1.4.

Cats are also primarily active at dawn, dusk, or through the night, and so the functional benefits of the multifocal lens may not be as critical in high ambient light during periods when activity levels are low. The cats eye would have a greater depth of focus when the

pupil was constricted, reducing the need for the DOF benefit conferred by the multifocal lens.

It is also noted that cats have a highly active pupil when hunting prey. A cat which is hunting in bright conditions will exhibit extreme variations in pupillary dilation from highly constricted in a resting state, to highly dilated when in a primed state shortly before pouncing on prey. We hypothesise that the variations in DOF and visual acuity as a result of these fluctuations might assist in hunting, but a study into this effect is beyond the scope of this thesis.

Chapter 6

Can monovision improve simulated 3D viewing?

The current chapter is concerned with an investigation into the validity of monovision as a means of reducing the vergence-accommodation conflict. We intend to perform two experiments to investigate different aspects of simulated 3D viewing using monovision lenses. In each experiment we have two conditions; the first is the no lens condition, which involves the participant wearing flat (plano-plano) lens over both eyes in additional to standard circular polarisers for simulated 3D viewing; and the second is the monovision condition in which the participant wears a flat piece of glass, with no refractive power, over the left eye and a 1D lens over the right eye. In all other respects the conditions are identical. The order of conditions is randomised between participants. The first experiment (the performance experiment) which will test the speed at which a participant can cross-fuse a stimulus, a 2 alternate forced choice (2AFC) task. The second experiment is concerned with their subjective comfort, and involves the a series of symptom questionnaires as well as a performance measure in the form of a 4AFC task.

We found that monovision is not an effective solution to the vergence accommodation

conflict. This is likely attributed to a decreased stereoacuity as most participants exhibited worse performance during the monovision condition. The subjective reports also indicated a preference for the no lens condition.

6.1. Background

Three-dimensional (3D) video has grown in popularity in previous years, yet a proportion of the population still have difficulty viewing simulated 3D imagery due to headaches and visual artefacts. There have been different approaches to solving this problem but here we propose a simple method which involves the application of different powered lenses over either eye to bridge the accommodative gap between images simulated at the screen and those closer to the observer. This is a method derived from a presbyopia correction called monovision; a vision correction technique where one eye is focused for near vision, and the other for far vision. Previous research suggests that in most cases an observer will become conscious of the sharper image, and the blurred image will be suppressed. The aim of this study is to investigate this technique as a potential means of reducing the discomfort associated with the vergence-accommodation conflict.

The human eye uses a number of different cues to estimate the depth of objects within the environment. One of these cues is vergence; the angle at which the eyes must rotate until their line of sight intersect (foveate) at the intended object to maintain retinal correspondence. The brain uses the rotation of the eyes, and the disparity in the 2-dimensional (2D) images projected onto each retina, to determine the relative position of objects within the environment. Stereopsis (the perception of 3D objects in response to the information from two eyes) was first described by Wheatstone in 1838. Wheatstone discovered that offset images would create the impression of a depth that was not consistent with the depth of the presented images, he used this discovery to build the first stereoscope. The Wheatstone Stereoscope is composed of two mirrors which direct the path of each eye to an independent image, each of which has a relative offset creating the illusion of depth (Wheatstone, 1838). The average inter-pupillary distance is 63 mm, and the majority of the western population

are within the range 50-75 mm (Dodgson, 2004). This separation requires the eyes to rotate to converge their line of sight to objects within the environment. The difference between these two images, the shifts in position of objects on the retina, allows the brain to construct a 3D representation of the visual field.

There have been many different techniques employed to illicit the illusion of 3D. Examples of recent and mainstream techniques include anaglyph 3D (colour filtered images), passive 3D (polarised images), active 3D (alternating images), and auto-stereoscopic (glasses-free 3D) imagery (Mendiburu, 2012). Each of these methods incur different benefits and disadvantages. Anaglyph 3D has the benefit of working on traditional display technologies, and only requires a basic set of coloured lenses which are very cheap to produce, but this technique also degrades the quality of the image by introducing false colouring (Woods & Harris, 2010). Passive 3D uses the same concept as anaglyph 3D but rather than using colour to create disparity, the images are presented side by side where the left eye uses one orientation of polarised light, while the other eye receives an image transmitted with the opposing orientation. This is done by projecting both images onto an appropriate material, or by alternating each line of pixels in a pixelated display. Active 3D uses lenses which switch between transparent and opaque depending on the refresh rate of the display. This allows either eye to receive a different image at a speed faster than we would perceive. This technique allows full resolution but the glasses are heavier and require power. Auto-stereoscopic displays do not require glasses but can only be used when the observer is positioned within a very limited viewing angle, perpendicular to the display (Holliman *et al.*, 2011).

These displays produce the illusion of depth by delivering an image to either eye, where each image is positioned with an offset relative to the distance of the screen from the observer. This offset causes the eyes to rotate so that their line of sight intersects at a plane closer or further from the display, creating a 'fused' image from two disparate images. The disparity between the two images causes the brain to assume that the images form an object which is not on the same plane as the screen, but rather the depth to which the lines of sight intersect, and the illusion of depth is created. An increase in the extent of simulated 3D

imagery in media has resulted in reports of discomfort, and television manufacturers have issued health warnings attached to the products they have released. This discomfort has been attributed to different causes. These precursors can include the wearing of glasses for extended periods, especially when the wearer is not used to them; ghosting, or cross-talk, which occurs when the polarising lenses don't fully filter out the opposing image due to lens quality or viewing angle; the introduction of flicker or visual artefacts associated with 3D production (e.g. occlusion or alignment); or other problems such as oblique viewing angles and image misalignment. The primary cause of visual discomfort is associated with a problem termed the vergence-accommodation conflict (Hoffman *et al.*, 2008).

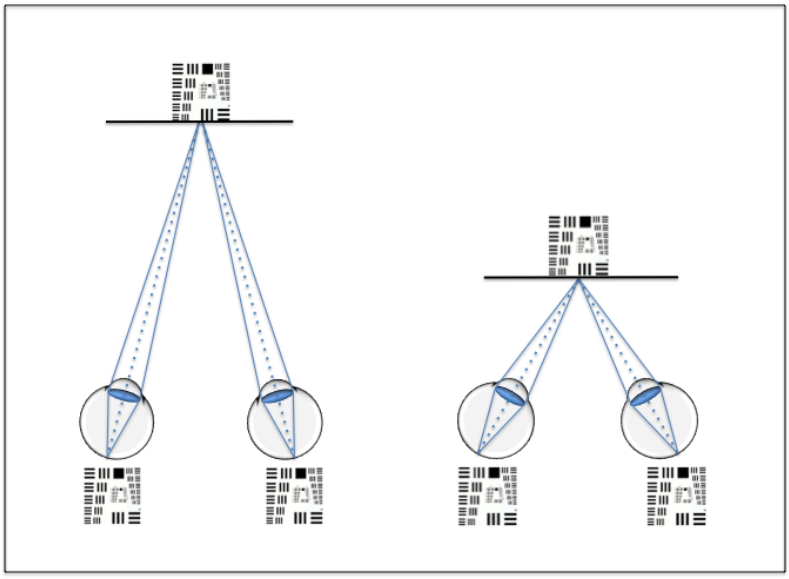

Figure. 6.1: On the left we see the effect of attending to an object that is at a distance, and on the right, an object that is closer. In both examples, vergence (the rotation of the eyes) and accommodation (the focal power of the eye) are coherent in the distance that they attend to.

Our investigation will exclusively use passive 3D technologies, but an alternative set-up was developed by researchers at Durham University which is intended to deliver the correct depth cue by placing a variable power lens in front of the eyes and adjusting the refractive

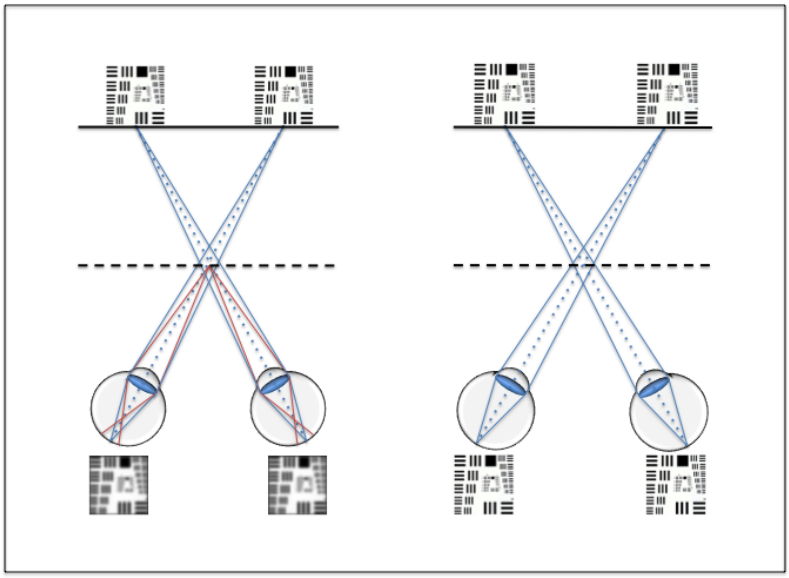

Figure. 6.2: Here we see the effect of simulating an object at a distance closer than the screen. The left, we see the effect when vergence and accommodation are linked, and as a consequence the retinal images become defocused. On the right, we see the effect when vergence and accommodation are not linked. In this situation we obtain a focused retinal image and perceive the illusion of 3D but, in this situation, the conflict in distance between vergence and accommodation may be responsible for decreased comfort.

strength of that lens depending on the simulated depth presented to the observer. The applied defocus will compensate for the accommodative gain that occurs when the vergence cue is altered to create the illusion of depth (Love *et al.*, 2009). This focal correction should reduce or remove the accommodation-vergence conflict. This focus-correct adaptive display has been in use for a series of experiments by researchers in Berkeley, in which the preliminary results suggest that such a set-up is preferable to traditional simulated 3D displays (Mackenzie *et al.*, 2010; Shibata *et al.*, 2011; Johnson & Banks, 2015).

This project will look at a less complex solution, inspired by a technique used to correct presbyopia, called monovision. The fundamental principle will be similar to that of the adaptive system; the observer will be presented with depth appropriate focal correction equivalent to the simulated depths presented. As there is no adaptive component to this

system, the focal cues must be presented to either eye and the brain left to interpret the signals. This is inspired by the ophthalmological correction for presbyopia called monovision.

6.1.1. Monovision

Monovision is a form of vision correction which is primarily used for the treatment of presbyopia. It involves adjusting one eye for distance vision and the other for near vision with the use of contact lenses, glasses, or intraocular lenses. This causes an attended object to be in better focus in one eye and worse focus in the other. An example of this is demonstrated in figure 6.3.

(a) Foreground focus (b) Background focus

Figure. 6.3: these two images highlight the effect of a stereogram with different focal positions in either eye. The left image shows the effect of having one eye for near vision, and the right image shows the focus for an image with distance vision. If we then cross-fuse these images into a single image (i.e. go cross-eyed until the two images merge) we find that both elephants are in focus, with a degree of image degradation (you may also suffer from a focal shift due to the change in vergence). This is due to the attentional system attempting to prioritise the sharp image, a phenomenon called binocular rivalry

Figure 6.3 demonstrates that, to a certain extent, an observer will prioritise the image from either eye which is in best focus. In this example, the elephants in the fused image become sharper despite only one position in either image being in-focus. This effect is called binocular rivalry (Levelt, 1965; Mitchell *et al.*, 2004), and it is this effect that we hope to exploit in our simulated 3D experiments.

The effectiveness of monovision correction in clinical applications is varied with patients

typically reporting improved vision but often following adjustment periods, as well as continued problems such as blurring, double vision, and poor night vision. There are some reports of aesthenopia (eye strain including headaches, blurred vision, fatigue and eye pain) after monovision surgery in presbyopic patients, although the majority of patients are satisfied with the outcome. (Xiao *et al.*, 2011). Greenbaum (2002) also noted that many patients prefer to have their dominant eye corrected for distance vision but there is little evidence that this change makes a significant difference to visual performance post-surgery. Alarcón *et al.* (2011) found that 90% patients who underwent monovision surgery retained a near and far visual acuity of 0.0 logMAR or better, but the discrepancy in the retinal image resulted in a significantly reduced contrast sensitivity function and stereoacuity. Erickson and Schor (1990) estimated that stereoacuity fell from 40-50 arc sec to 80-100 arc sec when participants used monovision correction. They also found a significant decline in contrast sensitivity. The decline in visual performance is supported by other studies (Kirschen *et al.*, 1999; Fawcett *et al.*, 2001).

Collins *et al.* (1994) documented that many patients who begin wearing monovision contact lenses often require a considerable period of time, days to weeks, to adjust to anisometropia. Their study found that 48% of subjects were comfortable with the change following a week of regular use, and 78% were satisfied after 8 weeks. In the 8-week study, they found that visual acuity did not change but participants reported increases in visual performance. This combined with an increase in satisfaction may be attributed to an adaptation to monovision (Collins *et al.*, 1994). Evans (2007) conducted a review of the monovision literature and found that the success rate of monovision in people already adapted to contact lenses was 59-67%. This figure differed depending on the pre-existing visual condition of the patient, and success rates were considerably higher in patients who accepted intra-ocular monovision but it is unknown whether this was due to the complications associated with reversing the procedure, the severity of pre-existing visual problems, or because of actual increases in quality of vision due to multifocal corneal shape introduced through LASIK procedures. This review also noted that the main limitations of monovision contact lenses

included an inability to suppress the opposing blurred image in low light conditions, the lack of an additional focal length between the short and long focal distances, but more importantly, for the application on 3D televisions, was the reduction in stereopsis which the authors stated was not widely noticed by patients in the literature but depending on the specific characteristics of the degradation may affect the quality of simulated 3D viewing (Evans, 2007).

The degree to which monovision is effective for vision correction over other techniques is debated but this project intends to investigate if such an application can improve 3D viewing. In this instance 'improve' can be characterised in different ways; the subject might experience greater subjective comfort or quality, or the participant might score better in performance related tasks. An example of monovision and its effect on focal distances and the vergence-accommodation conflict problem is detailed in figure 6.4.

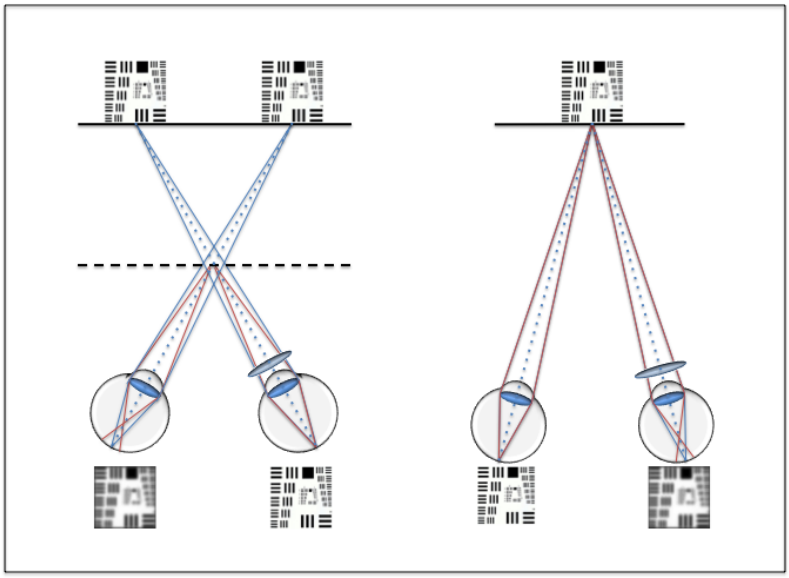

Figure. 6.4: the effect of using a monovision lens over the right eye is shown when the display simulated a an object closer to the observer in the left figure, and displays an object at the distance of the screen on the right. The retinal image is defocused in a single eye in either condition. This provides the observer with a means of reducing the vergence-accommodation conflict as the eyes can refocus to retain a clear image.

The application of monovision for 3D viewing aims to deliver a sharp image to either eye depending on the focal distance which has been simulated. This might not satisfy all simulated distances but would bridge the gap between the distance to the display and the focal distance associated with the change in vergence. Equivalently this provides two depths to which the observer can accommodate, rather than one, and it is this benefit which should confer an improvement in stereoscopic viewing.

6.2. Performance Experiment: Time to Fuse

This experiment was designed to test the speed at which a participant could cross-fuse a stimulus image and identify the orientation of its pattern. The stimulus was a random dot stereogram which, when fused, appeared as a sinusoidal grating composed of randomly positioned dots. The spatial frequency was set to 0.311 cycles/degree, but the phase was randomised to ensure variation in the stimulus between presentations. The peak to trough amplitude of the sinusoidal grating was 25 arcmin. The orientation of the grating was either -20° or +20°. The order in which the gratings were presented was randomised while ensuring that an equal number of both orientations were presented. The orientation of the grating was kept close to horizontal because disparity sensitivity is greater for horizontal corrugations, rather than vertical corrugations, and this also reduces the incidence of monocular artefacts Banks *et al.* (2004).

6.2.1. Methods

6.2.1.1. Participants

Participants were recruited from Physics Department staff, as well as members of the student population at Durham University. Participants were selected between the ages of 18 and 30 to reduce the instances of presbyopia and other age-related performance factors. Participants were instructed to wear vision correction if required, and preferably in the form of contact lenses. There may also be variations in participant competency based on anisometropia (differences in the power of either eye), which was not assessed prior to completion of

the experiment beyond asking the participant to disclose any prescriptive requirements. Participants were informed of potential risks (primarily fatigue/headaches), but were not informed of the hypotheses or specific details of the experiment until after the trials had been completed. The subjects were not paid for their time and light refreshments were provided during the rest period. One participant, RH1, was unable to cross-fuse the prerequisite test patterns and was discounted from the study. We did not test participants stereoacuity, and collaborators working in Berkeley on a similar project reported a high degree of subject variability in gross stereopsis. This may explain the participants who could not perform the tasks, and the inconsistencies in performance between participants.

The experiment was approved by Durham University Physics Department Ethics Committee, both in line with ethical concerns involving human participants, as well as general risk assessment. Initially participants were not offered financial incentive, but approval was later granted to offer entry into a prize draw for a £100 amazon gift voucher. They were informed of their right to withdraw at any point. Each participant's involvement was confidential and their data identifiable through a unique three character coding.

We initially tested 20 subjects but the data from 9 of those participants was excluded due to erroneous data. We removed participants whose data met certain exclusion criteria, this included a lapse rate in the no lens condition of greater than 15%, and and participant for whom the threshold was estimated as a negative value in either condition. These participants could not have been following protocol by allowing their eyes to remain converged at the simulated distance, and not attending to the text displayed between each stimulus interval (a solution to this problem is discussed in section 7).

6.2.1.2. Apparatus and Stimuli

Each condition was conducted in the same location, a small lab space, with the same equipment. The glasses were custom designed and each was fitted with a plano lens (no refractive power) in the left eye, and a lens with a given magnitude of power over the right eye. The power of this lens was 1D throughout both the performance and the comfort experiment.

The 3D display was an LG-D2343P 58cm Full-HD 3D monitor. The bespoke glasses were fitted with clip-on circular polarisers. The disparity between the images on the screen is calculated with reference to the distance between the participants eyes and the screen (viewing distance). A chin rest was fixed to the desk at a distance of 0.5 metres from the 3D display in order to reduce the error cause by drift in the position of the participant throughout the session. The participant fixated on a dot in the middle of the screen at the location where the stimulus appeared to ensure their gaze was appropriately positioned. This dot was blurred to reduce the awareness of the difference in strength of either lens between presentations. Text was introduced during the fixation period to encourage the participant to diverge their eyes to the correct depth between presentations, despite the presence of high contrast information subjects were not aware that each lens had a different focal power.

The random dot stereogram (RDS) was generated by creating an array of arbitrary size (512 x 512 pixels), and dividing this array into 1024 'windows' each of size 16 x 16 pixels. A single dot was then randomly placed within this pixel window. This created an array containing a fairly even distribution of dots. The horizontal disparity necessary to create the sinusoidal stereogram was calculated using an equation detailed by Banks *et al.* (2004) and defined in 6.1,

$$D(x, y) = (A/2)\cos[2\pi f(y\cos\alpha - x\sin\alpha) + \varphi] \tag{6.1}$$

where x and y are the coordinates of the dots, A is the peak to trough amplitude, f is the spatial frequency, α is the orientation, and φ is the phase of the sinusoidal grating (Banks *et al.*, 2004). The pixels composing each dot were then offset depending on their position to create the 3D sinusoidal effect.

This array of dots, containing stereoscopic information is then further offset so that the entire pattern appears closer to the participant. This is achieved by calculating the disparity between two images to create a depth at a given position, relative to the viewing distance

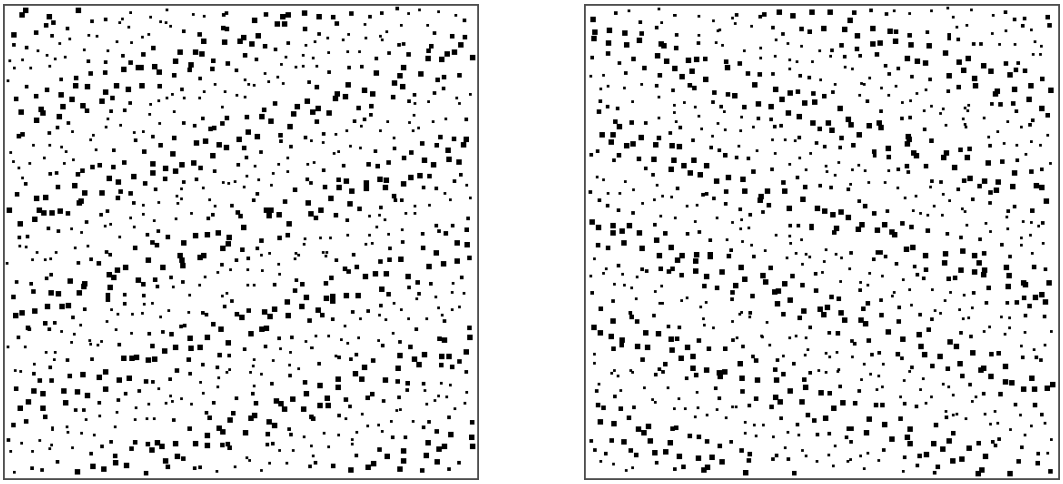

(a) -20° (b) 20°

Figure. 6.5: these two images show the stereogram at -20° and 20°. The size of the dots represent depth where larger dots would be presented with greater disparity to simulate a depth closer to the observer than the display. The smallest dots are those without disparity and would appear to be positioned at the depth of the display.

and inter-pupillary distance using 6.2,

$$D = -IVP \tag{6.2}$$

where D is the disparity require to simulate the correct magnitude of depth, I is the inter-pupillary distance, V is the viewing distance, and P is the magnitude of depth we intend to simulate. We approximated inter-pupillary distance (IPD) at 6 cm, which is close to the average IPD for a typical population (Dodgson, 2004). The viewing distance was 2D (0.5m), this resulted in a pixel resolution of 1.86 arcmin, and this resulted in a dot size of 7.44 arcmin (4x4 pixels). This resulted in the stimulus subtending 15.87°, and it was presented at 1D closer to the participant (i.e. at 3D from the participant). The stimulus remained at a constant size regardless of the simulated distance. The left eye would be focused on the display when the fixation dot was presented, simultaneously the right eye would be focused behind the display. When the stimulus was then presented at 3 dioptres from the participant, the eyes would converge and the accommodation process would bring

the right eye into focus and the left eye would be defocused with respect to the display distance. This allowed the eyes to converge and accommodate to a new position and still retain a sharp retinal image in one eye, which (as demonstrated in figure 6.3) allows the brain to interpret a coherent stereo image which appears largely in focus.

6.2.1.3. Procedure

The participant was introduced to the equipment, informed of their right to withdraw, and asked to complete the consent form. The participant was the asked to position their head comfortably in the chin rest, and make any necessary adjustments to their chair and position. The computer programme was initiated, and the lights dimmed. The experimenter then left the room and allowed the participant to progress through the instructions presented on-screen. This began with instructions informing the participant which pair of glasses to wear. The participant then undertook a series priming tasks to become accustomed to the magnitude of disparity and the degree to which they would need to cross-fuse each stimulus. These priming exercises began by cross-fusing a cross into a circle, which most participants found a comparatively difficult task, largely due to the size and lack of coherent stereo information. This was succeeded by a series of random dot stereograms (RDS) which began at a low disparity (0.2 dioptres) and increased in disparity, over 5 steps (steps of 0.2 dioptres), until equal to that used in the experiment. This allowed the participant to slowly become accustomed to the task. The participant had to correctly identify the orientation of the RDS on each presentation to allow them to progress to the successive step. If they answered incorrectly then the depth returned to 0.2 dioptres, and the priming phase began again. If the participant repeatedly failed to progress through the priming phase then they were excluded from the experiment.

Once the trial phase was completed the participant was presented with a screen informing them that the experiment was about to begin, this allowed them a moments rest from the test phase and allowed them to ensure they were sitting comfortably. The experiment began once they indicated their intention to continue with a keypress. The stimulus patterns were

presented sequentially using an adaptive staircase method from the PsychoPy python library (Peirce, 2007). The staircase method was designed (Dixon & Mood, 1948) to present an approximate threshold value in as few steps as possible through a 1-up/2-down method, whereby the presentation time would increase for every incorrect answer, but decrease for every two correct answers (Garca-Pérez, 1998; Klein, 2001). The stimulus was initially presented for 2 seconds, this time was then decreased by 0.4 seconds for every correct answer. Once the participant answered incorrectly the time would increase by 0.4 seconds, and the 1-up/2-down method would be implemented. The presentation time would then increase with each incorrect answer but only decrease if a given stimulus level was answered correctly in two consecutive presentations. After every two reversals, the time step would decrease by 50%, and this reduction would occur each time two reversals occurred until the time step had reduced to 0.025 second time steps. This staircase was used for 50 trials and then the experiment was reset to the starting values and repeated. This procedure was repeated for 4 sets of 50 trials; 200 trials in total. It was found that many participants did not perform optimally (or quite erratically) in the first set of 50 presentations. This sequence was excluded from the final results and considered an extension to the training phase.

Once the participant had completed the first trial with a random pair of glasses, they were asked to return and complete the second condition with the other pair of glasses. They were given a minimum of a 30 minute break, but were asked if they felt that their eyes had recovered from the initial session. The participant was given more time if any doubt was present. The glasses were also worn in a random order for each participant, this was to reduce the risk of a bias due to fatigue for the successive pair of glasses.

Figure 6.6 shows the response times for participant IM1. As can be seen in this figure, the participant begins responding with a stimulus interval of 2 seconds. This then decreases for each correct answer, but increases when the participant answers correctly.

The first session in each condition in figure 6.6 is erratic and does not follow the curve, or settle on a comparable concluding value, as compared with other successive trials. This effect

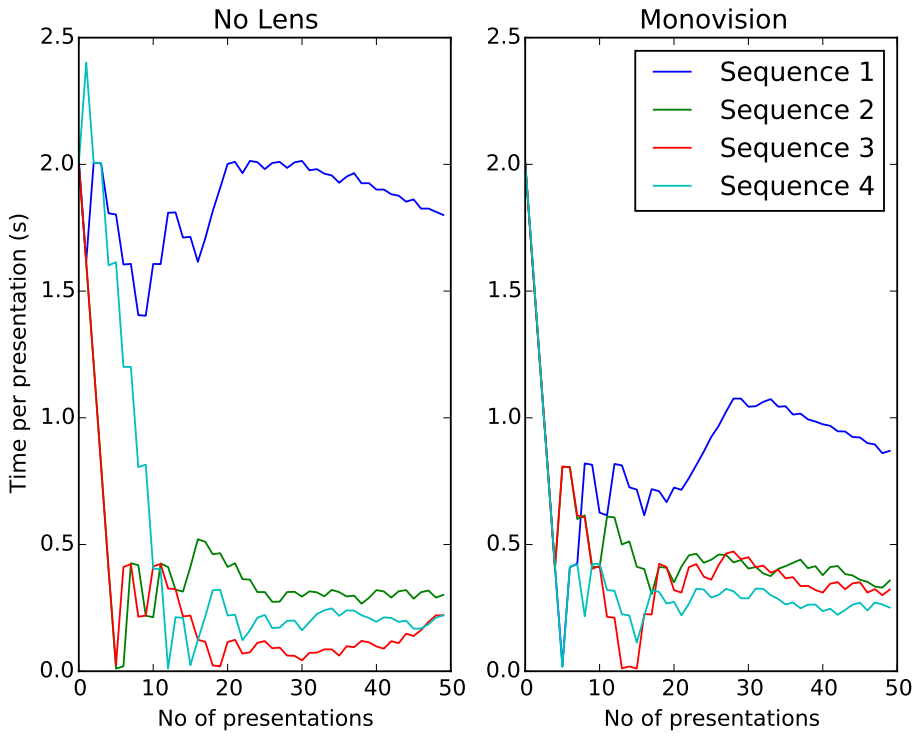

Figure. 6.6: the time intervals for the presentation of the stimulus throughout the course of the experiment for participant IM1. Each curve represents a set of 50 trials. The left hand plot refers to the no lens condition, while the right hand plot gives the timings for the monovision condition. A negative gradient shows that the participant answered correctly (initially for every presentation, then every second presentation following the first reversal). A plateau indicates where a correct answer was given once following the first reversal. A positive gradient follows an incorrect response.

was typical and we have assumed this is due to a familiarity effect such that the participant requires a number of trials (in addition to the training phase) to perform optimally during the data collection phase. In all participants we have discounted the initial 50 trials (i.e. the first curve as indicated in 6.6 as Sequence 1). As such the final analysis only contains 150 data points from each participant.

The curves displayed in each figure in the results section have typically been fitted using maximum likelihood criterion (Wichmann & Hill, 2001) with the python library Pypsignifit

3.0 (Fründ *et al.*, 2011), unless otherwise stated. This library has been developed for the analysis of psychophysical experiments, and the application of fitting psychometric functions. There are three aspects of statistical importance with regards to the fitted curves; the threshold plotted half way between the guessing rate (50% in the 2-AFC task or lower asymptote) and the upper asymptote (optimally 100% but may be lower depending on the subjects lapsing rate), we have called this the mid-point threshold; the slope of the curve at that point; and the lapsing rate (i.e. the upper asymptote of the curve as a consequence of incorrect answers at longer presentation intervals.) The 50% threshold on the curve changes in absolute position in the figure depending on the lapsing rate. If the lapsing rate is 0.04 (i.e. 4%), then the 50% threshold will be measured at 73% rather than 75%. This point on the curve has been used for the threshold as some participants may, for example, only ever perform at a 75% asymptote. In this way we measure the mid-point between chance and optimal performance. The slope of the curve at this position is variable depending on the strength of the threshold measurement. This is attributed to the participants confidence in the stimulus, and relates to their perception of changes in the independent variable (Green & Swets, 1966), or the reliability of determining a threshold due to the experimental design. A steep curve indicates that the observer can identify small changes in the independent variable, in this case the speed of presentation, while a shallow curve suggests that the participant can only differentiate very crude changes to the presentation time (Fründ *et al.*, 2011). The lapsing rate is a measure of the upper asymptote of the curve. This decreases from 1 due to errors that occur at greater independent variable values, in the case of this experiment this would include errors in fusing the stereogram when the time interval is large.

The curve is fitted by the function Ψ where,

$$\Psi(x;\theta) = \gamma + (1 - \gamma - \lambda)F(x;\theta) \tag{6.3}$$

where θ is the parameter vector (m, w, γ, λ). The parameters m and w determine the

shape of the psychometric function depending on the function used, where m relates to the horizontal shift of the slope of the curve and w relates to the distance in which the curve increases. γ is the guessing rate (50% in the 2AFC task), and λ is the lapsing rate (upper asymptote of the fitted curve based on general response errors). These curves are further explained in figure 6.7 (Fründ *et al.*, 2011).

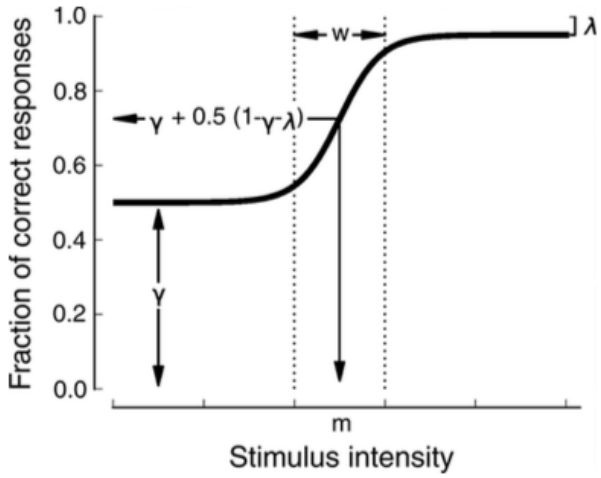

Figure. 6.7: the effect of different parameters in the shape of the fitted function. where λ and γ represent the upper (lapsing rate) and lower (guessing rate) asymptotes of the curve respectively. The parameters m and w relate to the horizontal shift and interval length of the slope respectively (Fründ *et al.*, 2011).

The function F used in equation 6.3 is the cumulative gaussian and is given by,

$$F(x;\alpha,\beta) = \frac{1}{1+\exp(-\frac{x-\alpha}{\beta})} \tag{6.4}$$

where α is equivalent to the 75% threshold, and β is the inverse of the slope of the function. These functions determine the fitted curve in each of the subsequent data figures.

6.2.2. Results

The results of this experiment are shown as values measured between the no lens condition (0D lenses over both eyes) and the monovision condition (a 0D lens over the left eye, and a

1D lens over the right eye). We collated the data for each participant and fitted a cumulative gaussian curve. We plotted thresholds and 95% confidence intervals at 50% on the curve between the upper and lower asymptotes (the relative position of these values on the figure depends on the lapsing rate associated with that data). An example of this curve fitted for the monovision and no lens conditions is shown in figure 6.8. This figure contains data from trials with participant EH1.

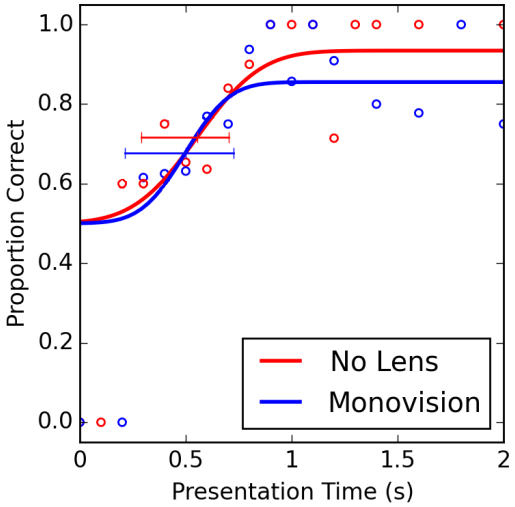

Figure. 6.8: the data for participant EH1. The red and black dots show the percentage of of correct answers at a given time point, and the associated curve is the cumulative gaussian fitted to that data. This participant has a mid-point threshold at 0.555s (at 71.7%) in the no lens condition, and 0.499 (at 67.8%) in the monovision condition. The participant exhibited a lapsing rate of 0.066 (6.6%) in the no lens condition but a lapsing rate of 0.145 (14.5%) in the monovision condition.

This figure shows that subject EH1 fused the stereogram into a cohesive image in comparable times for the monovision and no lens conditions. This is indicated in figure 6.8 by the relative positions of the curves and the estimated thresholds. The mid-point threshold is positioned at 0.499s in the monovision condition, and at 0.555s in the no lens condition. The mid-point threshold is offset from the expected 75% threshold due to the lapsing rate, and as a consequence is at the reduced position of 71.7% in the no lens conditions, and 67.8% in the monovision condition. The most striking result is the difference in the lapse

rate between the two conditions, where the lapse rate was higher in the monovision case (no lens = 0.066; monovision = 0.145). This trend was found across many participants.

If we plot this threshold value for each participant (as shown in figure 6.9) and subject the data to a Wilcoxon signed-rank test, we find that there is not a statistically significant difference between the two conditions (p=0.790).

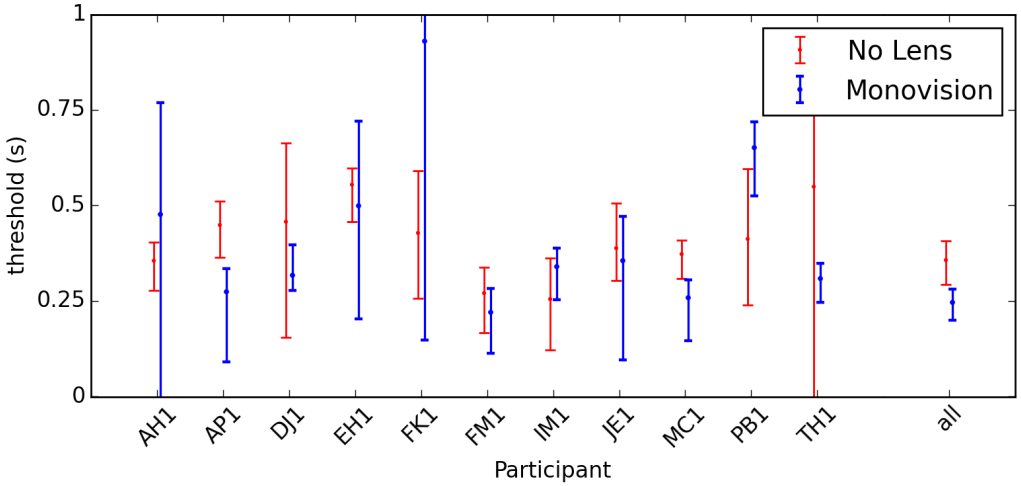

Figure. 6.9: the threshold for a position half way between the curve maximum and minimum, for each participant. The abscissa shows the participants identifier, and the ordinate shows the threshold as a proportion correct.

If we look at the lapsing rate (i.e the upper asymptote of the fitted curve) for all participants we see that this effect occurs in both conditions, but to a greater magnitude in the monovision condition. Figure 6.10 shows the lapse rate of each participant. It is clear that participants sometimes made errors during the no lens condition but these errors were more prevalent in the monovision condition.

The lapse rate was, for almost every participant, greater in the monovision condition than in the no lens condition (with the exception of participant PB1 for whom the estimated lapse rate was 0.076 in the no lens condition, and 0.069 in the monovision condition). Although the prevalence of errors above threshold was higher in the monovision case, the difference between both conditions was not significantly different (p=0.131). The slope of the curve

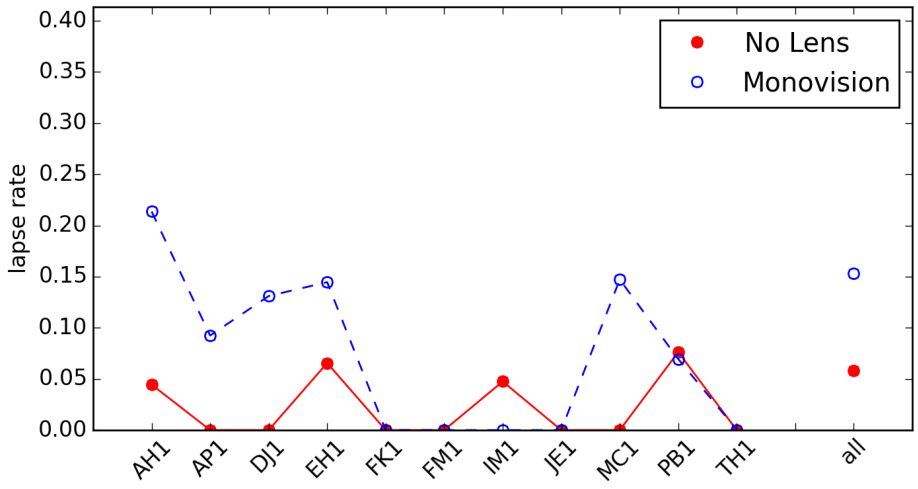

Figure. 6.10: the lapse rate for each participant. The abscissa shows the participants identifier, and the ordinate shows the lapse rate as a proportion correct (100x for percentage). The lapse rate is the maximum rate at which the participant answers correctly due to errors at the longer stimulus presentation times.

at the 50% threshold did differ between the two conditions, where it appears that the curve was often steeper in the monovision condition, and less so in the no lens condition, although the difference between the conditions is not statistically significant (p=0.248).

We took the data from each participant and collated it into a single figure, equivalent to that shown in figure 6.8. We than applied the same curve fitting algorithm to these data, as shown in figure 6.11. This generalised figure demonstrates the prevalent trends found throughout the experiment.

There is a lapse rate present in both conditions but the value is higher in the monovision condition; 0.054 (5.4%) in the no lens condition, and 0.144 (14.4%) in the monovision condition. This is contrasted by the decreased gradient of the slope of the cumulative gaussian in the no lens condition (0.294) vs. the monovision condition (0.096). The estimated threshold plotted for each curve suggests that the fusion rate is faster in the monovision condition but this may be a consequence of the increased lapsing rate. The threshold for the no lens condition is plotted at 0.36s and an absolute percentage rate of 72.3%, while the monovision

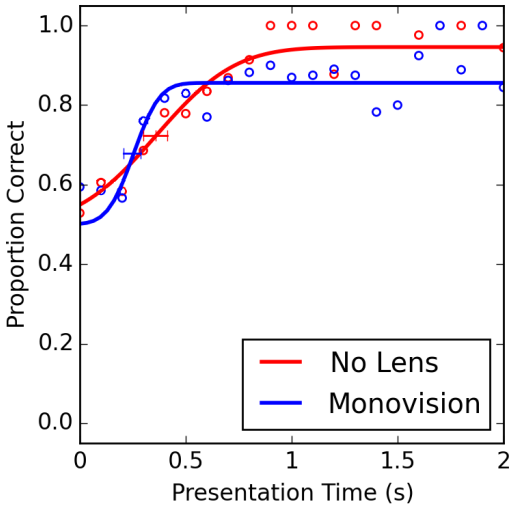

Figure. 6.11: This figure shows the collated data for all participants. The circles show the proportion correct at each time interval, and the curves are the cumulative gaussian fitted to that data. The no lens condition has a 50% curve threshold of 0.36s (at 72.1%), at which the slope is 0.294, and the lapse rate (upper asymptote) is 0.054 (5.4%). The monovision condition has a 50% curve threshold of 0.254s (at an absolute value of 67.1%), at which the slope of the curve is 0.096, and the lapsing rate was measured as 0.144 (14.4%).

threshold is plotted at 0.254s with an absolute percentage rate of 67.8%. Each participants data (thresholds, lapse rates, and slope gradients) can be seen in the appendix (figures B.1, B.2, and B.3).

6.2.3. Discussion

The experiment which has been conducted suggests that there is not a significant benefit, with regards to the speed and identification of patterns in a random dot stereogram, in monovision glasses over standard 3D glasses but nor was there a significant loss in the speed at which participants could perform stereoscopic fusion tasks. The thresholds estimated for each participant were not significantly different between the two conditions. There was also no statistically significant result with regards to the participants certainty of the stimulus around the threshold values (indicated by differences in the steepness of the slope of the estimates psychometric function).

It has been reported that monovision can impair stereopsis, particularly under certain conditions and before a period of adaptation (Evans, 2007). This may be due to the significant effect of blur information when solving binocular correspondence problems (Hoffman & Banks, 2010). Some studies suggest that stereoacuity is impaired even when monovision is long standing (Fawcett *et al.*, 2001) despite several accounts of individuals who subjectively report adaption after a period of time (Collins *et al.*, 1994; Johannsdottir & Stelmach, 2001). This suggests that despite no quantifiable improvement in stereopsis, participants may feel more comfortable with the effects of monovision after a period of adjustment, and the reduction in stereopsis might explain the partial increase in the lapse rate during the monovision condition.

The impairment of stereoacuity may or may not be a problem for recreational viewing, but due to the nature of this application it would not be feasible to allow an adaptation period prior to viewing. It should also be noted that there are many anecdotal accounts on the internet of people who have had difficulty viewing 3D movies following monovision correction, although the exact prescription and visual quality in each of these accounts is unknown. Additional studies may be required to further investigate the short term effects of monovision in recreational viewing. We have run an additional experiment (section 6.3) in addition to this one; investigating comfort and performance during continuous sustained viewing of a moving stereoscopic image using the no lens and monovision conditions.

6.3. Comfort Experiment: Visual Fatigue

In this experiment the participant viewed a stimulus (as shown in figure 6.12) composed of monocular stereo images which gradually changed in the magnitude of disparity and, consequently, perceived depth. The participant would maintain fixation on the target and perform a basic task as a performance related measure, but also as a means of reducing boredom or drift during the duration of the trial. This was a 4-alternative forced choice (4AFC) task which involved identifying which circle, out of four, was at a depth different to the others present in the stimulus. The user was presented with response feedback in

the form of a green (correct) or red (incorrect) stimulus colour change. The stimulus would oscillate from 0.25 dioptres (simulated depth behind the screen) to -1.5 dioptres (simulated depth in front of the screen).

The participant was also requested to complete a short questionnaire following each condition which allowed them to indicate the severity of symptoms they experienced during the trial. These symptoms included headaches, eye tiredness, blurry vision, etc. Each question was multiple choice using a 7-point Likert scale. One session questionnaire was completed following the no lens condition, then the same session questionnaire after the monovision condition, and finally a comparative questionnaire was issued which queried the participant on their preferences for either condition (the full questionnaire can be seen in the appendix).

6.3.1. Methods

6.3.1.1. Participants

This experiment was initially completed by cohort of participants who had completed the time-to-fuse experiment. They were aware of the experimental condition to varying degrees but each had been aware of the presence of a monovision focal arrangement in the previous condition (most participants were aware of this soon after wearing the glasses). Additional participants were recruited who were not aware of the experimental conditions. This was following ethical approval for all participants to be entered into a prize draw to win a £100 amazon gift voucher. Participants were not informed of the experimental condition and were only given instruction with regards to completing the task. All participants were informed of their right to withdraw from the study, or the prize draw. We subsequently excluded 10 participants after reviewing their data. This was due to erratic results which strongly suggest that the participant was not capable of completing the task. The final results are based on the data from 8 participants. This is a small sample size, which may impact the reliability of the results that we found, particularly in the qualitative data.

6.3.1.2. Apparatus and Stimuli

The apparatus was identical to that described in the previous experimental condition (detailed in 6.2.1.2) but the position of the equipment was changed to allow a reduced angular resolution and appropriately sized stimulus offset. The chin mount was now fitted at a distance of 2 metres from the display (LG-D2343P 58cm Full-HD 3D monitor). The glasses were identical (a pair glasses with no focal power in either lens, and a monovision pair which had a 1 dioptre lens in the right eye) but an additional pair of polarised glasses were introduced to the priming phase to reduce the likelihood that participant would notice the monovision condition, as well as ensuring that the priming tasks were consistent between sessions.

The stimulus consisted of a white diamond with an X through the centre. This stimulus would begin at -0.25 dioptres and appear to travel towards the participant as the disparity increased to a simulated distance of 1.5 dioptres relative to the position of the display. As the display was positioned at 0.5D (2m), this was equivalent to a distance ranging from 2D (0.5m) to 0.25D (4m) relative to the participant. The disparity, in pixels, equivalent to these simulated depths was calculated using equation 6.2. The stimulus took 5 seconds to travel between these two distances. The diamond stimulus subtended approximately 1.99° on the retina, and an example of the stimulus at a given disparity can be seen in figure 6.12.

The participant was presented with 4 circles within the stimulus pattern (as seen in Figure 6.12) every 3 seconds. The circles would be presented at a depth equivalent to the diamond stimulus, but one of these circles would have a slightly greater offset giving the impression that it is slightly closer than the others. This target circle would be presented with an offset of either 0,2,4,6, or 8 pixels. This pixel values are equivalent to a disparity of 0, 0.93, 1.86, 2.79, and 3.72 arcmin.

6.3.1.3. Procedure

The participant was invited into the room, and asked to sit comfortably in the chair before the chin rest. They were informed of their right to withdraw at any point during the study,

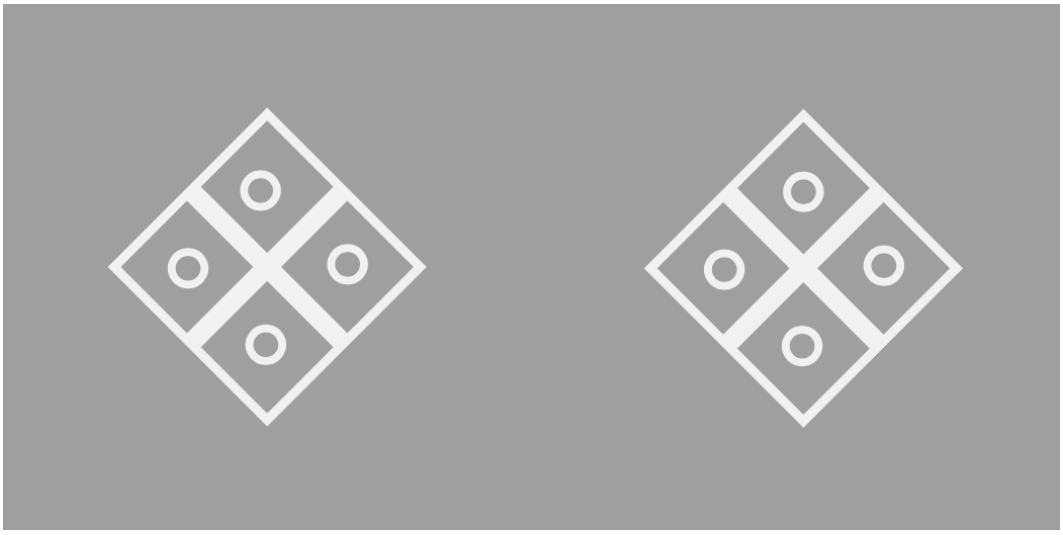

Figure. 6.12: the stimulus presented to the observer during the comfort experiment. Each diamond is presented to either eye by alternating the lines of pixels to match either the left or right polarisation of the screen. The observers polarised glasses then mask the opposing image to either eye such that the left diamond is presented to the right eye and the right diamond is presented to the left eye. This creates the illusion of depth to the position at which the line of sight intersects in front of the screen. The stimulus on this page can be cross-fused, there is one disparate circle.

and if they had not done so, they were asked to complete a consent form. The participant was informed that there were three pairs of glasses in front of them that would be used during the course of the experiment, each numbered. The first sub-session involved wearing the plastic 3D glasses and viewing the stimulus pattern for 1 minute while performing the 4-AFC task. This was to familiarise the participant with the task and allow them to experience the magnitude of disparity before initiating the main experiment. The results of this initial priming phase were not recorded.

At the start of the session, the computer randomly selected and asked the participant to wear one of the other two pairs of glasses by displaying its corresponding number. The participant then began the main session which involved viewing the stimulus for 10 minutes, and responding to the 4-AFC task. The stimulus was initially presented at 0.25 D (uncrossed disparity, i.e. behind the display), and the stereo images decreased in disparity

through 0 dioptres (equivalent depth of the display), and then continued moving towards the participant (crossed disparity, i.e. in front of the screen) at a simulated depth of 1.5D; this transition took 5 seconds. The circles were presented for the 4-AFC task at intervals of 3 seconds, and the participant responded to these presentations in real time. If the participant indicated the correct response by pressing the corresponding arrow key then the stimulus turned green for a short duration, and red if the participant responded incorrectly. The response would always be correct during presentations in which there was not a disparate circle (i.e. when all circles were displayed at the same depth).

Upon completion of the 10 minute session, the participant was asked to complete a session questionnaire which asked them to rate how they felt on a 7-point likert scale for symptoms including eye tiredness, blurry vision, nausea, neck and back tiredness, eye strain and headache. Another session was then arranged for the following day to allow sufficient recovery time. The procedure was then repeated but the computer would instruct the participant to wear the other pair of glasses. Following this second session the participant completed a second (identical) session questionnaire and the comparison questionnaire which asked them which session they preferred in terms of general fatigue, eye irritation, headache, nausea, and a statement of general preference for one session over the other.

We adjusted the data so that non-responses in the 4-AFC task were totalled, and 25% of this total was added to the correct rate, equivalent to the guess rate for the task. The participants were also given correct response feedback, regardless of their answer, each time there was no disparate circle (i.e. the display disparity was 0 arcmin). In order to correctly plot the data we recorded their responses for this task and plotted the correct number of responses for the curve fitting using the pypsignifit library (Fründ *et al.*, 2011). We also plotted the 4-AFC task on a logarithmic scale as increasing disparity is associated with a logarithmic decline in stereoacuity (Adams *et al.*, 2009).

6.3.2. Results

The results of this experiment show a decreased performance when using the monovision lenses, as well as decreased subjective preference. The session questionnaires asked the participant to rate the severity of symptoms that they experience during the session. The results of the session questionnaires for either condition (no lens or monovision) are shown in figure 6.13, where the bars represent the median values in the dataset.

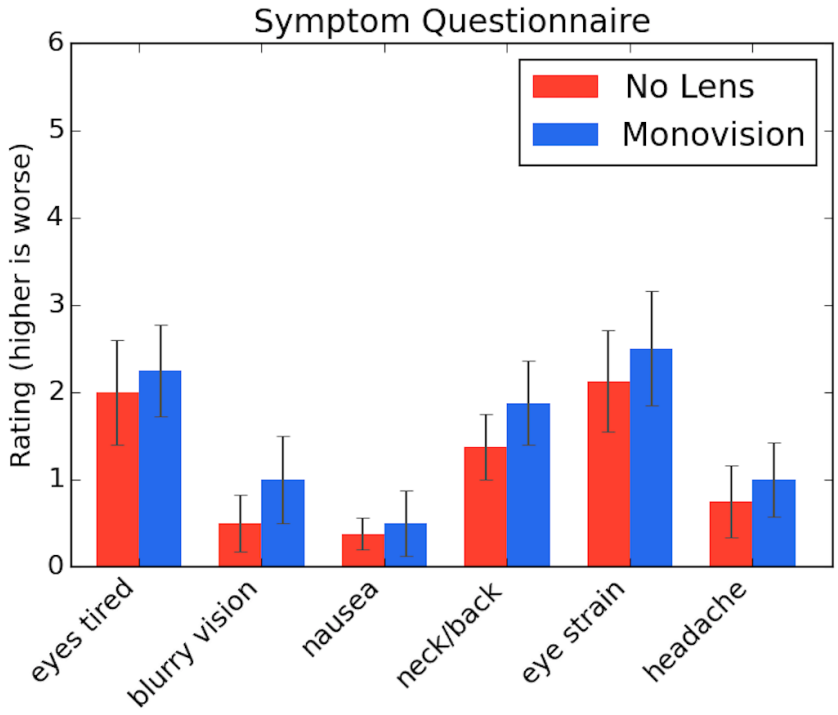

Figure. 6.13: the results of the session questionnaires, where the red bars represent the median of responses after the no lens condition, and the green bars represent the median of responses to the monovision condition. The responses are based on a 7-point likert scale (0-6), where 0 indicates no effect, and 6 indicates a severe effect of the symptom listed on the abscissa. There were no significant differences for any symptom between conditions (Wilcoxon signed-rank test)

The responses to symptoms experienced during either session suggests that there is little difference in the severity of the symptoms. The participants should not have felt any difference in neck strain between the two conditions unless the chair had been adjusted, or

they were fatigued due to extraneous factors. The only other symptom in which there was a difference in the median value of the reported severity of a symptom was eye tiredness, this is is shown in the left hand red and green bars in figure 6.13. When we compared the responses regarding each symptom in either condition to a Wilcoxon signed-rank test, we find that there is not a significant difference between the no lens and monovision conditions for any of the queried symptoms.

The results of the comparison questionnaire show that there was an overall preference for the no lens condition. The results are shown in figure 6.14. The range of available responses was from -3 to -1 indicating a strong to weak preference for the first session, 0 indicated that there was no difference between sessions, and 1 to 3 indicated a weak to strong preference for the second session. The order in which the participants conducted the experiments was randomised, so we normalised the responses to correspond to either the no lens or monovision condition (rather than the first and second sessions).

The symptoms in figure 6.14 are highlighted along the abscissa, and the value of the bar, based on the median of participant responses, indicates which session was preferred (i.e. which reduced the specific symptom). This is with the exception of the final value on the abscissa ('prefer') which was a simple indication of which condition the participant preferred. There was not a significant difference in the preference for either condition when asked about specific symptoms, but their overall preference (the right hand bar in figure 6.14) was significantly different as compared with the null hypothesis ($p=0.039$).

We also recorded the data which was produced through the 4-AFC task performed by the participant while watching the stimulus for each 10 minute session. The participant was asked to identify which circle was at a different disparity with respect to the stimulus and the other three circles. The data corresponding to their responses is shown in figure 6.15. This data shows the number of correct responses, the number of incorrect responses, and the number of times the participant did not respond.

The cohort of participants included in the final dataset could perform the task reasonably well at all disparity values, and only omitted a response on a small number of presentations

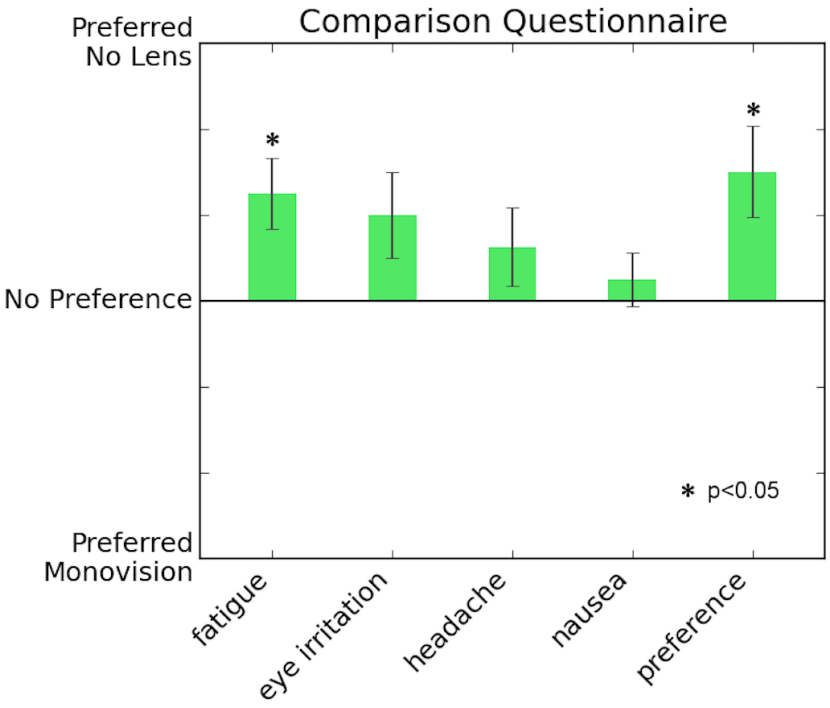

Figure. 6.14: the comparison questionnaire asked which session was worse for a range of symptoms, as well as an overall statement of preference for one session over the other. The median results from this questionnaire are generally weighted towards the no lens condition, with only 1 out of 8 participants indicating a preference for the monovision condition.

(typically below 20% of responses). The answers given in the no lens condition were consistently higher than those given in the monovision condition (with the exception of 0 disparity for which the participant was always correct, provided a response was given). The disparity of the circles did have a small effect on the proportion of incorrect answers but this trend is not very strong and, as such, the effect which dominates the increase in lapse rate between the conditions is unclear.

If we take the data for a single participant, and plot the proportion of correct answers and a cumulative gaussian function using the pypsignifit library (Früind *et al.*, 2011), we can calculate estimates for the thresholds, lapse rates, and steepness of the slope. The procedure was similar to that detailed in section 6.2.1.3. In figure 6.16, we see this data for participant

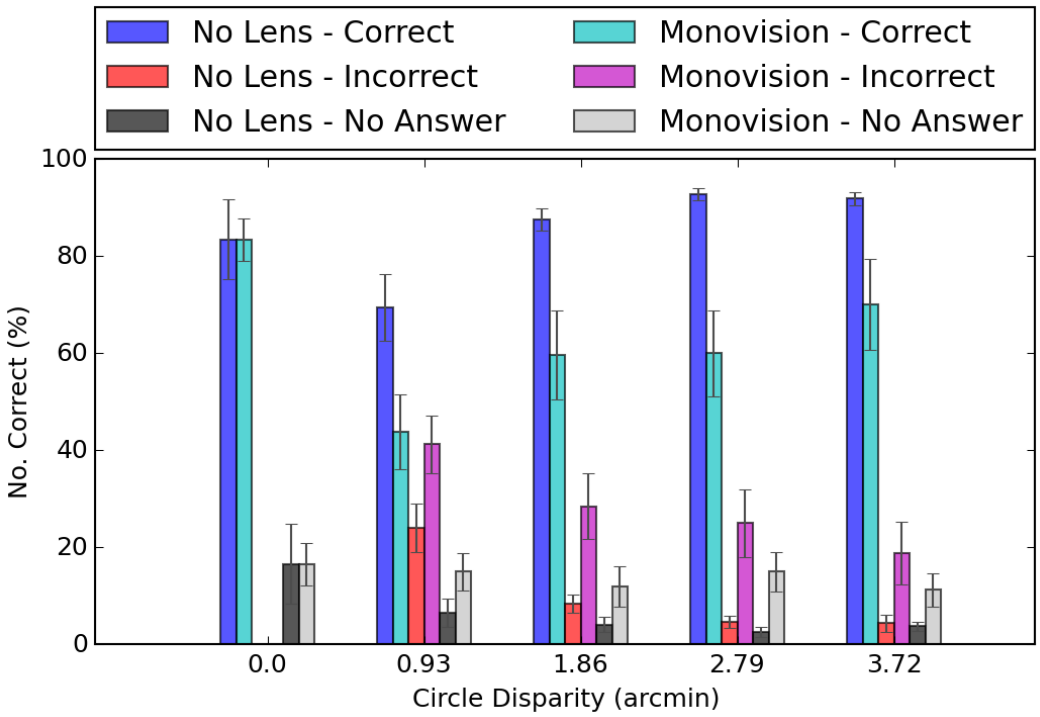

Figure. 6.15: the data from the 4-AFC task contains information regarding the number of correct responses, incorrect responses and non-responses (where the the participant did not provide a response). This data is provided for each of the disparity values.

HBR.

We fitted an equivalent curve to the data for each participant, and plotted the estimated thresholds and 95% confidence intervals, as shown in figure 6.17. The threshold between the values for the two conditions differ significantly (p=0.012). The slope (p=0.123) and lapse rate (p=0.208) of the two conditions differ, but not significantly. All data and fitted trend lines can be seen in the appendix (figures C.1, C.2, and C.3).

We then took the proportion of correct responses for each of the disparity value across all participants. In figure 6.18, we have fitted the curve to the mean correct responses in each condition. We can see that the fitted curves differ in the three primary parameters of the psychometric function (threshold, lapse rate, and slope).

The results presented up to this point include data from two participants who were

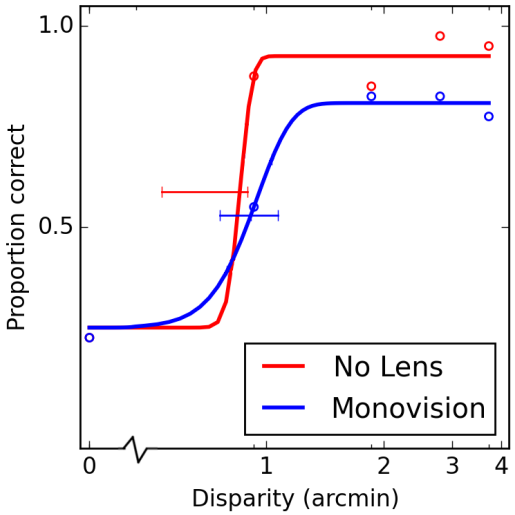

Figure. 6.16: The data and fitted cumulative gaussian for participant HBR, with 95% confidence intervals at the 50% threshold between the upper and lower asymptotes.

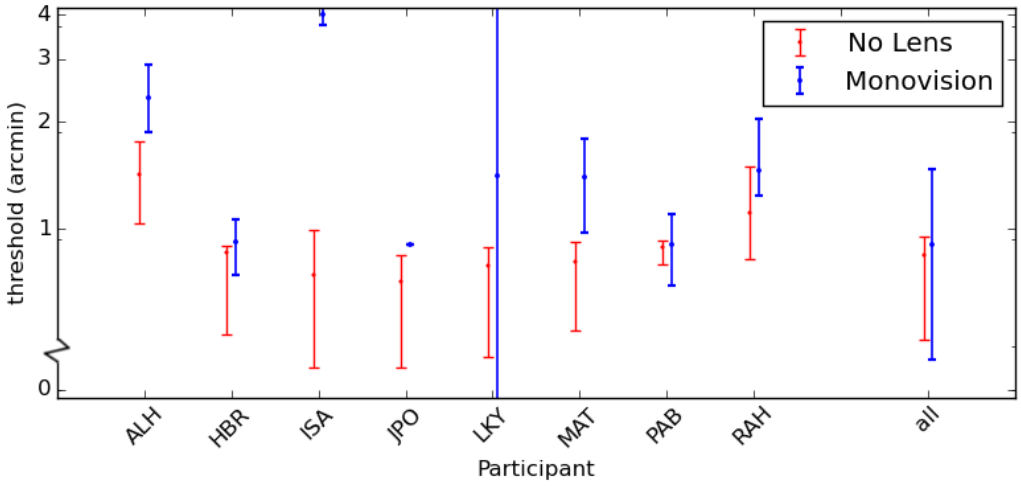

Figure. 6.17: The thresholds and 95% confidence intervals for each participant.

known to the experimenters, and were aware of the experimental condition. We have also run the tests with their data removed to ensure that they had not contaminated the results by introducing a bias. We found that the difference in threshold (full dataset in figure

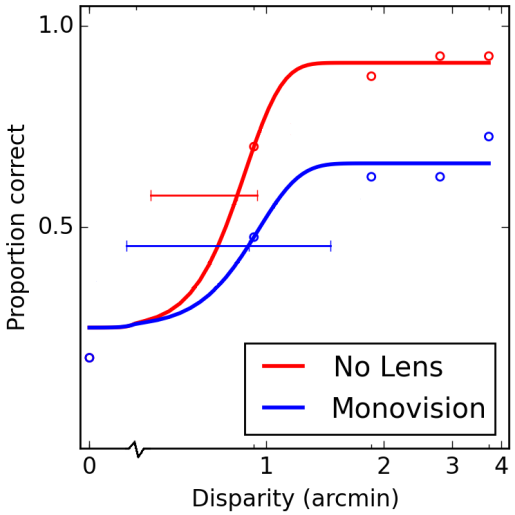

Figure. 6.18: the proportion of correct answers for each disparity value, where the disparity applies to the target circle. The curves are fitted by the pypsignifit library; the red curve is fitted to the no lens condition, and the green curve is fitted to the monovision condition.

6.18) also remained significant (p=0.028), while the difference in the slope and lapsing rate remained non-significant. These are consistent with the original findings. The effect on the questionnaire results was more pronounced, where the previously significant result regarding participant preference for one session over the other was no longer significant (p=0.149). As a consequence of removing these two participants, the 4-AFC task was unaffected (i.e. their performance did not deviate from the cohort) yet the qualitative was significantly altered. This should be taken into account when considering the implications of these findings. The related figures can be seen in the appendix (figures C.4 and C.5).

6.3.3. Discussion

The results of this experiment suggest that monovision is, on average, perceived to be a less preferable approach as compared with standard polarised lenses with no additional prescriptive power (additional to the observers normal prescription if required). The quantitative results of the experiment suggest that, despite a lack of difference in the severity of symptoms reported after each session, people tended to prefer the no lens condition as evidenced

by the comparative questionnaire. Although it is important to note that, while a preference for the no lens condition was given, this was not necessarily a significant difference.

The results from the 4-AFC task in the comfort experiment suggested that participants performed worse during the monovision condition. The overall disparity at which they could detect the target circle was increased as compared with the no lens condition, i.e. they required a larger change in position to identify the disparate circle. This suggests that their stereoacuity may have been compromised, a result which is supported by the data from the performance experiment in which participants tended to make a greater number of errors when wearing monovision glasses as compared with the no lens glasses.

Monovision may provide an observer with two points of focus, which may assist in reducing the vergence-accommodation conflict but other factors, such as the potential for reduced stereoacuity, result in a decrease performance and preference for this proposed solution.

Participant PAB explicitly reported the effect of perceptual rivalry during the comfort experiment, stating that they "noticed the switching of focus from left to right and could *feel* it". PAB noted that this felt uncomfortable at first, while other participants stated that they did not even identify a difference between the two sets of glasses when they were asked.

It is also important to take care when comparing the results from the performance study and the comfort study as the display distances were very different. This may influence the severity of the vergence-accommodation conflict, and other factors such as microfluctuations may affect the results due to depth of field.

6.4. Conclusions

The results of both experiments, the performance experiment and the comfort experiment, suggest that monovision may not be an effective solution to the problem of the vergence-accommodation conflict. This technique does provide the observer with two simultaneous focal points and, through binocular rivalry, they may be able to direct attentional priority to

the retinal image in best focus. Even if this effect holds, our results suggest that participants may not perform stereo-acuity tasks as accurately, and many also indicated a preference for the no lens glasses. The fusion task was marginally faster in the monovision condition during the time to fuse experiment, but this result was not significant, as such further testing with greater rigour and diversity of parameters (such as lens strengths) may prove informative, but the evidence in the literature supports the conclusion that monovision presents more complications than benefits.

This study would have benefited from testing participants prior to their involvement. This may have included visual acuity/refractive error testing for each eye, as well as a stereoacuity test. This would have complimented the results and given further insight into those participants who did prefer the monovision condition (participants JEH and PAB), or those who performed with greater speed or accuracy (participants JEH and TH1). We also did not test the participants dominant eye, and this may have an effect on the efficacy of monovision. The decline in performance, and negative subjective reports, are the biggest concern following the results of this study. This may be due to reduced stereoacuity, or simply because participants find monovision an unusual and unfamiliar perspective as initially documented by many who accept monovision as a form of presbyopia correction.

Richards (1970) have shown that it is possible that a proportion of the population suffer from stereoblindness, and degradation in stereopsis. They have attributed this to an inherited physiological capacity for stereoscopic processing in either hemisphere in the brain. They suggest that an individual lacking in this ability in either hemisphere may suffer stereoblindness. They note that their research suggests that a lack of stereopsis occurs in the population at about a rate of 2.9%, similar to the incidence of squint.

It is also possible that a bias in the decision making process for fast presentations could be influenced by the number of previous presentations of a given orientation. The participant's intuitive estimation of the probability of outcomes might be affected by the orientation history (Bogacz *et al.*, 2006). The presentation of each orientation was equal in number throughout the trial, but the order in which they occurred was not controlled. If the

participant had previously encountered a larger number of stimuli at -20° then they may be inclined to assume continuance in later trials which were faster than threshold. This could be reduced by randomising the trials over smaller sets of presentations such as 6-10, rather than randomised over a full-set of 50 presentations. The inverse of this problem is also possible, such that participants might assume a weighting towards the opposite of previous orientations. These potential biases can be eliminated through a more rigorous experimental design.

We collected no data regarding the activities the participant engaged in before and after the task. The participant was queried on their perceived level of fatigue, but answers were unanimously 'fine', which may suggest that people were predisposed to answer positively (Brown & Levinson, 1987). We also included a question regarding neck strain. This question was introduced as a null response (where the specific condition should not affect the outcome of the question) and the fact that a difference did exist between the two conditions may suggest that participants were inclined to answer negatively, not due to actual discomfort, but because of a performance bias where they have perceived that session negatively due to their perception of decreased performance.

6.5. Reducing discomfort with focus-correct dynamic-lens displays

This project was in collaboration with researchers at U.C. Berkeley who undertook a related set of experiments, but their investigation involved using a focus-correct display rather than monovision. This display contained variable lenses which changed their refractive power to match the simulated depth of the 3D display. This meant that vergence was equal to accommodation and resolved the vergence-accommodation conflict. They performed the same experiments (with slightly different parameters) as outlined in sections 6.2 and 6.3. They found that their focus-correct display enabled participants to perform better at stereoscopic fusion tasks (in both the 2-AFC and the 4-AFC tasks from either experiment), and overall participants preferred the focus-correct display as compared with traditional 3D viewing methods.

These finding differ from our results, and a key aspect would be the retention of binocular correlation, and a greater range of values where accommodation distance is equal to vergence distance. We speculate that monovision was poorly received due to decreased stereoacuity, and binocular correlation. The disadvantage of the focus-correct system is that it is large and expensive relative to other methods.

Chapter 7

Conclusion

This thesis has covered three distinct aspects of depth perception; the role of aberrations in dynamic accommodation control, the efficacy of monovision as a means of reducing the vergence accommodation conflict, and the function of different shaped pupils and multifocal lenses throughout different species. This section will summarise the findings relevant to each chapter.

Spherical aberration as a cue to the sign of defocus

This chapter investigated the presence of sign information in images formed on either side of focus, when spherical aberration (or astigmatism) is present in the optical system. The data was presented with reference to the human eye as dynamic accommodation control could, hypothetically, be driven by such information. When looking at images formed on either side of focus, astigmatism provides a clear difference in the contrast of spatial frequencies that are oriented parallel or perpendicular to the axis of astigmatism. Spherical aberration also produces images that are different on either side of focus, but the difference is not as apparent as in the astigmatism case. The data we provide shows that in the case of spherical aberration, sign information is present in the spatial frequency content of images, where the high spatial frequencies are attenuated on one side of focus, while on the other it is the low

spatial frequencies which are attenuated. It appears that there are no false positives in the range of defocus values close to best focus, so, in principle, this information could be used by the human visual system to determine the sign of defocus.

Future work

This series of simulations would ideally be followed by a psychophysical investigation to determine if observers can use spherical aberration as a cue to the sign of defocus. This would involve controlling all possible cues including; chromatic aberration, either through a monochromatically illuminated stimulus target or a more complex optical system that would neutralise the chromatic aberration of the eye; monochromatic aberrations, the observers natural aberrations would need to be controlled to isolate individual aberration terms and manipulate (i.e. increase, reduce, or invert) their spherical term according to experimental requirements; microfluctuations, this could be controlled through an variable focus lens or ensuring that their magnitude was less than the observers depth of focus. It may also be prudent to consider any potential cue from the Stiles-Crawford effect as a consequence of the vergence of light entering the eye, this is an effect which is less well documented in recent literature (although this may be due to the difficulty most participants experience in making correct focal steps without chromatic information).

In previous studies, only a limited demographic could estimate the sign of defocus when viewing stimuli under monochromatic conditions. The results of Chen *et al.* (2006) suggest that people vary considerably in their dependency on MCAs for accommodation control. It would also prove beneficial to measure the aberrations of individuals who could perform defocus estimation tasks and further analyse image formation to determine its role in depth estimation. This study could be extended by analysing a more complex model eye, one in which aberrations are combined to produce a complex wavefront representative of aberrations found in eyes of a typical population, such as those described by Porter *et al.* (2001).

An investigation into elongated pupils and multifocal lenses

This project covered a number of different aspects relating to pupils shapes in different species. The aspects of the collaborative project which are less related to depth perception found that pupil shape can be predicted with a high degree of accuracy when the diel activity and trophic strategy of a certain species is known. There also appears to be a relationship between the height of an animal and the pupil shape that it will exhibit. We also show that horizontally elongated pupils are associated with greater throughput of light to the retina across the transverse axis of the retina, and many species with horizontal pupils exhibit cyclovergence which causes the orientation of the pupil to remain parallel to the horizon.

The results of the simulations which model vertically elongated pupils, and multifocal lenses (with a basis in the feline ocular system), do not support the findings of Malmström and Kröger (2006) which suggest that the role of the pupil is to expose all areas of the multifocal lenses when the pupil is constricted. The outer zones of the multifocal lens were occluded when the eye was constricted, and any area which was exposed would make a negligible difference to image quality. We believe that the multifocal lens serves as a means of increasing depth of focus when the pupil is dilated (i.e. during scotopic or mesopic phases). The elongated pupil may serve to increase stereopsis during photopic phases, or simply to provide the animal with a greater range of control of pupillary area.

The other factor which was not considered in the scope of this project was the shape of the eye and retina. This may have a large effect on the image quality at, for example, different eccentricities. We assumed a cylindrical retina in the Zemax model, which introduces hyperopia or myopia at different positions for different pupil shapes, but the magnitude and position of these changes may be dependant on eye shape.

Future work

This study could be enhanced by extending the analysis to include more species. It may also prove beneficial to investigate exceptions to the findings, such as vertically oriented pupils in crocodiles, or horizontally oriented pupils in mongooses. These exceptions may give

additional insight into the function of the adaptations which have occurred due to ecological factors not considered by our study. Additional, comparative, studies could investigate pupil shape in animals which are not included in our subsection of the animal kingdom such as aquatic, avian, or invertebrate species. Additional analysis could be conducted to investigate the differences in benefit between graduated lenses and multifocal lenses for extending depth of focus. Measurements of different aspects of animal eyes would also enhance this study by providing estimates of the size and refractive power of different zones in multifocal lenses. The f-ratio of the eye of relevant species would also provide insight into the presence of adaptations which extend depth of focus. This would complement the theory that height and depth of focus plays a role in pupil shape, as well as providing a plausible case for multifocal lenses.

Can monovision improve simulated 3D viewing?

The viability of utilising monovision as a means of reducing the vergence-accommodation conflict was assessed through a series of psychophysical experiments. The speed at which a participant could cross-fuse a stimulus was measured by presenting a stereogram on the display for a certain length of time. This time decreased when the participant answered correctly, and increased when the participant answered incorrectly. We found that participants could cross-fuse the stimulus marginally faster in the monovision condition, but they were more prone to making mistakes (although neither of these results were statistically significant). The second experiment questioned the participants subjective comfort after viewing a moving stimulus for 10 minutes, while they performed a 4-AFC task. We found that participants preferred the traditional 3D glasses over the monovision glasses. They also performed better in the 4AFC task in the traditional condition. We attributed these findings to a decrease in stereoacuity, which is supported by the literature.

Future work

The number of participants who were eliminated from the study following data collection could have been reduced if an additional 3D acuity test had been employed. The titmus

stereo fly test may have removed participants who were incapable of performing the task to a sufficient standard. The priming phase could also have been a little more rigorous in its elimination of people who could not perform the task well. The cross and circle exercise should be removed as it provided the participant with little information and was comparatively difficult. It would be more beneficial to position the circle and cross below a random dot stereogram to act as a guide towards fusing the pattern where coherent stereo information would allow them to sustain the fixation. The delivery of positive feedback when the participant answered questions that had 0 disparity may also lead to a bias whereby the participant may learn to attend to features which are otherwise uninformative. It may be better to provide the feedback associated with a randomly selected circle, regardless of the assigned disparity.

The time to fuse experiment should be adapted to ensure that the participant converged and diverged on each presentation. It was noted that some participants performed better than anticipated due to an ability to maintain fusion between presentations. This resulted in the elimination of the expected 'guess rate' as the participant could perform better than chance. The presentation of an RDS at the simulated distance, and then a second at the distance of the screen, each requiring a correct response may eliminate this bias from the experiment. If more time was granted then testing participants for anisometropia, and determining eye dominance, might allow the experimental parameters to be adjusted to suit each participant. It would also prove beneficial to measure each participants inter-pupillary distance to reduce the error in depth estimation.

The results of this experiment correlate with findings in the literature regarding stereopsis, and appear to give good evidence to the efficacy of monovision in recreational 3D viewing, but future studies would benefit from the amendments suggested here.

Appendix A

Species

This section contains a list of all species included in the statistical analysis in section 5.1.1.

Species	Common Name	Diel Activity	Foraging Mode	Pupil Shape
Acanthophis antarcticus	Common death adder	Polyphasic	Ambush	Vertical
Acanthophis hawkei	Not found	Polyphasic	Ambush	Vertical
Acanthophis praelongus	Not found	Nocturnal	Ambush	Vertical
Acanthophis pyrrhus	Desert death adder	Nocturnal	Ambush	Vertical
Acanthophis rugosus	Not found	Polyphasic	Ambush	Vertical
Acanthophis wellsi	Not found	Polyphasic	Ambush	Vertical
Acrochordus arafurae	Not found	Nocturnal	Active	Circular
Antaresia childreni	Children's python	Nocturnal	Ambush	Vertical
Antaresia maculosa	Not found	Nocturnal	Ambush	Vertical
Antaresia perthensis	Not found	Nocturnal	Ambush	Vertical
Antaresia stimsoni	Not found	Nocturnal	Ambush	Vertical
Aspidites melanocephalus	Not found	Nocturnal	Ambush	Vertical
Aspidites ramsayi	Not found	Nocturnal	Ambush	Vertical
Austrelaps ramsayi	Not found	Diurnal	Active	Circular
Austrelaps superbus	Lowland copperhead	Diurnal	Active	Circular
Cacophis harriettae	Not found	Nocturnal	Active	Subcircular
Demansia angusticeps	Not found	Diurnal	Active	Circular
Demansia calodera	Not found	Diurnal	Active	Circular
Demansia olivacea	Not found	Diurnal	Active	Circular
Demansia papuensis	Not found	Diurnal	Active	Circular
Demansia psammophis	Not found	Diurnal	Active	Circular
Demansia quaesitor	Not found	Diurnal	Active	Circular
Demansia rimicola	Not found	Diurnal	Active	Circular
Demansia rufescens	Not found	Diurnal	Active	Circular
Demansia simplex	Not found	Diurnal	Active	Circular
Demansia torquata	Not found	Diurnal	Active	Circular
Demansia vestigiata	Not found	Diurnal	Active	Circular
Dendrelaphis punctulata	Not found	Diurnal	Active	Circular
Denisonia devisi	Mud adder	Nocturnal	Ambush	Subcircular
Denisonia maculata	Ornamental snake	Nocturnal	Ambush	Subcircular
Drysdalia coronoides	White-lipped snake	Polyphasic	Active	Circular
Drysdalia mastersii	Not found	Nocturnal	Active	Circular
Drysdalia rhodogaster	Not found	Nocturnal	Active	Circular
Echiopsis curta	Not found	Nocturnal	Ambush	Subcircular
Elapognathus coronata	Not found	Polyphasic	Active	Circular
Elapognathus minor	Short-nosed snake	Nocturnal	Active	Circular
Furina barnardi	Not found	Nocturnal	Active	Subcircular
Furina diadema	Not found	Nocturnal	Active	Subcircular
Furina ornata	Not found	Nocturnal	Active	Subcircular
Furina tristis	Not found	Nocturnal	Active	Subcircular
Hemiaspis damelii	Not found	Nocturnal	Active	Circular
Hemiaspis signata	Not found	Polyphasic	Active	Circular
Hoplocephalus bitorquatus	Not found	Nocturnal	Ambush	Circular
Hoplocephalus bungaroides	Broad-headed snake	Nocturnal	Ambush	Circular
Hoplocephalus stephensii	Not found	Nocturnal	Ambush	Circular
Liasis fuscus	Not found	Nocturnal	Ambush	Vertical

Table A.1

Liasis olivaceus	Not found	Nocturnal	Ambush	Vertical
Morelia amethistina	Not found	Nocturnal	Ambush	Vertical
Morelia bredli	Not found	Nocturnal	Ambush	Vertical
Morelia carinata	Not found	Nocturnal	Ambush	Vertical
Morelia oenpelliensis	Not found	Nocturnal	Ambush	Vertical
Morelia spilota	Not found	Nocturnal	Ambush	Vertical
Morelia viridis	Not found	Nocturnal	Ambush	Vertical
Notechis scutatus	Tiger snake	Diurnal	Active	Circular
Oxyuranus microlepidotus	Inland taipan	Diurnal	Active	Circular
Oxyuranus scutellatus	Coastal taipan	Diurnal	Active	Circular
Pseudechis australis	Not found	Polyphasic	Active	Circular
Pseudechis butleri	Not found	Nocturnal	Active	Circular
Pseudechis colletti	Collett's snake	Nocturnal	Active	Circular
Pseudechis guttatus	Not found	Diurnal	Active	Circular
Pseudechis porphyriacus	Red-bellied black snake	Diurnal	Active	Circular
Pseudonaja nuchalis	Not found	Polyphasic	Active	Circular
Pseudonaja textilis	Eastern brown snake	Diurnal	Active	Circular
Simoselaps approximans	Not found	Nocturnal	Active	Circular
Simoselaps australis	Not found	Nocturnal	Active	Circular
Simoselaps bertholdi	Not found	Polyphasic	Active	Subcircular
Simoselaps fasciolatus	Not found	Nocturnal	Active	Subcircular
Simoselaps littoralis	Not found	Polyphasic	Active	Subcircular
Suta suta	Not found	Nocturnal	Active	Subcircular
Tropidechis carinatus	Not found	Polyphasic	Active	Circular
Tropidonophis mairii	Not found	Nocturnal	Active	Circular
Felis catus	Domestic cat	Polyphasic	Ambush	Vertical
Felis silvestris	Wildcat	Polyphasic	Ambush	Vertical
Felis libyca	African wildcat	Polyphasic	Ambush	Vertical
Felis bieti	Chinese mountain cat	Nocturnal	Ambush	Vertical
Felis margarita	Sand cat	Nocturnal	Ambush	Vertical
Felis nigripes	Blackfooted cat	Nocturnal	Ambush	Vertical
Felis chaus	Jungle cat	Polyphasic	Ambush	Vertical
Otocolobus manul	Pallas' cat	Polyphasic	Ambush	Circular
Prionailurus rubiginosus	Rusty-spotted cat	Nocturnal	Ambush	Vertical
Prionailurus bengalensis	Leopard cat	Polyphasic	Ambush	Vertical
Prionailurus viverrinus	Fishing cat	Nocturnal	Ambush	Vertical
Prionailurus planiceps	Flat-headed cat	Polyphasic	Ambush	Vertical
Puma concolor	Cougar	Nocturnal	Ambush	Circular
Puma yagouaroundi	Jaguarundi	Diurnal	Ambush	Circular
Acinonyx jubatus	Cheetah	Diurnal	Active	Circular
Lynx pardinus	Iberian lynx	Polyphasic	Ambush	Subcircular
Lynx lynx	Lynx	Polyphasic	Ambush	Subcircular
Lynx canadensis	Canada lynx	Polyphasic	Ambush	Subcircular
Lynx rufus	Bobcat	Polyphasic	Ambush	Subcircular
Leopardus pardalis	Ocelot	Nocturnal	Ambush	Vertical
Leopardus wiedii	Margay	Nocturnal	Ambush	Vertical
Leopardus braccatus	Pantanal cat	Polyphasic	Ambush	Vertical
Leopardus colocolo	Colocolo	Polyphasic	Ambush	Vertical
Leopardus geoffroyi	Geoffroy's cat	Nocturnal	Ambush	Vertical
Leopardus guigna	Kodkod	Polyphasic	Ambush	Vertical

Table A.2

Leopardus tigrinus	Oncilla	Polyphasic	Ambush	Vertical
Caracal caracal	Caracal	Polyphasic	Ambush	Subcircular
Caracal aurata	African golden cat	Polyphasic	Ambush	Vertical
Caracal serval	Serval	Nocturnal	Ambush	Vertical
Pardofelis temminckii	Asian golden cat	Diurnal	Ambush	Circular
Pardofelis marmorata	Marbled cat	Nocturnal	Ambush	Vertical
Panthera leo	Lion	Nocturnal	Ambush	Circular
Panthera onca	Jaguar	Polyphasic	Ambush	Circular
Panthera pardus	Leopard	Polyphasic	Ambush	Circular
Panthera tigris	Tiger	Nocturnal	Ambush	Circular
Panthera uncia	Snow leopard	Polyphasic	Ambush	Circular
Neofelis nebulosa	Clouded leopard	Nocturnal	Ambush	Vertical
Crocuta crocuta	Spotted hyena	Nocturnal	Active	Vertical
Genetta genetta	Common genet	Nocturnal	Ambush	Vertical
Canis lupus	Gray wolf	Nocturnal	Active	Circular
Canis latrans	Coyote	Diurnal	Active	Circular
Canis simensis	Ethiopian wolf	Polyphasic	Active	Circular
Canis aureus	Golden jackal	Polyphasic	Active	Circular
Canis adustus	Side-striped jackal	Nocturnal	Active	Circular
Canis mesomelas	Black-backed jackal	Nocturnal	Active	Circular
Cuon alpinus	Dhole	Diurnal	Active	Circular
Lycaon pictus	African wild dog	Polyphasic	Active	Circular
Cerdocyon thous	Crab-eating fox	Nocturnal	Ambush	Vertical
Lycalopex culpaeus	Culpeo	Polyphasic	Ambush	Vertical
Lycalopex fulvipes	Darwin's fox	Polyphasic	Active	Vertical
Lycalopex griseus	South american gray fox	Nocturnal	Ambush	Vertical
Lycalopex gymnocercus	Pampas fox	Nocturnal	Ambush	Vertical
Lycalopex sechurae	Sechuran fox	Nocturnal	Ambush	Vertical
Lycalopex vetulus	Hoary fox	Nocturnal	Active	Vertical
Chrysocyon brachyurus	Maned wolf	Polyphasic	Ambush	Circular
Speothos venaticus	Bush dog	Diurnal	Active	Circular
Vulpes lagopus	Arctic fox	Polyphasic	Ambush	Vertical
Vulpes vulpes	Red fox	Polyphasic	Ambush	Vertical
Vulpes velox	Swift fox	Nocturnal	Ambush	Vertical
Vulpes macrotis	Kit fox	Nocturnal	Ambush	Vertical
Vulpes corsac	Corsac fox	Nocturnal	Ambush	Vertical
Vulpes chama	Chama fox	Nocturnal	Ambush	Vertical
Vulpes pallida	Pale fox	Nocturnal	Ambush	Vertical
Vulpes bengalensis	Bengal fox	Polyphasic	Ambush	Vertical
Vulpes cana	Blanfords fox	Nocturnal	Ambush	Vertical
Vulpes rueppelli	Rueppell's fox	Nocturnal	Ambush	Vertical
Vulpes zerda	Fennec fox	Nocturnal	Active	Vertical
Urocyon cinereoargenteus	Gray fox	Nocturnal	Ambush	Vertical
Urocyon littoralis	Island fox	Polyphasic	Active	Vertical
Otocyon megalotis	Bat-eared fox	Nocturnal	Active	Vertical
Nyctereutes procyonoides	Raccoon dog	Nocturnal	Ambush	Vertical
Bassaricyon gabbi	Northern olingo	Nocturnal	Herbivorous	Horizontal
Cryptoprocta ferox	Fossa	Polyphasic	Ambush	Vertical
Fossa fossana	Malagasy civet	Nocturnal	Active	Vertical
Galidia elegans	Ring-tailed mongoose	Diurnal	Active	Horizontal

Table A.3

Suricata suricatta	Meerkat	Diurnal	Active	Horizontal
Herpestes auropunctatus	Small asian mongoose	Diurnal	Active	Horizontal
Helogale parvula	Common dwarf mongoose	Diurnal	Active	Horizontal
Cynictis penicillata	Yellow mongoose	Polyphasic	Active	Horizontal
Paracynictis selousi	Selous' mongoose	Nocturnal	Ambush	Horizontal
Ailurus fulgens	Red panda	Polyphasic	Herbivorous	Subcircular
Camelus bactrianus	Bactrian camel	Diurnal	Herbivorous	Horizontal
Camelus dromedarius	Dromedary	Diurnal	Herbivorous	Horizontal
Lama glama	Llama	Diurnal	Herbivorous	Horizontal
Lama guanicoe	Guanaco	Diurnal	Herbivorous	Horizontal
Vicugna pacos	Alpaca	Diurnal	Herbivorous	Horizontal
Vicugna vicugna	Vicuna	Diurnal	Herbivorous	Horizontal
Hippopotamus amphibius	Hippopotamus	Nocturnal	Herbivorous	Horizontal
Hexaprotodon liberiensis	Pygmy hippopotamus	Nocturnal	Herbivorous	Horizontal
Equus ferus	Horse	Diurnal	Herbivorous	Horizontal
Equus africanus	Donkey	Diurnal	Herbivorous	Horizontal
Equus quaga	Plains zebra	Diurnal	Herbivorous	Horizontal
Okapia johnstoni	Okapi	Diurnal	Herbivorous	Horizontal
Giraffa camelopardalis	Giraffe	Polyphasic	Herbivorous	Horizontal
Odocoileus virginianus	White-tailed deer	Polyphasic	Herbivorous	Horizontal
Gazella dorcas	Dorcas gazelle	Nocturnal	Herbivorous	Horizontal
Tapirus terrestris	Brazilian tapir	Polyphasic	Herbivorous	Circular
Tapirus indicus	Malayan tapir	Nocturnal	Herbivorous	Circular
Tapirus bairdii	Baird's tapir	Nocturnal	Herbivorous	Circular
Tapirus pinchaque	Mountain tapir	Polyphasic	Herbivorous	Circular
Ceratotherium simum	White rhinoceros	Polyphasic	Herbivorous	Circular
Diceros bicornis	Black rhinoceros	Polyphasic	Herbivorous	Circular
Rhinoceros unicornis	Indian rhinoceros	Polyphasic	Herbivorous	Circular
Loxodonta africana	African elephant	Diurnal	Herbivorous	Circular
Elephas maximus	Asian elephant	Diurnal	Herbivorous	Circular
Connochaetes taurinus	Common wildebeest	Diurnal	Herbivorous	Horizontal
Bison Bison	American bison	Diurnal	Herbivorous	Horizontal
Bison Bonasus	European bison	Diurnal	Herbivorous	Horizontal
Litocranius walleri	Gerenuk	Diurnal	Herbivorous	Horizontal
Ourebia ourebi	Oribi	Polyphasic	Herbivorous	Horizontal
Raphicerus campestris	Steenbok	Diurnal	Herbivorous	Horizontal
Procapra gutturosa	Mongolian gazelle	Polyphasic	Herbivorous	Horizontal
Oreotragus oreotragus	Klipspringer	Polyphasic	Herbivorous	Horizontal
Redunca redunca	Bohor reedbuck	Nocturnal	Herbivorous	Horizontal
Pelea capreolus	Grey rhebok	Diurnal	Herbivorous	Horizontal
Cervus elaphus	Red deer	Polyphasic	Herbivorous	Horizontal
Pudu mephistophiles	Pudu	Polyphasic	Herbivorous	Horizontal
Mazama gouazoubira	Gray brocket	Polyphasic	Herbivorous	Horizontal
Tragulus napu	Greater mouse-deer	Nocturnal	Herbivorous	Horizontal
Hyemoschus aquaticus	Water chevrotain	Nocturnal	Herbivorous	Horizontal
Tragulus javanicus	Java mouse-deer	Nocturnal	Herbivorous	Horizontal
Procavia capensis	Rock hyrax	Polyphasic	Herbivorous	Horizontal
Heterohyrax brucei	Yellow-spotted rock hyrax	Diurnal	Herbivorous	Horizontal
Equus zebra	Mountain zebra	Diurnal	Herbivorous	Horizontal
Equus hemionus	Onager	Polyphasic	Herbivorous	Horizontal

Table A.4

Cynomys ludovicianus	Black-tailed prairie dog	Diurnal	Herbivorous	Circular
Tamias striatus	Eastern chipmunk	Diurnal	Herbivorous	Circular
Sus scrofa	Wild boar	Polyphasic	Herbivorous	Circular
Sus barbatus	Bornean bearded pig	Diurnal	Herbivorous	Circular
Chrysemys picta	Painted turtle	Diurnal	Active	Circular
Pseudemys alabamensis	Alabama red-bellied cooter	Diurnal	Active	Circular
Alligator mississippiensis	American alligator	Nocturnal	Ambush	Vertical
Crocodylus porosus	Saltwater crocodile	Nocturnal	Ambush	Vertical
Sphenodon punctatus	Northern tuatara	Nocturnal	Ambush	Vertical
Gekko gecko	Tokay gecko	Nocturnal	Ambush	Vertical
Iguana Iguana	Green iguana	Nocturnal	Herbivorous	Subcircular
Xenosaurus Grandis	Knob-scaled lizard	Diurnal	Ambush	Circular
Agkistrodon piscivorus	Cottonmouth	Polyphasic	Ambush	Vertical
Coluber constrictor	Yellow-bellied racer	Diurnal	Ambush	Circular
Boa constrictor	Boa constrictor	Nocturnal	Ambush	Vertical
Pituophis catenifer	Western gopher snake	Diurnal	Active	Circular
Sistrurus catenatus	Massasauga rattlesnake	Polyphasic	Ambush	Vertical
Thamnophis sirtalis	Common garter snake	Polyphasic	Ambush	Circular

Table A.5

Appendix B

Time to Fuse

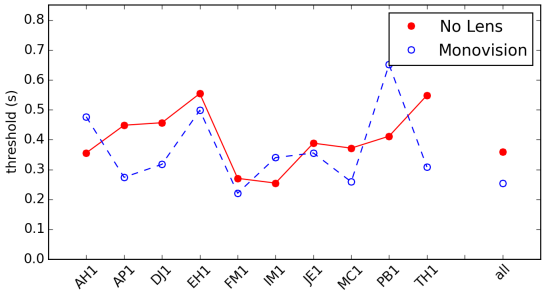

Figure. B.1: the threshold for a position half way between the curve maximum and minimum, for each participant. The abscissa shows the participants identifier, and the ordinate shows the threshold as a proportion correct.

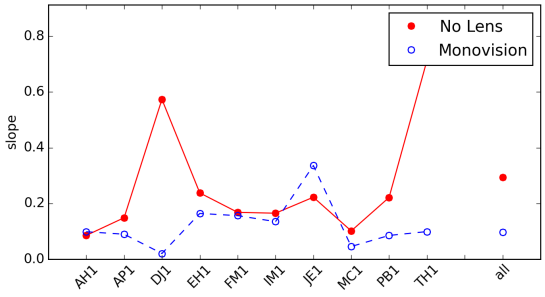

Figure. B.2: the slope of the curves at the mid-point threshold for each participant. The abscissa shows the participants identifier, and the ordinate shows the gradient of the slope at a mid-point on the curve. This slope is associated with subject uncertainty with regards to the stimulus, i.e. a distinct threshold has not been established due the effect of the independent variable in the given condition.

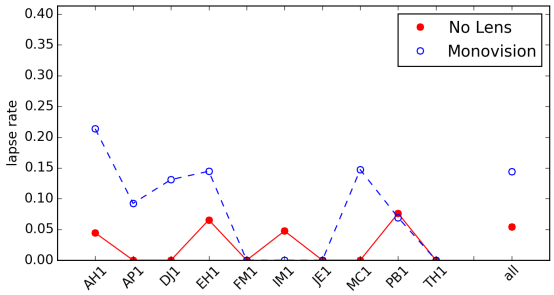

Figure. B.3: the lapse rate for each participant. The abscissa shows the participants identifier, and the ordinate shows the lapse rate as a proportion correct (100x for percentage). The lapse rate is the maximum rate at which the participant answers correctly due to errors at the longer stimulus presentation times.

Appendix C

Comfort

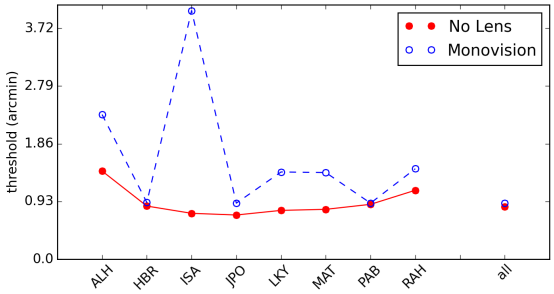

Figure. C.1: the thresholds for the no lens and monovision conditions estimated for each participant listed on the abscissa (no lens vs. Monovision: p=0.026)

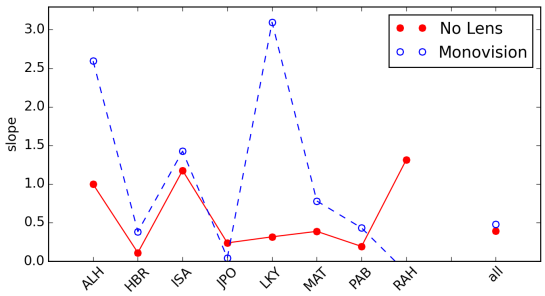

Figure. C.2: the slopes for the no lens and monovision conditions estimated for each participant listed on the abscissa. (no lens vs. Monovision: p=0.081)

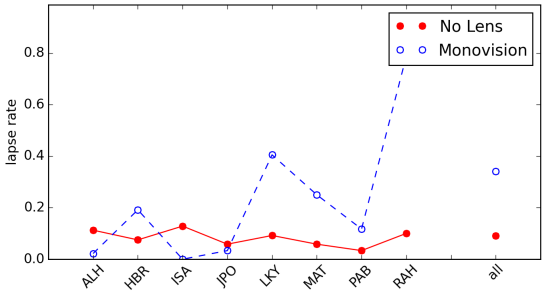

Figure. C.3: the lapse rates for the no lens and monovision conditions estimated for each participant listed on the abscissa. (no lens vs. Monovision: p=0.137)

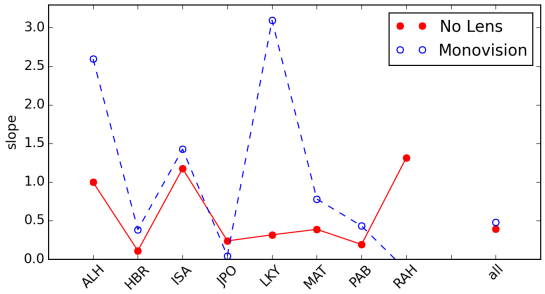

Figure. C.4: The session questionnaire data with participants LKY and MAT removed, who were known to the experimenters.

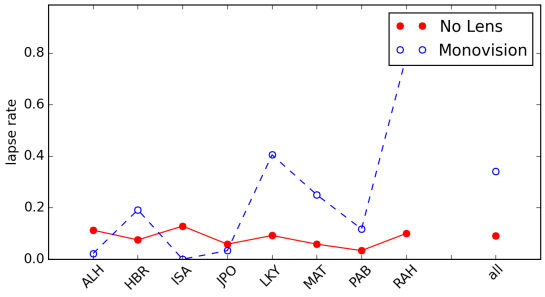

Figure. C.5: The comparison questionnaire data with participants LKY and MAT removed, who were known to the experimenters.

References

Adams, W. E., Leske, D. A., Hatt, S. R., & Holmes, J. M. (2009, February). Defining real change in measures of stereoacuity. *Ophthalmology*, *116*(2), 281–5. Retrieved from `http://www.pubmedcentral.nih.gov/articlerender.fcgi?artid=3903340\&tool=pmcentrez\&rendertype=abstract` doi: 10.1016/j.ophtha.2008.09.012

Aggarwala, K. R., Kruger, E. S., Mathews, S., & Kruger, P. B. (1995). Spectral bandwidth and ocular accommodation. *J. Opt. Soc. Am.*, *12*(3), 450–455.

Alarcón, A., Anera, R. G., Villa, C., Jiménez del Barco, L., & Gutierrez, R. (2011, September). Visual quality after monovision correction by laser in situ keratomileusis in presbyopic patients. *J. Cataract Refract. Surg.*, *37*(9), 1629–35. Retrieved from `http://www.sciencedirect.com/science/article/pii/S0886335011008753` doi: 10.1016/j.jcrs.2011.03.042

Applegate, R. A., Sarver, E. J., & Khemsara, V. (2002, January). Are all aberrations equal? *J. Refract. Surg.*, *18*(5), S556–62. Retrieved from `http://www.ncbi.nlm.nih.gov/pubmed/12361157`

Armaly, M. F. (1969, February). The Size and Location of the Normal Blind Spot. *Arch. Ophthalmol.*, *81*(2), 192–201. Retrieved from `http://archopht.jamanetwork.com/article.aspx?articleid=629422` doi: 10.1001/archopht.1969.00990010194009

Artal, P., & Guirao, a. (1998, November). Contributions of the cornea and the lens to the aberrations of the human eye. *Opt. Lett.*, *23*(21), 1713–5. Retrieved from `http://www.ncbi.nlm.nih.gov/pubmed/18091893`

Artal, P., & Tabernero, J. (2010). Optics of human eye : 400 years of exploration from Galileo s time. *Appl. Opt.*, *49*(16), 123–130.

Bailey, I. L., & Lovie, J. E. (1976, November). New design principles for visual acuity letter charts. *Am. J. Optom. Physiol. Opt.*, *53*(11), 740–5. Retrieved from `http://www.ncbi.nlm.nih.gov/pubmed/998716`

Banks, M. S. (2012). *Personal Communication.*

Banks, M. S., Gepshtein, S., & Landy, M. S. (2004, March). Why is spatial stereoresolution so low? *J. Neurosci.*, *24*(9), 2077–89. Retrieved from `http://www.ncbi.nlm.nih.gov/pubmed/14999059` doi: 10.1523/JNEUROSCI.3852-02.2004

Berson, D., Dunn, F., & Takao, M. (2002). Phototransduction by retinal ganglion cells that set the circadian clock. *Science (80-.).*, *295*, 1070–1073. Retrieved from `http://www.sciencemag.org/content/295/5557/1070.short`

Bogacz, R., Brown, E., Moehlis, J., Holmes, P., & Cohen, J. D. (2006, October). The physics of optimal decision making: a formal analysis of models of performance in two-alternative forced-choice tasks. *Psychol. Rev.*, *113*(4), 700–65. Retrieved from `http://`

www.ncbi.nlm.nih.gov/pubmed/17014301 doi: 10.1037/0033-295X.113.4.700

Bowmaker, J. K., & Dartnall, H. J. (1980, January). Visual pigments of rods and cones in a human retina. *J. Physiol.*, *298*, 501–11. Retrieved from http://www.pubmedcentral.nih.gov/articlerender.fcgi?artid=1279132\&tool=pmcentrez\&rendertype=abstract

Brach, V. (1977). The functional significance of the avian pecten: a review. *Condor*. Retrieved from http://www.jstor.org/stable/1368009

Brischoux, F., Pizzatto, L., & Shine, R. (2010, September). Insights into the adaptive significance of vertical pupil shape in snakes. *J. Evol. Biol.*, *23*(9), 1878–85. Retrieved from http://www.ncbi.nlm.nih.gov/pubmed/20629855 doi: 10.1111/j.1420-9101.2010.02046.x

Brown, B., Yap, M. K., & Fan, W. C. (1993, April). Decrease in stereoacuity in the seventh decade of life. *Ophthalmic Physiol. Opt.*, *13*(2), 138–42. Retrieved from http://www.ncbi.nlm.nih.gov/pubmed/8265147

Brown, P., & Levinson, S. C. (1987). *Politeness: Some Universals in Language Usage*. Cambridge University Press. Retrieved from https://books.google.com/books?hl=en\&lr=\&id=OG7W8yA2XjcC\&pgis=1

Campbell, F., & Westheimer, G. (1960). Dynamics of the Accommodation Responses of the Human Eye. *J. Physiol.*, *151*, 285–295.

Campbell, F. W., & Robson, J. G. (1968). Application of Fourier Analysis to the Visibility of Gratings. *J. Physiol.*(197), 551–566.

Campbell, F. W., Robson, J. G., & Westheimer, G. (1958). Fluctuations of Accommodation under Steady Viewing Conditions. *J. Physiol.*, *145*, 579–594.

Campbell, F. W., & Westheimer, G. (1959, June). Factors influencing accommodation responses of the human eye. *J. Opt. Soc. Am.*, *49*(6), 568–71. Retrieved from http://www.ncbi.nlm.nih.gov/pubmed/13655156

Cartmill, M. (2002). Explaining Primate Origins. In E. M. Peregrine N, Ember C (Ed.), *Phys. anthropol. orig. readings method pract.* (pp. 42–52). Pearson Education.

Chalupa, L., & Werner, J. (2004). *The visual neurosciences*. Retrieved from https://books.google.co.uk/books?hl=en\&lr=\&id=AN-sdYjcyvAC\&oi=fnd\&pg=PR13\&dq=visual+neuroscience+Chalupa,+L.+Werner,+J\&ots=46WZ1IuzYB\&sig=kEnqWbVf1VKx04h0-5P4Wh-hrYM

Changizi, M. a., & Shimojo, S. (2008, October). "X-ray vision" and the evolution of forward-facing eyes. *J. Theor. Biol.*, *254*(4), 756–67. Retrieved from http://www.ncbi.nlm.nih.gov/pubmed/18682253 doi: 10.1016/j.jtbi.2008.07.011

Charman, W. N., & Heron, G. (1988). Fluctuations in accommodation : a review. *Ophthal. Physiol. Opt.*, *8*, 153–164.

Chen, L., Kruger, P. B., Hofer, H., Singer, B., & Williams, D. R. (2006). Accommodation with higher-order monochromatic aberrations corrected with adaptive optics. *J. Opt. Soc. Am. A*, *23*(1), 1–8.

Chin, S. S., Hampson, K. M., & Mallen, E. a. H. (2009, May). Role of ocular aberrations in dynamic accommodation control. *Clin. Exp. Optom.*, *92*(3), 227–237. Retrieved from http://doi.wiley.com/10.1111/j.1444-0938.2009.00361.x doi: 10.1111/j.1444-0938.2009.00361.x

Collins, M., Bruce, A., & Thompson, B. (1994, November). Adaptation to monovision. *Int. Contact Lens Clin.*, *21*(11-12), 218–224. Retrieved from http://www.sciencedirect

.com/science/article/pii/089289679490054X doi: 10.1016/0892-8967(94)90054-X

Collins, M., Davis, B., & Wood, J. (1995, September). Microfluctuations of steady-state accommodation and the cardiopulmonary system. *Vision Res.*, *35*(17), 2491–502. Retrieved from http://www.ncbi.nlm.nih.gov/pubmed/8594816

Crozier, W., & Wolf, E. (1944). Flicker response contours for the sparrow, and the theory of the avian pecten. *J. Gen. Physiol.*. Retrieved from http://jgp.rupress.org/content/27/4/315.abstract

D. G. Pelli, J. G. R. A. J. W. J. (1988). The design of a new letter chart for measuring contrast sensitivity. *Clin. Vis. Sci.*, *2*(3), 187–199. Retrieved from http://citeseerx.ist.psu.edu/viewdoc/summary?doi=10.1.1.321.5971

Dai, G. (2008). *Wavefront optics for vision correction* (No. February). SPIE Press. Retrieved from http://ebooks.spiedigitallibrary.org/book.aspx?bookid=110 doi: 10.1117/3.769212

De Groot, S. G., & Gebhard, J. W. (1952). Pupil Size as Determined by Adapting Luminance. *J. Opt. Soc. Am.*, *42*(7), 492–495.

Dixon, W., & Mood, A. (1948). A method for obtaining and analyzing sensitivity data. *J. Am. Stat. ...*. Retrieved from http://www.tandfonline.com/doi/abs/10.1080/01621459.1948.10483254

Dodgson, N. A. (2004). Variation and extrema of human interpupillary distance. *Proc. SPIE*, *5291*(January), 36–46.

Eadie, A. (1995, July). The use of coherence functions in the study of ocular mechanisms. *Ophthalmic Physiol. Opt.*, *15*(4), 311–317. Retrieved from http://www.sciencedirect.com/science/article/pii/027554089500080W doi: 10.1016/0275-5408(95)00080-W

Erickson, P., & Schor, C. (1990, January). Visual function with presbyopic contact lens correction. *Optom. Vis. Sci.*, *67*(1), 22–8. Retrieved from http://www.ncbi.nlm.nih.gov/pubmed/2407989

Evans, B. J. W. (2007, September). Monovision: a review. *Ophthalmic Physiol. Opt.*, *27*(5), 417–39. Retrieved from http://www.ncbi.nlm.nih.gov/pubmed/17718882 doi: 10.1111/j.1475-1313.2007.00488.x

Fairhall, A. L., Burlingame, C. A., Narasimhan, R., Harris, R. A., Puchalla, J. L., & Berry, M. J. (2006, November). Selectivity for multiple stimulus features in retinal ganglion cells. *J. Neurophysiol.*, *96*(5), 2724–38. Retrieved from http://jn.physiology.org/content/96/5/2724.short doi: 10.1152/jn.00995.2005

Fawcett, S. L., Herman, W. K., Alfieri, C. D., Castleberry, K. A., Parks, M. M., & Birch, E. E. (2001, December). Stereoacuity and foveal fusion in adults with long-standing surgical monovision. *J. AAPOS*, *5*(6), 342–7. Retrieved from http://www.jaapos.org/article/S109185310170818X/fulltext doi: 10.1067/mpa.2001.119785

Fernandes, P. (2013). Adaptation to multifocal and monovision contact lens correction. *Optom. Vis. ...*. Retrieved from http://journals.lww.com/optvissci/Abstract/2013/03000/Adaptation_to_Multifocal_and_Monovision_Contact.7.aspx

Fincham, E. (1951). Tthe accommodation reflex and its stimulus. *Br. J. Ophthalmol.*, *35*, 381–394. Retrieved from http://www.ncbi.nlm.nih.gov/pmc/articles/PMC1323765/

Flitcroft, D. I. (1990, December). A neural and computational model for the chromatic

control of accommodation. *Vis. Neurosci.*, *5*(6), 547–55. Retrieved from http://www.ncbi.nlm.nih.gov/pubmed/2085470

Forrester, J., Dick, A., & McMenamin, P. (2015). *The eye: basic sciences in practice*. Retrieved from https://books.google.co.uk/books?hl=en\&lr=\&id=3i93BwAAQBAJ\&oi=fnd\&pg=PP1\&dq=The+Eye:+Basic+Sciences+in+Practice\&ots=T2mwX84_Ib\&sig=LSHZPfo3PHc3AYSu36uMw7Z9w_U

Fründ, I., Haenel, N. V., & Wichmann, F. A. (2011, January). Inference for psychometric functions in the presence of nonstationary behavior. *J. Vis.*, *11*(6), 16–. Retrieved from http://www.journalofvision.org/content/11/6/16 doi: 10.1167/11.6.16

Fry, G. (1939). Further experiments on the accommodation convergence relationship. *Am J Optom*. Retrieved from http://scholar.google.co.uk/scholar?q=fry+1939+accommodation+convergence\&btnG=\&hl=en\&as_sdt=0,5\#0

Gambra, E., Wang, Y., Yuan, J., Kruger, P. B., & Marcos, S. (2010, September). Dynamic accommodation with simulated targets blurred with high order aberrations. *Vision Res.*, *50*(19), 1922–7. Retrieved from http://www.pubmedcentral.nih.gov/articlerender.fcgi?artid=2926285\&tool=pmcentrez\&rendertype=abstract doi: 10.1016/j.visres.2010.06.015

Garca-Pérez, M. A. (1998, June). Forced-choice staircases with fixed step sizes: asymptotic and small-sample properties. *Vision Res.*, *38*(12), 1861–1881. Retrieved from http://www.sciencedirect.com/science/article/pii/S0042698997003404 doi: 10.1016/S0042-6989(97)00340-4

Garnham, L., & Sloper, J. J. (2006, January). Effect of age on adult stereoacuity as measured by different types of stereotest. *Br. J. Ophthalmol.*, *90*(1), 91–5. Retrieved from http://www.pubmedcentral.nih.gov/articlerender.fcgi?artid=1856927\&tool=pmcentrez\&rendertype=abstract doi: 10.1136/bjo.2005.077719

Gray, L. S., Winn, B., & Gilmartin, B. (1993, October). Accommodative microfluctuations and pupil diameter. *Vision Res.*, *33*(15), 2083–90. Retrieved from http://www.ncbi.nlm.nih.gov/pubmed/8266650

Green, D. M., & Swets, J. A. (1966). *Signal Detection Theory and Psychophysics*. John Wiley and Sons. Retrieved from https://books.google.co.uk/books/about/Signal_Detection_Theory_and_Psychophysic.html?id=yYsQAQAAIAAJ\&pgis=1

Greenbaum, S. (2002, August). Monovision pseudophakia. *J. Cataract Refract. Surg.*, *28*(8), 1439–1443. Retrieved from http://www.sciencedirect.com/science/article/pii/S088633500201218X doi: 10.1016/S0886-3350(02)01218-X

Greene, H. A., & Madden, D. J. (1987, October). Adult age differences in visual acuity, stereopsis, and contrast sensitivity. *Am. J. Optom. Physiol. Opt.*, *64*(10), 749–53. Retrieved from http://www.ncbi.nlm.nih.gov/pubmed/3688177

Hammond, P., & Mouat, G. S. V. (1985). The relationship between feline pupil size and luminance. *Exp Brain Res*, *59*, 485–490.

Hampson, K. M., Munro, I., Paterson, C., & Dainty, C. (2005, July). Weak correlation between the aberration dynamics of the human eye and the cardiopulmonary system. *J. Opt. Soc. Am. A*, *22*(7), 1241–50. Retrieved from http://www.ncbi.nlm.nih.gov/pubmed/16053145http://www.osapublishing.org/viewmedia.cfm?uri=josaa-22-7-1241\&seq=0\&html=true doi: 10.1364/JOSAA.22.001241

Heath, J. E., Northcutt, R. G., & Barber, R. P. (1969). Rotational Optokinesis in Reptiles

and its Bearing on Pupillary Shape. *Z. Vergl. Phyiologie*, *62*, 75–85.

Heesy, C. P. (2004, November). On the relationship between orbit orientation and binocular visual field overlap in mammals. *Anat. Rec. A. Discov. Mol. Cell. Evol. Biol.*, *281*(1), 1104–10. Retrieved from http://www.ncbi.nlm.nih.gov/pubmed/15470671 doi: 10.1002/ar.a.20116

Heesy, C. P. (2005, June). Function of the mammalian postorbital bar. *J. Morphol.*, *264*(3), 363–80. Retrieved from http://www.ncbi.nlm.nih.gov/pubmed/15844100 doi: 10.1002/jmor.10334

Hess, R. F., & Carney, L. G. (1979, May). Vision through an abnormal cornea: a pilot study of the relationship between visual loss from corneal distortion, corneal edema, keratoconus, and some allied corneal pathology. *Invest. Ophthalmol. Vis. Sci.*, *18*(5), 476–83. Retrieved from http://www.ncbi.nlm.nih.gov/pubmed/437949

Hofer, H., Artal, P., Singer, B., Aragón, J. L., & Williams, D. R. (2001, March). Dynamics of the eye's wave aberration. *J. Opt. Soc. Am. A. Opt. Image Sci. Vis.*, *18*(3), 497–506. Retrieved from http://www.ncbi.nlm.nih.gov/pubmed/11265680

Hoffman, D. M., & Banks, M. S. (2010, January). Focus information is used to interpret binocular images. *J. Vis.*, *10*(5), 13. Retrieved from http://jov.arvojournals.org/article.aspx?articleid=2121047 doi: 10.1167/10.5.13

Hoffman, D. M., Girshick, A. R., & Banks, M. S. (2008). Vergenceaccommodation conflicts hinder visual performance and cause visual fatigue. *J. Vis.*, *8*(3), 1–48. doi: 10.1167/8.3.33.Vergence

Holliman, N. S., Dodgson, N. A., Favalora, G. E., & Pockett, L. (2011, June). Three-Dimensional Displays: A Review and Applications Analysis. *IEEE Trans. Broadcast.*, *57*(2), 362–371. Retrieved from http://ieeexplore.ieee.org/articleDetails.jsp?arnumber=5754618 doi: 10.1109/TBC.2011.2130930

Johannsdottir, K. R., & Stelmach, L. B. (2001). Monovision: a review of the scientific literature. *Optom.Vis.Sci.*, *78*(1040-5488), 646–651.

Johnson, G. L. (1901). *Contributions to the comparative anatomy of the mammalian eye.* Retrieved from http://books.google.co.uk/books/about/Contributions_to_the_comparative_anatomy.html?id=Sln-QBMsP3EC\&pgis=1

Johnson, P., & Banks, M. S. (2015). *Personal Communication.*

Kelber, A., & Roth, L. S. V. (2006, March). Nocturnal colour vision–not as rare as we might think. *J. Exp. Biol.*, *209*(Pt 5), 781–8. Retrieved from http://www.ncbi.nlm.nih.gov/pubmed/16481567 doi: 10.1242/jeb.02060

Kelber, A., Vorobyev, M., & Osorio, D. (2003, February). Animal colour vision–behavioural tests and physiological concepts. *Biol. Rev. Camb. Philos. Soc.*, *78*(1), 81–118. Retrieved from http://www.ncbi.nlm.nih.gov/pubmed/12620062

Kiel, J. W. (2010). *Anatomy.* Morgan & Claypool Life Sciences. Retrieved from http://www.ncbi.nlm.nih.gov/books/NBK53329/

Kirschen, D. G., Hung, C. C., & Nakano, T. R. (1999, December). Comparison of suppression, stereoacuity, and interocular differences in visual acuity in monovision and acuvue bifocal contact lenses. *Optom. Vis. Sci.*, *76*(12), 832–7. Retrieved from http://www.ncbi.nlm.nih.gov/pubmed/10612404

Klein, S. a. (2001, November). Measuring, estimating, and understanding the psychometric function: A commentary. *Percept. Psychophys.*, *63*(8), 1421–1455. Retrieved from http://www.springerlink.com/index/10.3758/BF03194552 doi: 10.3758/

BF03194552

Koretz, J. F., Handelman, G. H., & Phelps Brown, N. (1984, January). Analysis of human crystalline lens curvature as a function of accommodative state and age. *Vision Res.*, *24*(10), 1141–1151. Retrieved from http://www.sciencedirect.com/science/article/pii/0042698984901688 doi: 10.1016/0042-6989(84)90168-8

Kotulak, J. C., & Schor, C. M. (1986, January). The accommodative response to subthreshold blur and to perceptual fading during the Troxler phenomenon. *Perception*, *15*(1), 7–15. Retrieved from http://www.ncbi.nlm.nih.gov/pubmed/3774480

Kröger, P. B., López-Gil, N., & Stark, L. (2001). Accommodation and the StilesCrawford effect: theory and a case study. *Ophthalmic Physiol. Opt.*, *21*(5), 339–351. Retrieved from http://www.sciencedirect.com/science/article/pii/S0275540801000047 doi: 10.1016/S0275-5408(01)00004-7

Kröger, P. B., Mathews, S., Katz, M., Aggarwala, K. R., & Nowbotsing, S. (1997, September). Accommodation without feedback suggests directional signals specify ocular focus. *Vision Res.*, *37*(18), 2511–26. Retrieved from http://www.ncbi.nlm.nih.gov/pubmed/9373683

Kröger, R. H., Campbell, M. C., Fernald, R. D., & Wagner, H. J. (1999, April). Multifocal lenses compensate for chromatic defocus in vertebrate eyes. *J. Comp. Physiol. A.*, *184*(4), 361–9. Retrieved from http://www.ncbi.nlm.nih.gov/pubmed/10377973

Kruger, P. B., Nowbotsing, S., & Aggarwala, K. R. (1995). Small Amounts of Chromatic Aberration Influence Dynamic Accommodation. *Optom. Vis. Sci.*, *72*(9), 656–666.

Kruger, P. B., & Pola, J. (1986, January). Stimuli for accommodation: blur, chromatic aberration and size. *Vision Res.*, *26*(6), 957–71. Retrieved from http://www.ncbi.nlm.nih.gov/pubmed/3660618

Kruger, P. B., Stark, L. R., & Nguyen, H. N. (2004, November). Small foveal targets for studies of accommodation and the Stiles-Crawford effect. *Vision Res.*, *44*(24), 2757–67. Retrieved from http://www.sciencedirect.com/science/article/pii/S0042698904003232 doi: 10.1016/j.visres.2004.06.013

Land, M. (2006, March). Visual Optics: The Shapes of Pupils. *Curr. Biol.*, *16*(5), R165–R167. Retrieved from http://linkinghub.elsevier.com/retrieve/pii/S0960982206011912 doi: 10.1016/j.cub.2006.02.041

Levelt, W. (1965). *On binocular rivalry* (Doctoral dissertation). Retrieved from http://pubman.mpdl.mpg.de/pubman/item/escidoc:77195/component/escidoc:513080/Levelt_Binocular_Rivalry_1965.pdf

Love, G. D. (2012). *Personal Communication.*

Love, G. D., Hoffman, D. M., Hands, P. J. W., Gao, J., Kirby, A. K., & Banks, M. S. (2009, August). High-speed switchable lens enables the development of a volumetric stereoscopic display. *Opt. Express*, *17*(18), 15716–25. Retrieved from http://www.pubmedcentral.nih.gov/articlerender.fcgi?artid=3056506\&tool=pmcentrez\&rendertype=abstract

Mackenzie, K. J., Hoffman, D. M., & Watt, S. J. (2010). Accommodation to multiple-focal-plane displays: Implications for improving stereoscopic displays and for accommodation control. *J. Vis.*, *10*(8), 1–20. doi: 10.1167/10.8.22.Introduction

Malmström, T., & Kröger, R. H. H. (2006, January). Pupil shapes and lens optics in the eyes of terrestrial vertebrates. *J. Exp. Biol.*, *209*(Pt 1), 18–25. Retrieved from http://www.ncbi.nlm.nih.gov/pubmed/16354774 doi: 10.1242/jeb.01959

Mann, I. (1924). The function of the pecten. *Br. J. Ophthalmol.*. Retrieved from http://www.ncbi.nlm.nih.gov/pmc/articles/PMC512927/

Mannos, J., & Sakrison, D. (1974, July). The effects of a visual fidelity criterion of the encoding of images. *IEEE Trans. Inf. Theory*, *20*(4), 525–536. Retrieved from http://ieeexplore.ieee.org/articleDetails.jsp?arnumber=1055250 doi: 10.1109/TIT.1974.1055250

Marcos, S., & Burns, S. A. (2000, January). On the symmetry between eyes of wavefront aberration and cone directionality. *Vision Res.*, *40*(18), 2437–47. Retrieved from http://www.ncbi.nlm.nih.gov/pubmed/10915884

Markwell, E. L., Feigl, B., & Zele, A. J. (2010, May). Intrinsically photosensitive melanopsin retinal ganglion cell contributions to the pupillary light reflex and circadian rhythm. *Clin. Exp. Optom.*, *93*(3), 137–49. Retrieved from http://www.ncbi.nlm.nih.gov/pubmed/20557555 doi: 10.1111/j.1444-0938.2010.00479.x

Mendiburu, B. (2012). *3D Movie Making: Stereoscopic Digital Cinema from Script to Screen*. CRC Press. Retrieved from https://books.google.com/books?hl=en\&lr=\&id=36B5AgAAQBAJ\&pgis=1

Michelson, A. (1927). *Studies in optics*. Chicago Ill.: The University of Chicago Press.

Millodot, M. (2004). *Dictionary of Optometry and Visual Science*. Butterworth-Heinemann. Retrieved from https://books.google.co.uk/books/about/Dictionary_of_Optometry_and_Visual_Scien.html?id=P2ZqAAAAMAAJ\&pgis=1

Milner, A., & Goodale, M. (1995). *The visual brain in action*. Retrieved from http://www.cse.buffalo.edu/~shapiro/Courses/CSE575/FSslides/psyche-4-12-milner.html

Mitchell, J. F., Stoner, G. R., & Reynolds, J. H. (2004, May). Object-based attention determines dominance in binocular rivalry. *Nature*, *429*(6990), 410–3. Retrieved from http://dx.doi.org/10.1038/nature02584 doi: 10.1038/nature02584

Monticone, P. P., & Menozzi, M. (2011, February). A review on methods used to record and analyze microfluctuations of the accommodation in the human eye. *J. Eur. Opt. Soc. Rapid Publ.*, *6*(April 2010), 1–7. Retrieved from https://www.jeos.org/index.php/jeos_rp/article/view/11003 doi: 10.2971/jeos.2011.11003

Nijkamp, M. D., Dolders, M. G. T., de Brabander, J., van den Borne, B., Hendrikse, F., & Nuijts, R. M. M. A. (2004, October). Effectiveness of multifocal intraocular lenses to correct presbyopia after cataract surgery: a randomized controlled trial. *Ophthalmology*, *111*(10), 1832–9. Retrieved from http://www.aaojournal.org/article/S0161642004008450/fulltext doi: 10.1016/j.ophtha.2004.05.023

Pau, H., & Kranz, J. (1991, May). The increasing sclerosis of the human lens with age and its relevance to accommodation and presbyopia. *Graefe's Arch. Clin. Exp. Ophthalmol.*, *229*(3), 294–296. Retrieved from http://link.springer.com/10.1007/BF00167888 doi: 10.1007/BF00167888

Peirce, J. W. (2007, May). PsychoPy–Psychophysics software in Python. *J. Neurosci. Methods*, *162*(1-2), 8–13. Retrieved from http://www.pubmedcentral.nih.gov/articlerender.fcgi?artid=2018741\&tool=pmcentrez\&rendertype=abstract doi: 10.1016/j.jneumeth.2006.11.017

Percival, A. (1892). The relation of convergence to accommodation and its practical bearing. *Ophthal. Rev*. Retrieved from http://scholar.google.co.uk/scholar?q=The+relation+of+convergence+to+accommodation+and+its+

practical+bearing\&btnG=\&hl=en\&as_sdt=0,5\#0

Pettigrew, J. D., & Sanderson, K. J. (1986). *Visual Neuroscience*. CUP Archive. Retrieved from https://books.google.com/books?id=3KU8AAAAIAAJ\&pgis=1

Phillips, S., & Stark, L. (1977, April). Blur: A sufficient accommodative stimulus. *Doc. Ophthalmol.*, *43*(1), 65–89. Retrieved from http://link.springer.com/10.1007/BF01569293 doi: 10.1007/BF01569293

Pinz, A., Bernögger, S., Datlinger, P., & Kruger, A. (1998, August). Mapping the human retina. *IEEE Trans. Med. Imaging*, *17*(4), 606–19. Retrieved from http://ieeexplore.ieee.org/articleDetails.jsp?arnumber=730405 doi: 10.1109/42.730405

Porter, J., Guirao, A., Cox, I. G., & Williams, D. R. (2001). Monochromatic aberrations of the human eye in a large population. *J. Opt. Soc. Am*, *18*(8), 1793–1803.

Prange, S., Gehrt, S. D., & Wiggers, E. P. (2004). Influences of Anthropogenic Resources on Raccoon (Procyon lotor) Movements and Spatial Distribution. *J. Mammal.*, *85*(3), 483–490.

Ramachandran, V. (1992). Blind spots. *Sci. Am.*. Retrieved from http://apps.usd.edu/coglab/schieber/pdf/Ramachandran1992.pdf

Regan, D., & Neima, D. (1984). Low-contrast letter charts in early diabetic retinopathy, ocular hypertension, glaucoma, and Parkinson's disease. *Br. J. Ophthalmol.*, *68*, 885–889. Retrieved from http://bjo.bmj.com/content/68/12/885.short

Richards, W. (1970, August). Stereopsis and stereoblindness. *Exp. Brain Res.*, *10*(4), 380–388. Retrieved from http://link.springer.com/10.1007/BF02324765 doi: 10.1007/BF02324765

Richdale, K. (2006). Comparison of multifocal and monovision soft contact lens corrections in patients with low-astigmatic presbyopia. *Optom. Vis. ...*. Retrieved from http://journals.lww.com/optvissci/Abstract/2006/05000/Comparison_of_Multifocal_and_Monovision_Soft.5.aspx

Riva, C., & Cranstoun, S. (1994). Choroidal blood flow in the foveal region of the human ocular fundus. *... Vis. Sci.*. Retrieved from http://www.researchgate.net/profile/Charles_Riva/publication/15197490_Choroidal_blood_flow_in_the_foveal_region_of_the_human_ocular_fundus/links/09e4150871174a680f000000.pdf

Rodieck, R. (1998). *The first steps in seeing*. Retrieved from http://sinauerd.nextmp.net/media/wysiwyg/tocs/FirstStepsInSeeing.pdf

Roth, L. S. V., & Kelber, A. (2004, December). Nocturnal colour vision in geckos. *Proc. Biol. Sci.*, *271 Suppl*(December), S485–7. Retrieved from http://www.pubmedcentral.nih.gov/articlerender.fcgi?artid=1810110\&tool=pmcentrez\&rendertype=abstract doi: 10.1098/rsbl.2004.0227

Russ, J. C. (2006). *The Image Processing Handbook, Fifth Edition*. CRC Press. Retrieved from http://books.google.com/books?id=Vs2AM2cWl1AC\&pgis=1

Sheard, C. (1934). The prescription of prisms. *Am. J. Optom.*. Retrieved from http://scholar.google.co.uk/scholar?q=The+prescription+of+prisms\&btnG=\&hl=en\&as_sdt=0,5\#0

Shibata, T., Kim, J., Hoffman, D. M., & Banks, M. S. (2011, January). The zone of comfort: Predicting visual discomfort with stereo displays. *J. Vis.*, *11*(8), 11. Retrieved from http://www.pubmedcentral.nih.gov/articlerender.fcgi?artid=

3369815\&tool=pmcentrez\&rendertype=abstract doi: 10.1167/11.8.11

Snellen, H. (1863). *Dr. H. Snellen's Probebuchstaben zur Bestimmung der Sehschaerfe*. Retrieved from https://books.google.co.uk/books?hl=en\&lr=\&id=0D4JAAAAIAAJ\&oi=fnd\&pg=PA3\&dq=Probebuchstaben+zur+Bestimmung+der+Sehsch\%C3\%A4rfe\&ots=zsuFscTJ4X\&sig=LNZUez6eUrDKUwlVs5nbwGKh4dc

Spector, R. H. (1990). Visual Fields. In H. Walker, W. Hall, & J. Hurst (Eds.), *Clin. methods hist. phys. lab. exam.* (3rd ed.). Butterworths. Retrieved from http://www.ncbi.nlm.nih.gov/books/NBK220/

Sperry, J. H., Blouin-Demers, G., Carfagno, G. L. F., & Weatherhead, P. J. (2010, June). Latitudinal variation in seasonal activity and mortality in ratsnakes (Elaphe obsoleta). *Ecology*, *91*(6), 1860–6. Retrieved from http://www.ncbi.nlm.nih.gov/pubmed/20583726

Stamper, R. (1984). The effect of glaucoma on central visual function. *Trans. Am. Ophthalmol. ....* Retrieved from http://www.ncbi.nlm.nih.gov/pmc/articles/PMC1298679/

Stanford University School of Medicine Website. (2015). *Fundoscopic Exam.* Retrieved from http://stanfordmedicine25.stanford.edu/the25/fundoscopic.html

Stark, L. R., Lee, R. S., Kruger, P. B., Rucker, F. J., & Ying Fan, H. (2002, June). Accommodation to simulations of defocus and chromatic aberration in the presence of chromatic misalignment. *Vision Res.*, *42*(12), 1485–98. Retrieved from http://www.ncbi.nlm.nih.gov/pubmed/12074944

Stark, L. R., Strang, N. C., & Atchison, D. a. (2003, December). Dynamic accommodation response in the presence of astigmatism. *J. Opt. Soc. Am. A, Opt. image Sci. visions*, *20*(12), 2228–36. Retrieved from http://www.ncbi.nlm.nih.gov/pubmed/14686501

Stark, L. R., & Takahashi, Y. (1965). Absence of an Odd-Error Signal Mechanism in Human Accommodation. *IEEE Trans. BIO-MIEDICAL Eng.*, *12*(3), 138–146.

Stiles, W. S. (1937, June). The Luminous Efficiency of Monochromatic Rays Entering the Eye Pupil at Different Points and a New Colour Effect. *Proc. R. Soc. B Biol. Sci.*, *123*(830), 90–118. Retrieved from http://rspb.royalsocietypublishing.org/content/123/830/90 doi: 10.1098/rspb.1937.0045

Strang, N. (2000). The accommodation response can improve visual performance in the presence of astigmatism. *... Vis. ....* Retrieved from https://scholar.google.co.uk/scholar?lookup=0\&q=The+accommodation+response+can+improve+visual+perfor-+mance+in+the+presence+of+astigmatism\&hl=en\&as_sdt=0,5\#0

Takeda, T., Hashimoto, K., Hiruma, N., & Fukui, Y. (1999, June). Characteristics of accommodation toward apparent depth. *Vision Res.*, *39*(12), 2087–2097. Retrieved from http://www.sciencedirect.com/science/article/pii/S0042698998002582 doi: 10.1016/S0042-6989(98)00258-2

Tessier-Lavigne, M. (2000). Visual processing by the retina. *Princ. Neural Sci.*. Retrieved from http://www.weizmann.ac.il/neurobiology/labs/ulanovsky/sites/neurobiology.labs.ulanovsky/files/uploads/kandel_ch26_retina.pdf

Thibos, L., Still, D., & Bradley, A. (1996). Characterization of spatial aliasing and contrast sensitivity in peripheral vision. *Vision Res.*. Retrieved from http://www.sciencedirect.com/science/article/pii/004269899500109D

Thorpe, S., Fize, D., & Marlot, C. (1996). Speed of processing in the human visual system. *Nature*. Retrieved from http://fias.uni-frankfurt.de/~triesch/courses/

260object/papers/SpeedOfProcessing.pdf

Wandell, B. A. (1995). *Foundations of Vision*. Sinauer Associates. Retrieved from https://books.google.co.uk/books/about/Foundations_of_Vision.html?id=5uhqAAAAMAAJ\&pgis=1

Westheimer, G. (2008, December). Directional sensitivity of the retina: 75 years of Stiles-Crawford effect. *Proc. Biol. Sci.*, *275*(1653), 2777–86. Retrieved from http://www.pubmedcentral.nih.gov/articlerender.fcgi?artid=2572678\&tool=pmcentrez\&rendertype=abstract doi: 10.1098/rspb.2008.0712

Wheatstone, C. (1838). Contributions to the physiology of vision.–Part the first. On some remarkable, and hitherto unobserved, phenomena of binocular vision. *Philos. Trans. R. Soc. ...*. Retrieved from http://www.jstor.org/stable/108203

Wichmann, F. a., & Hill, N. J. (2001, November). The psychometric function: II. Bootstrap-based confidence intervals and sampling. *Percept. Psychophys.*, *63*(8), 1314–1329. Retrieved from http://www.springerlink.com/index/10.3758/BF03194545 doi: 10.3758/BF03194545

Wilcox, J. G., & Barlow, H. B. (1975, December). The size and shape of the pupil in lightly anaesthetized cats as a function of luminance. *Vision Res.*, *15*(12), 1363–5. Retrieved from http://www.ncbi.nlm.nih.gov/pubmed/1210019

Wilson, B. J., Decker, K. E., & Roorda, A. (2002). Monochromatic aberrations provide an odd-error cue to focus direction. *Op. Soc. Am.*, *19*(5), 833–839.

Winn, B., Charman, W. N., Pugh, J. R., Heron, G., & Eadie, a. S. (1989, March). Perceptual detectability of ocular accommodation microfluctuations. *J. Opt. Soc. Am. A.*, *6*(3), 459–62. Retrieved from http://www.ncbi.nlm.nih.gov/pubmed/2709192

Winn, B., Pugh, J. R., Gilmartin, B., & Owens, H. (1990a, October). Arterial pulse modulates steady-state ocular accommodation. *Curr. Eye Res.*, *9*(10), 971–5. Retrieved from http://www.ncbi.nlm.nih.gov/pubmed/2276274

Winn, B., Pugh, J. R., Gilmartin, B., & Owens, H. (1990b, January). The frequency characteristics of accommodative microfluctuations for central and peripheral zones of the human crystalline lens. *Vision Res.*, *30*(7), 1093–9. Retrieved from http://www.ncbi.nlm.nih.gov/pubmed/2392837

Wirm, B., & Gilmartin, B. (2007, December). Current perspective on microfluctuations of accommodation. *Ophthalmic Physiol. Opt.*, *12*(2), 252–256. Retrieved from http://doi.wiley.com/10.1111/j.1475-1313.1992.tb00301.x doi: 10.1111/j.1475-1313.1992.tb00301.x

Woods, A. J., & Harris, C. R. (2010, February). ¡title¿Comparing levels of crosstalk with red/cyan, blue/yellow, and green/magenta anaglyph 3D glasses¡/title¿. In A. J. Woods, N. S. Holliman, & N. A. Dodgson (Eds.), *Is&t/spie electron. imaging* (pp. 75240Q–75240Q–12). International Society for Optics and Photonics. Retrieved from http://proceedings.spiedigitallibrary.org/proceeding.aspx?articleid=775972 doi: 10.1117/12.840835

Xiao, J., Jiang, C., & Zhang, M. (2011). Pseudophakic monovision is an important surgical approach to being spectacle-free. *Indian J. Ophthalmol.*, *59*(6), 481–5. Retrieved from http://www.pubmedcentral.nih.gov/articlerender.fcgi?artid=3214420\&tool=pmcentrez\&rendertype=abstract doi: 10.4103/0301-4738.86318

Yi, F., Robert Iskander, D., & Collins, M. (2011, May). Depth of focus and visual acuity with primary and secondary spherical aberration. *Vision Res.*, *51*(14), 1648–1658.

Retrieved from http://www.ncbi.nlm.nih.gov/pubmed/21609729 doi: 10.1016/j.visres.2011.05.006

Young, L. K. (2011). *Ocular higher-order aberrations and visual performance* (Unpublished doctoral dissertation).

Young, L. K., Love, G. D., & Smithson, H. E. (2013, January). Different aberrations raise contrast thresholds for single-letter identification in line with their effect on cross-correlation-based confusability. *J. Vis.*, *13*(7), 12. Retrieved from http://www.journalofvision.org/content/13/7/12.fullhttp://www.ncbi.nlm.nih.gov/pubmed/23788460 doi: 10.1167/13.7.12